Università
degli Studi
di Ferrara

DOCTORAL COURSE IN
PHYSICS

CYCLE XXX

DIRECTOR Prof. Eleonora Luppi

ARCHAEOMETRICAL TECHNIQUES APPLIED TO CULTURAL HERITAGE AND TO OTHER DISCIPLINES

Scientific/Disciplinary Sector (SDS) FIS/07

Candidate
Dott. Vivarelli Arianna

Supervisor
Prof. Petrucci Ferruccio Carlo

Co-supervisor
Dr. Bernardi Adriana

Years 2014/2018

SUMMARY

INTRODUCTION

The term archaeometry literally means "measure of the ancient". It is now well-established that this is a multidisciplinary field in which the exact sciences give their contribution to the field of cultural heritage for the studies aimed at its knowledge, conservation and restoration. So usually chemical, physical, biological techniques, etc. are made available to the culture, becoming typically, if not exclusively, archaeometric techniques. In the same way, some techniques quite consolidated in the study of cultural heritage could be extended to other specialized subjects to offer an alternative to more traditional analysis, for example in terms of speed, affordability or easiness of interpretation.

This continuous exchange between hard sciences and archaeometry, and the correlated multidisciplinary nature, link the different research themes addressed. After a first part dedicated to the analysis of thermal performances of innovative materials, mainly through microclimatic monitoring in historical buildings, in the second phase of this thesis the application of two archaeometric image techniques was extended to sectors of social impact, such as fluid-dynamics and agrifood. In the case, Schlieren interferometry for the visualization of air flow in sanitary environments, and reflectance spectroscopy for the analysis of edible oils.

The first two years of research were carried out at the Institute of Atmospheric Sciences and Climate (ISAC) of the CNR of Padua. The covered topics mainly concerned the analysis of the internal microclimate in historical buildings, in particular the effects on energy efficiency and human comfort related to the use of thermal buffering and insulating materials. These materials were studied and / or developed in the context of recent European projects (MESSIB and EFFESUS), funded within the 7th Framework Programme. Indeed, most of the current developments in energy efficiency address new construction without dealing with the unique problems of historic structures and consequently they are not acceptable for built heritage due to the necessity of preserving integrity and authenticity. Therefore, the study on new technologies and the application of new materials in the field of cultural heritage is of primary importance for an effective conservation and discounting to current needs of sustainability of the world heritage.

The project MESSIB (acronym of “Multisource Energy Storage System integrated in Buildings”) had the purpose to develop, evaluate and demonstrate a multi-source energy storage system integrated into buildings. The basic idea of the project was to provide a buffer to balance fluctuations in energy supply and demand, through the integration of new materials and technologies based on energy storage.

Within this project, my research was focused on the phase change materials (PCMs), used to stabilize the temperature over short-term time cycles, thanks to their ability to store and release the latent thermal energy during the transition from the solid to the liquid state and vice versa.

Even though the use of PCMs in civil buildings has been a main research topic for the last decades and a large literature has been published, no specific reference to cultural heritage has been found. Indeed, the most common and so far effective application of PCMs in the civil field turns out to be one of the main barriers for their use in cultural heritage. In fact, the solution of incorporating the PCMs in construction materials is possible only for new or refurbished buildings, not always for historical ones, because this operation would require an invasive intervention on the building. Last, but not least, in heritage buildings the use of PCMs has to be evaluated in terms of not only human comfort and energy saving benefits, but also taking into account conservation issues. Hence, the most feasible application of PCMs' technology in cultural heritage would be to place boards of different materials incorporating PCMs. These panels can be sized according to the dimensions of the room and they can be easily installed and removed according to the specific needs.

In this thesis, this potentially new application of the PCMs' technology to heritage objects was evaluated. Firstly, the thermal behaviour of PCMs when incorporated into a specific building material was studied by comparing the performances of different types of paraffin waxes - in the form of powder and emulsion with melting points at 21 and 26°C - incorporated in plaster and silicone. The experimentation concerned the demonstration of the effectiveness of PCMs, the reproducibility of results and the most performing material among those under examination. Secondly, the possibility of applying PCM technology to historic buildings and / or objects of cultural heritage and the related barriers were assessed, through tests performed both in laboratory and in field - at the Santa Croce Opera Museum in Florence and at the Archaeological Museum in Novelda-Alicante (Spain). In particular, by transposing their use from the civil sector, a configuration was simulated for which the work of art would be in contact with the PCM, and pro and cons of this methodology were analysed.

The project EFFESUS (acronym of "Energy Efficiency for EU Historic Urban Districts' Sustainability") aimed to develop and demonstrate through case studies a methodology to evaluate and select energy efficiency interventions, based on both new and existing technologies compatible with historic-artistic values. The results of the project were the development of: 1) new technologies and materials to improve significantly the thermal properties of the building envelope; 2) a multi-scale data model for energy management in historical districts; 3) the Decision Support System (DSS), a software tool to support the identification of the best energy efficiency solution.

Within this project, my research was focused on the analysis of the effects on microclimate inside historic buildings after the installation of the following insulating materials: i) aerogel fibre for use in cavities behind the interior fittings of the wall; ii) insulating mortar for internal use; iii) reflective outer coating.

In addition to the intrinsic innovative aspect of the materials, specifically developed by some project partners, their evaluation through traditional techniques, such as temperature and heat flux measurements, thermal transmittance etc. has revealed worthy to study their impact especially in the frame of the needs of renovation of the large cultural heritage patrimony.

Firstly, a literature research was carried out to draw up a state of the art about the common impact indicators used to evaluate the retrofitting measures and solutions, implemented to improve indoor air quality and thermal comfort, to be further integrated into the DSS.

Secondly, the above mentioned insulating materials were installed in 3 case studies (3 historical buildings located in Glasgow, United Kingdom – Benediktbeuern, Germany – Istanbul, Turkey) and the performances of the retrofit interventions were evaluated. In particular, the actions consisted in the definition of the monitoring plan in each demonstration site, continuous data collection and analysis, comparison of the environmental conditions and the energy consumption with and without the intervention. At the end, the materials were analysed in terms of applicability, performance, durability, removability and compatibility with the historic structure. In particular, the improvement of energy efficiency and internal thermal comfort for human well-being was demonstrated.

The last year of research was carried out at the Laboratory of Archaeometry of the University of Ferrara and has pursued two distinct aims.

The first objective was to create a Schlieren optical system, able to visualize the streak-like appearance of fluid flow due to small changes in the refractive index, arising from variations in pressure and/or temperature of air. As a dynamic and straightforward viewing tool, the system is primarily applied to conduct qualitative visual studies.

The implementation of a Schlieren system to be applied to the heating, ventilation and air conditioning (HVAC) studies for the analysis of the air movements and the impact of the plants is an interesting alternative to the gas tracers or Particle Image Velocimetry systems. Indeed, the advantages of the use of the Schlieren technique, instead of traditional fluid dynamic studies, consist in the sensitivity to changes, non-invasiveness since it does not interfere with the flow and speed of diagnostic by returning an image, which immediately indicates the direction of the airflow. By using Schlieren technique, for example, it is possible to set differently the operating parameters of HVAC systems in real time, displaying immediately the effect of the change, without the need for post-analysis or modelling of collected data.

The final objective would be properly to monitor the air movements produced by the functioning of the heating / air conditioning / purification systems, in order to improve their operating conditions according to the place of installation. In particular, in sanitary environments, it would be worthwhile to have no impact of the airflow on the human body, in order to reduce the risk of infections, by moving away the transported microbial load from the patients, with consequent benefits on both people health and costs of medical care.

The experimental work focused on understanding the potentiality of the system built in the laboratory, in particular to estimate the sensitive volume of the working area, to quantify the sensitivity to changes in the refractive index, and finally to demonstrate the sensitivity of the system to pressure variations in both static and perturbed conditions. The goal was to understand the basic conditions to work in real environments.

The second objective was to test the use of image spectroscopy for the prompt analysis of olive oil samples. This technique is usually carried out in archaeometric studies to detect at different times the alterations of the pictorial layer not yet perceptible to the human eye. Therefore, the main goal was to understand if image spectroscopy could be a reliable and prompt technique to be extended to the analysis of edible oils, a research field not yet explored by this technique.

Spectroscopy, in general, is a non-destructive technique that allows the qualitative determination of organic compounds; in fact, as the nature and the composition of the sample vary, the absorption bands in the electromagnetic spectrum differ in intensity and frequency values. For this reason, it has become a powerful analytical tool in food research. Among the different variety of oils, the absorption bands show slight differences due to the quantity variation of the components (in particular β-carotene, chlorophyll *a* and *b*), and/or to the presence of sealing agents, in turn function of the type of cultivation, the place of production, the climatic conditions.

Usually, oil samples are analysed in laboratory with quite expensive multispectral / hyperspectral devices. The advantages of the use of image spectroscopy would be portability and affordability in terms of costs respectively, at the expense of spectral resolution. The final aim of this task would be to build a portable and low cost device for a beginning individuation of possibly counterfeited samples to be labelled for further and deeper analyses with more specific techniques.

The challenge of the experimental work of this thesis was to validate the technique by obtaining reflectance / transmittance spectra similar to those obtained with the spectrophotometer. After several preliminary tests for the identification of the appropriate configuration, six samples of extra virgin olive oil were analysed. The reflectance values were then object of calculation to obtain the corresponding transmittance values to be compared to those collected with the spectrophotometer.

SECTION A - MICROCLIMATE MONITORING TO STUDY THE THERMAL PERFORMANCE OF INNOVATIVE MATERIALS IN HISTORICAL BUILDINGS

Main passive interventions to optimize the energy performance of buildings

The energy saving has assumed an increasing importance in the last few years and has been one of the primary objectives of governments and institutions, both for the reduction of fuel consumption and procurement costs, and for the reduction of atmospheric emissions of polluting substances, first of all carbon dioxide (CO_2), with consequent benefits for the environment.

Therefore, there is also a renewed interest in those aspects of architecture, which lead to thermal comfort in buildings with minimum expenditure of conventional energy. After the "Kyoto Protocol" ratified in 1997, with which the participating nations committed themselves to reduce CO_2 emissions, Europe issued the Community Directive 2002/91/CE on the energy performance of buildings. In Italy, the directive was implemented by the Legislative Decree 192/2005, supplemented and amended by various subsequent measures, including the D.P.R. 2/04/2009 no. 59 and the decree of the Ministry of economic development 26/06/2009. Furthermore, the UNI TS 11300 standard, issued by the Italian National Unification Agency, is the reference for the national application of Directive 2002/91/EC. Finally, the legislative decree 4/7/2014 n. 102 implements the Directive 2012/27/EU, which amends the Directives 2009/125/EC and 2010/30/EU and repeals the Directives 2004/8/EC and 2006/32/EC.

It is important to point out that the aforementioned standards do not exhaust the complex regulatory framework, which is constantly evolving, also in consideration of the technological progress and the evolution of market laws.

The interventions aimed at optimizing the energy performance of buildings can be passive, if one acts on the enclosure, or active, in the event one intervenes on the plants. This thesis will focus only on the first category of interventions.

Passive interventions are based on the control of the amount of thermal energy that the building exchanges with the environment. Therefore, these interventions consist essentially in the thermal insulation of the opaque walls, in the replacement of the fixtures and in the shielding. Moreover, these interventions are closely linked to external microclimatic conditions. For this reason, especially in temperate climates where considerable seasonal and daily temperature variations occur, it is important to find a balance between the different seasonal needs, taking into account the thermal balance of the building throughout the entire solar year.

In particular, during the winter the main objective is to favor the production, capture and accumulation of heat inside the building, limiting at the same time the thermal dispersions towards the outside. The first result can be achieved by maximizing the exploitation of solar energy, the second by improving the overall thermal insulation of transparent and opaque closures.

On the contrary, during the summer, cooling optimization is achieved by minimizing the incident solar radiation and dissipating the heat in excess by optimizing the capacity of the enclosure to store and re-emit heat with a certain time lag.

In this way, it is possible to integrate the performance of active plants, reducing the demand for primary energy necessary for the achievement of comfort conditions.

Passive heating

The amount of heat exchanged by a body per unit of surface is calculated through the transmittance parameter, U, defined as the heat flow that passes through a unit surface subjected to temperature differences equal to 1 K (UNI EN ISO 6946) and it is related to the thickness and thermal conductivity of the layers that compose the body. The thermal conductivity, λ, represents the capacity that a material has to conduct heat: it is defined as the amount of heat, measured in Watt, that flows every second through 1 m^2 of material with a thickness of 1 mm with a temperature difference between inside and outside of 1 K.

In general, the insulating properties of an opaque wall therefore depend on the thickness and thermal conductivity of the materials composing it.

In this sense, the massive walls that generally characterize the historical buildings have a medium level of thermal conductivity in face of high thicknesses. If the insulation of the walls is insufficient, it is possible to integrate the wall system with special layers of insulating material, whose very low thermal conductivity allows to considerably improving the thermal performance in face of limited thickness.

However, it must be taken into account that the addition of a new component to the opaque envelope may have negative implications on the hygrometric behavior of the walls with possible formation of interstitial condensation. In particular, the presence of high porosity materials is more commonly found in traditional buildings, alongside the use of construction elements generally without vapor barrier or waterproofing. For this reason, the choice of thermal insulation must conform to the permeability and breathability of the existing wall system or be counterbalanced by alternative measures for the dissipation of excess internal humidity.

Another issue to keep in mind in insulation interventions is related to the needs of fruition of spaces and the possible reduction of useful volumes, especially if the insulating material is applied inside the building. In this case, it is possible to adopt very high-performance components, such as heat-reflecting insulators, with extremely thick layers.

Finally, for the insulation of a building it is also necessary to limit the discontinuities in the thermal properties of the enclosure, defined as thermal bridges, which put the outer surfaces in contact with the internal surfaces by means of elements with high heat conductivity. Thermal bridges can be of shape or structure. In the first case, they occur in the corner areas between homogeneous materials; in the second, they appear at the connection between elements with different thermal characteristics. During the winter, thermal bridges cause the internal surface temperature to decrease, with the risk of causing condensation; during the summer, on the contrary, they allow the penetration of heat from the outside towards the inside, causing overheating of internal air.

The reduction of thermal bridges is linked to the continuity of the behavior towards heat flow of the individual components through the entire surface of the wall. In the case an insulating layer is introduced, whose thermal conductivity is usually much lower than that of traditional closures, it is important to ensure a homogeneous lining of the envelope, whether external or internal.

The insulating layer can be placed in the following ways:

- external insulating layer
- internal insulating layer
- internal or external thermal insulating plaster.

The positioning of the insulating layer marks the boundary between the internal and external thermal conditions, influencing the building's response to the climate.

The insulation of the external façade moderates the thermal fluctuations both on surface and air temperature, so the environment takes much time to heat and cool but keeps the same temperature longer. Moreover, the external insulation does not alter the internal volumes and, if applied continuously, the effect of thermal bridges decreases.

When the shape of the building strongly limits the continuity of an external coating, it is possible to apply the insulating layer inside. In this case, the mass of the wall is removed as thermal mass and therefore the response to internal temperature variations is faster;

however, the use of masonry as a heat accumulation and dissipation system is prevented. Furthermore, the intervention determines a reduction in the tread surface and makes difficult the limitation of the structural thermal bridges between horizontal and vertical surfaces.

In case of application of a layer of thermal insulating plaster, the degree of insulation is lower because of the reduced thickness and the limited insulation properties of the materials, but it can sometimes be the only possible intervention. The thermal insulating plaster can be applied both externally and internally in completely similar ways.

Passive cooling

With regard to passive cooling techniques applied to the envelope, they can be divided into two classes of intervention. The first is based on preventive projects aimed at reducing external thermal contributions before they invest the building, with external solar shading or by acting on the morphology of the envelope surfaces and their finishing. The second class is based on the control of the ways in which these thermal flows can pass through the closures and then be dissipated, working on the design and calculation of the thermal capacity and the insulating power of the materials and introducing natural or controlled ventilation systems.

The surface finishing changes the amount of solar energy that is reflected or absorbed by the materials, propagating towards the inside of the building. The amount depends on the angle of incidence, on the roughness of the surface and on the reflection coefficient, defined as albedo, of the materials used. The albedo represents the percentage of radiation that is reflected by the material: it strongly influences the propagation of solar energy into the environment, both dispersing it towards the atmosphere and redirecting it towards the neighboring structures. The albedo values depend on different characteristics of the material, including color and roughness.

In the market, also exist materials and pigments, called cool materials, characterized by a very high value of the albedo in face of variable coloring and superficial treatments. These materials can also be used for normal maintenance works, providing good reflection performance of solar radiation without altering the aesthetic character of the building.

In temperate climates, the thermal inertia of the walls becomes particularly important during the cooling period, where there is a greater thermal variability between the night and day periods.

The control of thermal inertia is carried out by means of the two parameters: the phase shift and the attenuation, which respectively represent the ability to delay and reduce the effect of a temperature variation between the internal and external surfaces.

The phase shift, φ, is the time delay between the maximum of the thermal flow entering the internal environment and the maximum temperature of the external environment. The attenuation factor is the ratio between the dynamic thermal transmittance module and the thermal transmittance in stationary conditions (UNI EN ISO 13786), and indicates the reduction of the amplitude of the thermal wave when passing from the outside into the environment through the structure in question. The thickness, density and specific heat of the materials used influences these two factors.

In the case of a building without thermal insulation, heat dissipation can naturally occur through the walls.
In a building with an insulating layer on the outer side, the thermal loads transmitted through the walls are almost eliminated. It is therefore necessary to use radiative or convective cooling strategies to dissipate internal loads during cooler periods.
In a building provided with an insulating layer on the inside, the temperature changes between night and day time increase, therefore the importance of thermal dissipation by ventilation is reduced.

One possibility of innovative intervention concerns the use of phase change materials (PCM). They have a melting point near the ambient temperature: this makes them capable of accumulating latent thermal energy during the transition from the solid state to the liquid state and releasing it in the reverse passage, without varying their temperature during the process.
For building applications, paraffinic organic compounds or hydrated salts with melting point between 18° and 25°C are used. The most common application involves the addition of microcapsules, with a diameter of 2-20 µm, to traditional materials (e.g. plasterboard panels or plasters for the internal lining), in order to obtain performing components with traditional laying methods. These components have an extremely high thermal inertia with reduced thickness and are compatible with current maintenance work. The disadvantages are related to the difficulty of controlling the specific behavior of the materials and their high flammability.

Among this wide variety of solutions, the doctoral research dealt with the possible application of PCM in cultural heritage and the testing of three innovative insulating materials - namely aerogel, radiant reflective coating, lime-based mortar - installed in historical buildings. Their thermal performances were demonstrated by means of microclimate analysis through laboratory experiments, simulation in real-world conditions and monitoring in practical case studies.

1 PHASE CHANGE MATERIALS (PCM)

1.1 PCM AS ENERGY STORAGE MATERIALS

In the last 20 years, a large part of scientific research has dealt with thermal energy accumulators, which include Phase Change Materials (PCMs). The concept behind the energy storage in general – and the thermal one in particular - is to provide a buffer device in buildings that balances the fluctuations between the supply and the energy demand, which can vary with different time cycles: short (daily), intermediate (weekly), long and seasonal. PCMs allow daily cycle of energy storage.

In general, short-term thermal storage can be differentiated into:

- sensitive systems, in which the thermal energy is stored by raising the temperature of a material. In this case, the accumulated amount of heat is calculated as follows:

$$Q = \int_{Ti}^{Tf} mC_p \Delta T$$

Where:

Ti = initial temperature of the substance
Tf = final temperature of the substance
m = mass of the substance
Cp = specific heat of the substance

- phase change systems, where the amount of stored heat is calculated as follows:

$$Q = \int_{Ti}^{Tm} mC_p dT + ma_m \Delta h_m + \int_{Tm}^{Tf} mC_p dT$$

Where:

T_m = melting temperature of the material
a_m = fraction of molten material
Δh_m = latent melting heat of the material per unit of mass

The working principle of phase change materials is the following: during the phase transition, the material absorbs heat and stores a high amount of energy, keeping its temperature constant and returning the heat outside only when a lowering of temperature occurs. The greater the latent melting heat, the greater will be the heat stored at a constant temperature.

In particular, during the solid-liquid transition, the phase change material begins to melt when the temperature of the environment reaches the melting point of the material concerned, which is specific to each substance. The PCM absorbs heat (latent liquefaction heat) from the environment when it starts to melt and will continue until it is completely melted. If the temperature continues to increase even after the complete melting of the material, the PCM will no longer be able to absorb the heat and then there will be an increase in the temperature of the environment. With regard to the liquid-solid passage, it is observed that when the temperature drops, the PCM gives off the previously stored heat (latent solidification heat) and return to the solid state.

Solid-liquid, liquid-solid phase changes involve a higher latent heat exchange than solid-solid transformations, where heat is accumulated in the transition from one crystalline form to another. Compared to liquid-gas transformations, on the other hand, they are characterized by a lower latent heat accumulation, however they allow a much smaller volume variation (in the order of 10% or less). The type of accumulation that exploits the change in solid-liquid and vice-versa, is therefore economically more convenient and generally the most used thank to the high density of accumulation.

Thermal energy storage systems using PCMs have been a main topic in research for the last decades and they have been recognized as one of the advanced technologies in enhancing energy efficiency and sustainability of buildings, as well as potentially reducing energy cost (Tyagi V.V., 2011). A large number of research studies and review papers provide a detailed characterization of PCMs, in terms of classification of materials and their properties, major applications in buildings and related problems (Tyagi V.V., 2011) (Tyagi V.V., 2007) (Cabeza L. F., 2011) (Khudhair A.M., 2004) (Zalba B., 2003). In general, the use of PCMs in buildings has two main advantages: enhancing indoor thermal comfort for occupants due to the reduced temperature fluctuations, and lowering global energy consumption due to the load reduction/shifting. Nevertheless, the success of their use depends on many factors such as the type and amount of PCMs, the encapsulation method, the location of PCMs in the building structure, the building design and orientation, the equipment design and selection, the climate conditions and so forth.

1.1.1 CLASSIFICATION OF PCMS AND TYPES OF ENCAPSULATION

Phase change materials can be divided into three broad categories: organic materials, inorganic materials and eutectic mixtures.

Organic PCMs can be divided into two groups: paraffins and non-paraffins. Both types are, in general, substances that can melt and solidify several times without segregation and without consequent degradation over time. Moreover, they solidify with a low value or in the absence of the sub-cooling phenomenon.

The paraffins are a mixture of solid hydrocarbons, mainly alkanes (in a percentage ranging from 75% to 100%), insoluble in water and in acids and are obtained from the processing of petroleum. These are compounds that at room temperature present a consistency similar to that of wax and are used in a wide temperature range ranging from 5.5°C to 80°C. In paraffins, the melting point increases with the increase in the number of carbon atoms present in them. It is therefore possible to control the melting temperature and fix it in the desired temperature range.

The non-paraffin category is the largest among the potential PCMs, thus with the most varied properties. In general, non-paraffinic PCMs can be divided into two subgroups: fatty acids and other non-paraffin organic PCMs. Unlike paraffins, which have very similar properties, each of these materials has its own specific characteristics.

The materials of inorganic origin are generally divided into hydrated salts and metallic materials. Compared to the organic ones, they generally have a higher latent heat which, however, tends to degrade over time. Because of this worsening of performance, they are less studied and appreciated than organic PCMs, with the exception of hydrated salts.

The hydrated salts can be seen as alloys of salts and water that form a typical crystalline solid (general formula $AB * nH_2O$) and the phenomena of liquefaction and solidification are in fact a dehydration and hydration of the salt itself.

The category of metals includes metals with low melting temperatures and eutectic metals.

The eutectic mixtures, subdivided into organic, inorganic and organic-inorganic eutectics, are solutions of two or more components, each of which melts and solidifies congruently and simultaneously without segregation, at a lower temperature than that of the single substances, forming a mixture of the component crystals. These materials are still under study and there is not sufficient information on thermo-physical properties, even if the disadvantage deriving from their excessive weight is relevant.

The main advantages and disadvantages of organic and inorganic PCMs are summarized in Table 1 (Tyagi V.V., 2007).

MATERIALS	ADVANTAGES	DISADVANTAGES
Paraffin	- chemically/thermally stable < 500°C; - solidify at temperature > 0°C; - congruent melting without segregation; - compatibility with the main building materials; - high latent melting heat; - limited volume variation; - good nucleation properties; - safe and non-reactive; - predictability of behavior; - recyclable; - subcooling not relevant	- low thermal conductivity in the solid state; - flammable (problem solved using a suitable container); - very expensive when mixtures of refined oil are used; - oxidative thermal aging (problem solved through the use of an appropriate antioxidant); - can react with the hydration products in the cement and present changes in odor and volume; - incompatibility with plastic containers
Organic non-paraffin	- high latent melting heat; - no supercoiling; - wide range of use (from 8°C to 130°C)	- flammability; - low thermal conductivity; - various levels of toxicity; - instability at high temperatures; - greater cost than paraffins
Hydrated salts	- high thermal conductivity; - greater density than paraffins; - high melting enthalpy; - high latent heat per unit of volume; - exact melting point; - compatibility with plastics; - easily available; - non-flammable; - low costs	- incongruent melting; - may become inactive after several cycles; - corrosivity; - can not be microencapsulated; - cycle stability is only guaranteed if certain conditions are met; - subcooling (crystallize at a temperature lower than the melting temperature); - hygroscopic; - need to use a container (it is therefore impossible to impregnate the construction material).

TABLE 1 - MAIN ADVANTAGES AND DISADVANTAGES OF ORGANIC AND INORGANIC PCMS

PCMs are unlikely to be used untied, because there would be a constant risk of moving the liquid phase to a different point from the original location. The hydrated salts, for example, are free to move in the common building materials and can exude from the surface; their water content can also change due to changes in humidity inside and outside the material. Likewise, the hydrocarbons, if dissolved in a slightly viscous liquid, risk to flow inside the materials with which they are mixed. The organic PCMs can also evaporate and spread in the ambient air, increasing the concentration of volatile organic compounds (VOCs). If you then think about the paraffins and their high flammability, it is advisable to cover them with a fireproof material.

These drawbacks can be overcome by including PCMs in sealed containers that also act as exchangers; in fact, the spread of the use of phase change materials depends on the development of effective containment methods (Verma, 2008).

The problems related to the phase change and the nature of the used substances, require the use of expensive materials with specific characteristics of mechanical resistance, flexibility, corrosion resistance, structural and thermal stability and easy management. Containment must act as a barrier between the PCM and the surrounding environment (capable of preventing material losses, ingress or leakage of water, oxygen penetration and consequent oxidation) and must provide a sufficient surface area for heat exchange, with good heat conducting characteristics.

The containment techniques can be divided into two categories: storage tanks with exchangers (Bulk Storage) and encapsulation. The encapsulation of the PCMs in physically and chemically stable polymeric nanoparticles is highly required in order to overcome some practical problems of dimensional instability, corrosiveness, low thermal conductivity, compatibility, etc. There are two main encapsulation modes, namely macro- and micro-encapsulation.

Macro-encapsulation provides that a significant amount of PCMs, which can vary from a few grams to a kilogram, be contained in discrete units, which can vary from a few millimetres (3-5 mm) up to a dozen centimetres. The shape of the macro-capsules is designed according to the use (panels, spheres, tubes, bags or other); they can be made of various materials, including plastic and some types of metals (steel or aluminium); they can be rigid or flexible; they can be used directly as heat exchangers or can be incorporated into other materials. An additive, specific to the particular application, provides a matrix in which PCMs are homogeneously distributed. Neither the additive nor the load-bearing structure modify the crystalline structure of PCMs.

Despite the wide variety of energy storage systems achievable through a careful selection of the geometry and materials of the capsules, macro-encapsulation has not led to great results due to the difficulty encountered in the heat transfer due to the phase change. During the energy extraction, in fact, the liquid solidifies on the exchange surface and creates an immobile layer of solid material with low thermal conductivity which, continuing to increase, prevents heat transfer.

Micro-encapsulation is a chemical or physical process that allows the incorporation of solid or liquid particles (dimensions from 1 to 1000μm in diameter) inside a solid shell. The individual particles of solid material define the core of the capsule, while the continuous film of high molecular weight polymeric coating material is the shell. The material contained in the core and the coating process define the type of microcapsule (Figure 1):

- Mononuclear microcapsules comprising only the shell around the nucleus;
- Polynuclear micro-capsules having multiple nuclei included in the shell;
- Matrix encapsulation in which the core material is uniformly distributed within the shell.

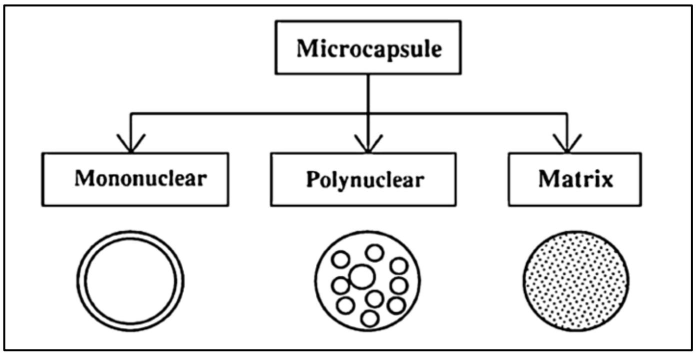

FIGURE 1 – MICROCAPSULE TYPOLOGY

The microcapsules can be made in the form of:

- aqueous dispersion: the micro-particles are single with a diameter of 2-20 μm;
- powder: the micro-particles are grouped into secondary particles of greater size (0.1-0.3mm).

Microencapsulation processes and particle size influence the temperatures at which phase transitions occur. The shell enclosing the PCMs allows heat transfer only by conduction, so it must have a high thermal conductivity to guarantee a good energy transfer rate.

The microencapsulation can be applied only to hydrophobic PCMs, so the paraffins are particularly suitable for the purpose. In addition, the coated particles can be used in any matrix compatible with the containment film, therefore it is possible to incorporate the phase change materials into common building materials, such as concrete and plaster, in a simple and economical way.

In fact, during the last decade, research has been focused on suitable methods to incorporate PCMs within buildings. In particular, organic PCMs micro-encapsulated in construction materials (gypsum, plaster, concrete) has been widely promoted as a passive solution to reduce energy consumption and to improve thermal comfort (Farid M.M., 2004) (Romero-Sanchez M. D., 2012) (Kuznik F., 2011) (Chen C., 2008) (Felix Regin A., 2008).

In this study, commercially available paraffin waxes PCMs micro-encapsulated in a stable polymeric shell were used for thermal energy storage. They were selected based on their features, such as easy availability, low prices, high thermal storage densities, good chemical stability, wide range of melting temperatures, which highly increases the number of applications in different buildings and locations according to the climatic conditions.

1.2 PCM IN CULTURAL HERITAGE

1.2.1 POSSIBLE APPLICATIONS AND BARRIERS

The idea of using PCMs in the field of cultural heritage was born from the possibility verified in the civil to reduce the thermal fluctuations within a confined environment. In fact, it is well known that environmental thermos-hygrometric variations can negatively affect the conservation of historical-artistic artefacts. By the use of PCMs, we aim, therefore, to stabilize the temperature by acting directly indirectly on the conservation environment.

The application of innovative materials and technologies in the field of cultural heritage is not, however, an easily feasible practice. We cannot think of intervening in the same way that we would operate on any civil house. In buildings classified as cultural heritage, the following aspects must mainly be respected:

- To limit the physical impact of the installation of new systems. Therefore, particular attention may be paid not to damage the structural and architectural elements of the building;
- To preserve the aesthetics of the works of art and their historical value, avoiding interventions that hinder their correct reading or looking for strategies to reduce the visual impact;
- To guarantee the correct preservation of the historical building itself, as well as of the works of art kept in it. It is essential that particular microclimatic conditions are respected, especially in terms of stability, so as to ensure conditions as constant as possible within the optimal values of conservation;
- To pay particular attention to the safety of works of art and to safeguard the well-being of the public user. These new technologies must not release pollutants that are dangerous for human health or for the conservation of works; they must be reliable even in case of malfunctioning and do not become sources of disturbance (noise, smell, etc.).

For this reason, the most common and so far effective application of PCMs in the civil field turns out to be one of the main barriers for their use in Cultural Heritage. In fact, the solution of incorporating the PCMs in construction materials is possible only for new or refurbished buildings, not always for historical ones, because this operation would require an invasive intervention on the building.

For the analysis of the viability of using PCMs as thermal energy storage materials in Cultural Heritage applications, different aspects have been analysed, including in each case the specific barriers (Romero M.D., 2012).

1.2.1.1 GENERAL BARRIERS

Efficiency and climate control

The efficiency depends on several factors: amount of PCMs, method of incorporation, sub cooling phenomena, etc. Moreover, PCMs are materials with low thermal conductivity. This characteristic can be considered as an advantage or as a limitation depending on the application. For some applications higher thermal conductivity is required (when high heat transfer rates is needed); therefore, PCMs should be addicted with fillers or incorporated in matrix in order to increase their thermal conductivity.

The performance of PCMs depends also on the optimal selection of the properties of the PCM in function of the local indoor microclimate, mainly its melting temperature and heat capacity. It needs to study preventively the environment to arrive at the best choice. In fact, a wrong choice of the PCMs characterised by a certain melting point reduce the effectiveness of the use of the product. The most important thing is to select the melting temperature in the range of the average temperature of the environment, so that there are always variations to lower and higher temperatures. In this case, the PCM will change from solid to liquid or liquid to solid and the energy will be stored or release with the phase change.

Reliability

With the optimized selection of PCMs, no problems of reliability are expected. Problems due to leakage of the PCMs or poor durability must be evaluated prior final application of the PCMs.

Operation & Maintenance

PCMs used as passive systems for thermal energy storage do not require any operation or maintenance. Therefore, only the initial economic investment is required. The reduction in the use of heating and cooling systems because of the use of PCMs will imply a direct reduction in the electricity bill.

For an optimum effectiveness of PCMs, it is important to be sure that after the heat storage of the PCM, the energy stored is completely released during the cooling process, in order to get the PCM ready for the next storage cycle. In some office buildings, this is done just by opening windows for a while at night.

Lifetime and costs

Durability of PCMs has to be evaluated previously to final application. Insufficient long-term stability of the storage materials and containers is a problem that has limited the widespread use of latent heat stores. This poor stability is due to two factors: poor stability of the material properties due to thermal cycling, and/or corrosion between the PCM and the container (e.g. hydrated salts show corrosion problems when in contact to metal substrates; in historical buildings the presence of metal pipes is very frequent so a particular care has to be taken).

PCMs have high price compared to some construction materials. Sometimes for a required phase change temperature, PCMs are not market available or there is not large-scale availability. There are numerous substances as potential PCMs but not commercially available. In addition, the costs of a given technology are greatly influenced by the particular application and the benefits obtained with the use of such technology.

Payback period is also depending on the price of the PCM, as no further maintenance works are required. Even, it has to be considered that the benefits of PCMs are directly on the electricity bill. Therefore, it is expected that the payback period will be very short.

Lack of standards, codes and certification

There is in general a lack of standard theoretical and experimental models to study the behaviour of PCMs when incorporated into the construction materials, as well as to evaluate their effectiveness and compare results of a PCM respect to another and from one laboratory to another laboratory. There is considerable uncertainty about the property values provided by manufacturers.

However, certification of the effectiveness of the PCMs would be required in terms of energy storage capacity of the PCM and quantification of the reduction in energy consumption when using PCMs. Final users, architects and other stakeholders require this information in order to recommend the use of these materials. This is particular true in special environment as museums, churches or historical buildings.

1.2.1.2 ARCHITECTURAL INTEGRATION

Aesthetics and materials properties

From the architectural point of view, the main barrier for the use of PCMs into cultural heritage is the method to incorporate the PCMs. For civil constructions, it is possible to incorporate PCMs into construction materials by different methods: in the bulk, by impregnation, coatings, etc. However, the situation is different for Cultural Heritage where the incorporation of PCMs in existing architectonical elements can change their aesthetic and other properties (porosity, permeability, etc.).

For this reason, the application of PCMs in Cultural Heritage may be similar to the application in the civil field, but restricted to museum panels or boards of different materials incorporating PMCs in contact with the roof/walls of historic buildings, only if not painted, nor decorated. Another possible use of these boards would be for example at the occasion of temporary exhibitions inside museums: these panels can be sized according to the dimensions of the room and they can be easily installed and removed according to the specific needs.

Particular properties of some construction materials such as porosity or permeability should not be modified, because they are extremely important in determining the hygrometric behaviour of the material with respect to the environmental conditions and so in the related risk of damage. For example, a variation in the pore size distribution may anticipate the condensation process inside the micro pores or interest a greater portion of the material itself. In addition, a change in the permeability of the material may affect its equilibrium moisture content with the well know consequences.

Dimensions

Depending on the material where the PCM will be incorporated, the size of the PCM could be a restriction or not. Considering the microencapsulated PCM, the only space restrictions are those related to the construction material where the PCMs will be incorporated: pore size distribution, pore diameter, etc. The smaller the particle size will be better for a higher percentage of PCM incorporation into the porosity of the construction material.

Considering macro-encapsulated PCMs, the size of the containers will depend on the available space to be placed.

__Installation__

Passive PCMs embedded in building materials for thermal energy storage in buildings and thermal fluctuations reduction do not require any specific installation, except the placement of the construction materials where they are incorporated – in case of micro-encapsulated PCMs – or of the containers – in case of macro-encapsulated PCMs.

The use of PCMs integrated with existing thermal systems can be mainly found as heat transfer fluids for solar system or water heating, but these uses are currently being developed for civil applications, and are not specific for Cultural Heritage.

1.2.1.3 SAFETY

__Fire and explosion__

This aspect is second in order of importance, after aesthetic compatibility and integrity, as it concerns the implementation of new materials or technologies to cultural heritage.

Most common PCMs are paraffins. One of the main drawbacks in the use of paraffins as PCMs is that they can be flammable. The problem of the risk of fire is particular considered in buildings where precious works of art are conserved or exhibited. Currently, for some applications where fire risk is high, PCMs are incorporated as micro- or macro-encapsulation including flame retardant compounds. Therefore, flammability of paraffin waxes can be reduced.

However, in the unlikely event of a fire, building materials may be exposed to substantially higher temperatures, that may even reach 800°C. In this case, paraffin-based PCMs are expected to evaporate, since the boiling point of most paraffins lies below 350°C. As a result, in the case the PCM encapsulation shell is broken, the produced paraffin vapours may be released to the porous structure of the materials where it is embedded and, through mass diffusion processes, emerge to the main combustion region. In this case, paraffin vapours are expected to ignite, thus adversely affecting the building’s fire resistance characteristics.

The situation with other PCMs such as hydrated salts is different, because they contain water in their formulation. In case of high temperatures in the environment, water will be released, decreasing the environment temperature and therefore, reducing the risk of fire.

Pressure

The purpose of using PCMs for Cultural Heritage applications implies the use of PCMs working at melting temperature close to the ambient and human comfort temperatures, and with solid to liquid phase change. Therefore, any problem with pressure will be found.

Environmental risk and pollutant emissions

The different PCMs can contain toxic compounds that could be dangerous for visitors and works of art. The most common PCMs are based on paraffin waxes or hydrated salts. Normally they are ecologically harmless and non-toxic. Moreover, paraffin waxes are chemically inert and stable below 500°C. The most important danger could be the emission of VOCs, but the measurements in field and laboratory demonstrated that at normal condition the emissions are under the threshold levels.

1.2.2 EVALUATION OF PCM TECHNOLOGY IMPACT IN CH

A potentially new application of the PCMs' technology to heritage objects was evaluated (Bernardi A., 2014). Model samples and real objects in contact with materials incorporating PCMs were monitored both in laboratory and on the field, and the effects of the use of PCMs on their thermal behaviour were studied. Hence, the advantages and disadvantages related to this application of PCMs' technology were evaluated with respect to conservation issues.

1.2.2.1 LABORATORY TESTS

The PCMs selected for testing were paraffin based provided by the company BASF:

- Micronal® DS 5001 X, in powder form with melting temperature of approximately 26°C, density of 250-350 kg/m^3 and latent heat capacity of ca. 110 kJ/kg.
- Micronal® DS 5029 X, in powder form with melting temperature of approximately 21°C, density of 250-350 kg/m^3 and latent heat capacity of ca. 90 kJ/kg.
- Micronal® DS 5000 X, a water-based solution with melting temperature of approximately 26°C, density of 0.9 g/cm^3, viscosity of 100-300 mPa•s and solid content of 45%.

The above mentioned PCMs were included in 2 different materials: silicon and gypsum. For the latter, PCMs were embedded in gypsum plasterboards; they were dispersed and mixed together with the gypsum powder in order to get a homogeneous distribution of PCMs into the bulk of the panel.

Thermal behaviour of PCMs in controlled conditions

The PCMs used for testing were included in 1 set of samples with silicon and 2 sets of samples with gypsum, composed as follows:

- set of silicon: control silicon, silicon with Micronal® DS 5029 X (called silicon + PCM 21) and silicon with Micronal® DS 5001 X (called silicon + PCM 26). Dimensions: 20 x 20 x 0.5 cm with 10% wt PCMs incorporated.
- 1st set of gypsum: gypsum control, gypsum with Micronal® DS 5001 X (called gypsum + PCM 26) and gypsum with Micronal® DS 5000 X (called gypsum + PCM 26 emulsion). Dimensions: 20 x 20 x 2 cm with 10% wt PCMs incorporated;
- 2nd set of gypsum: gypsum control, gypsum with Micronal® DS 5001 X (called gypsum + PCM 26) and gypsum with Micronal® DS 5029 X (called gypsum + PCM 21). Dimensions 40 x 40 x 1.4 cm with 20% wt PCMs incorporated.

The surface temperature of the silicon and gypsum samples was monitored on both sides (upper and bottom) under thermal cycles in controlled conditions (silicon set, gypsum set 1) and in climatic chamber (gypsum set 2) by means of platinum thermo-resistances previously calibrated (accuracy 0.1°C) with the aim to evaluate the efficiency of these materials in reducing thermal fluctuations.

The experimental device used for testing silicon and gypsum set 1 samples is shown in Figure 2. The heating/cooling cycles were generated by an air conditioning system, which threw air into a box, on whose upper surface the panels were placed.

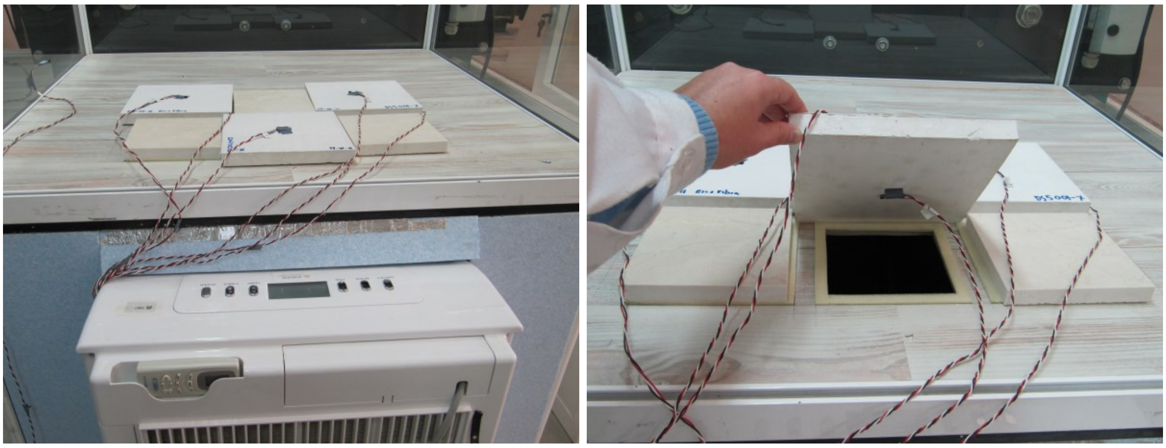

FIGURE 2 - EXPERIMENTAL DEVICE TO EVALUATE THERMAL BEHAVIOUR OF SILICON AND GYPSUM SET 1 SAMPLES UNDER THERMAL CYCLES (IMAGE COURTESY OF AIDICO)

Figure 3 shows the temperatures of air and of the different silicon samples on the upper side. The maximum temperature of the control silicon is higher (1°C) than the sample containing PCM 21, while it is similar to the one of the sample containing PCM 26. The thermal behavior of the silicon with PCM 26 is generally intermediate between the control and the silicon with PCM 21.

The heating process is slower for the samples with PCMs, mainly for the silicon with PCM 21. For example, in order to get temperatures higher than 28°C, the silicon with PCM 21 requires 30 min more than the control silicon, indicating the thermal energy storage by the PCM. The silicon with PCM 26 takes 10 min more than the control sample. Therefore, the PCM 21 seems to be more effective as thermal energy storage material than PCM 26 when incorporated to silicon.

The cooling process is also slower for the silicon with PCM 21 (it requires longer time to get lower temperatures than the control sample, i.e. 20 min more to get to 18°C) and it reaches a minimum temperature lower of 1°C than the control sample. The cooling process for the silicon with PCM 26 is slightly slower than the control sample, but finally the same temperature values are obtained.

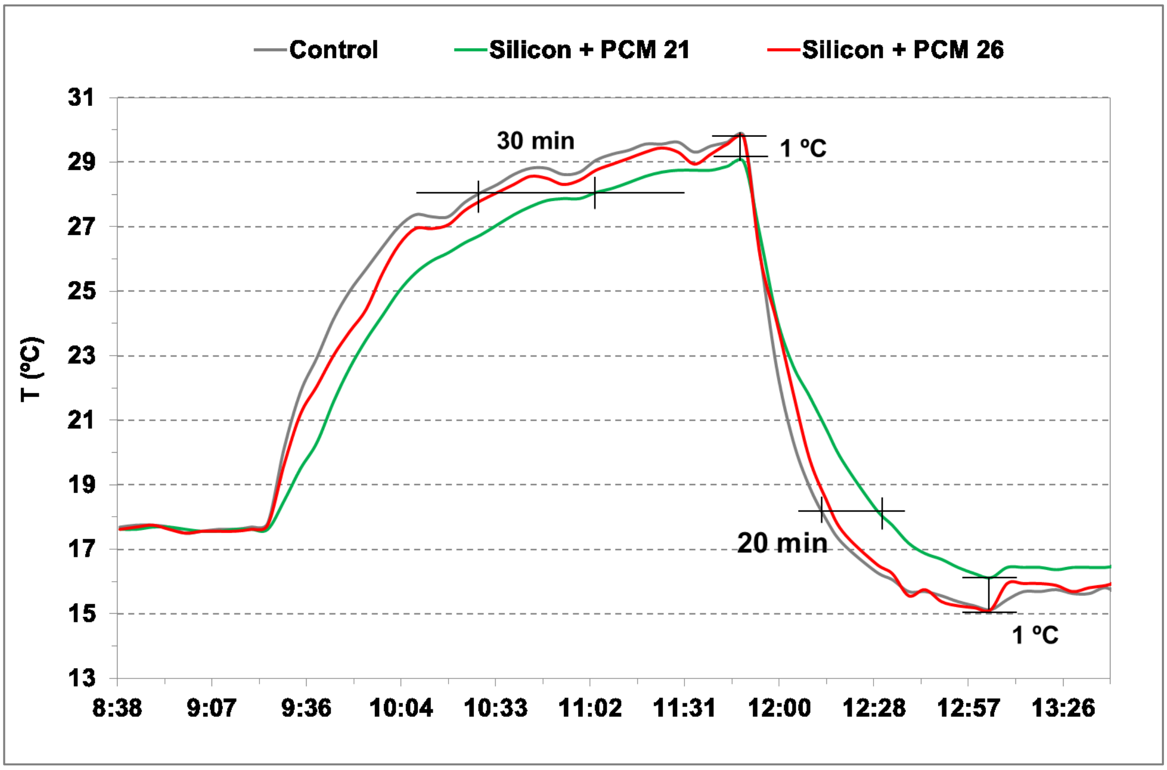

FIGURE 3 - AIR TEMPERATURE AND UPPER SURFACE TEMPERATURES OF THE DIFFERENT SILICON SAMPLES (IMAGE COURTESY OF AIDICO)

Similar results were obtained with other thermal cycles, concluding that the thermal behavior of the silicon samples is reproducible and confirming the higher effectiveness of the PCM 21 as thermal energy storage material respect to PCM 26 when included into the silicon formulation.

Contrary to what was expected, the maximum temperature at the bottom surface of the silicon with PCM 26 is slightly higher than the control sample. Minimum temperatures obtained for the silicon with PCM 26 are lower than the control sample and the silicon with PCM 21. Therefore, the obtained results pointed out also an important drawback related to the use of silicon samples incorporating PCMs. In fact, the temperature difference between the bottom and upper surfaces of each piece slightly increases with the presence of PCMs. The measured thermal gradients were:

- control silicon = 4.2°C
- silicon + PCM 21 = 4.9°C
- silicon + PCM 26 = 5.2°C.

The results of the laboratory tests performed on the gypsum samples were similar to the previous ones for both the bottom and upper surfaces: reduction of the maximum temperature and a time delay to reach the highest temperature (Figure 4).

Moreover, the gypsum samples containing PCMs showed a slower cooling process compared to the gypsum control samples, and higher minimum temperatures, mainly for the PCM 26 emulsion. Therefore, the heat storage/release capacity of the PCMs when incorporated to gypsum was confirmed.

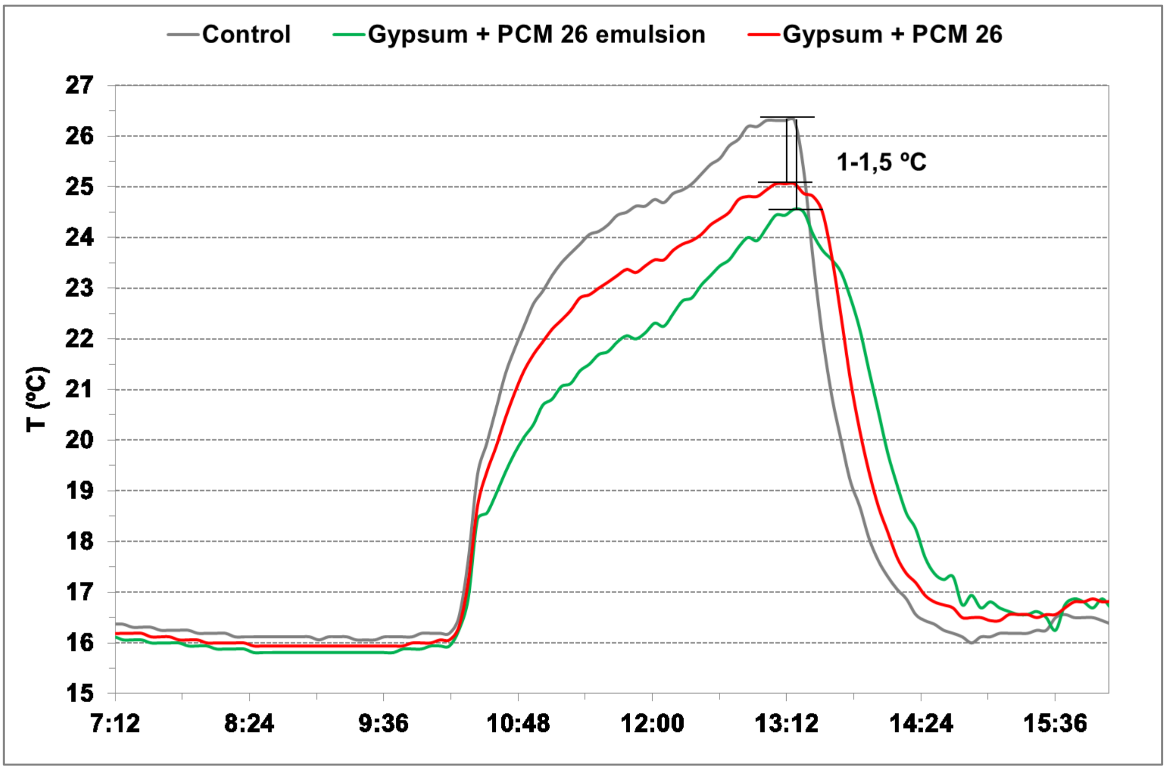

FIGURE 4 - AIR TEMPERATURE AND UPPER SURFACE TEMPERATURES
OF THE DIFFERENT GYPSUM SAMPLES

The analysis of the thermal gradient between the bottom and upper gypsum surfaces gave similar results as those obtained for the silicon samples and confirmed the drawback. The measured thermal gradients were:

- control gypsum = 5.7°C
- gypsum + PCM 26 emulsion = 6.5°C
- gypsum + PCM 26 = 6.2°C

Similar results were obtained during other thermal cycles, concluding that the thermal behavior of the gypsum samples is reproducible.

The gypsum panel set 2 was tested in climatic chamber, where it was possible to study the behavior of the samples under heating and cooling cycles characterized by different amplitudes and frequencies. The cycles were carried out during several days and the results were reproducible.

As already pointed out in the previous tests, the effect of PCM 21 was more evident than PCM 26 in both heating and cooling processes (Figure 5). In fact, the use of PCM leads to a reduction of the area under the curve respectively less than 0.2% for PCM 26 and of about 1.4% for PCM 21 in both processes. These values are directly related to the quantity of thermal energy stored by the two different kind of PCMs.

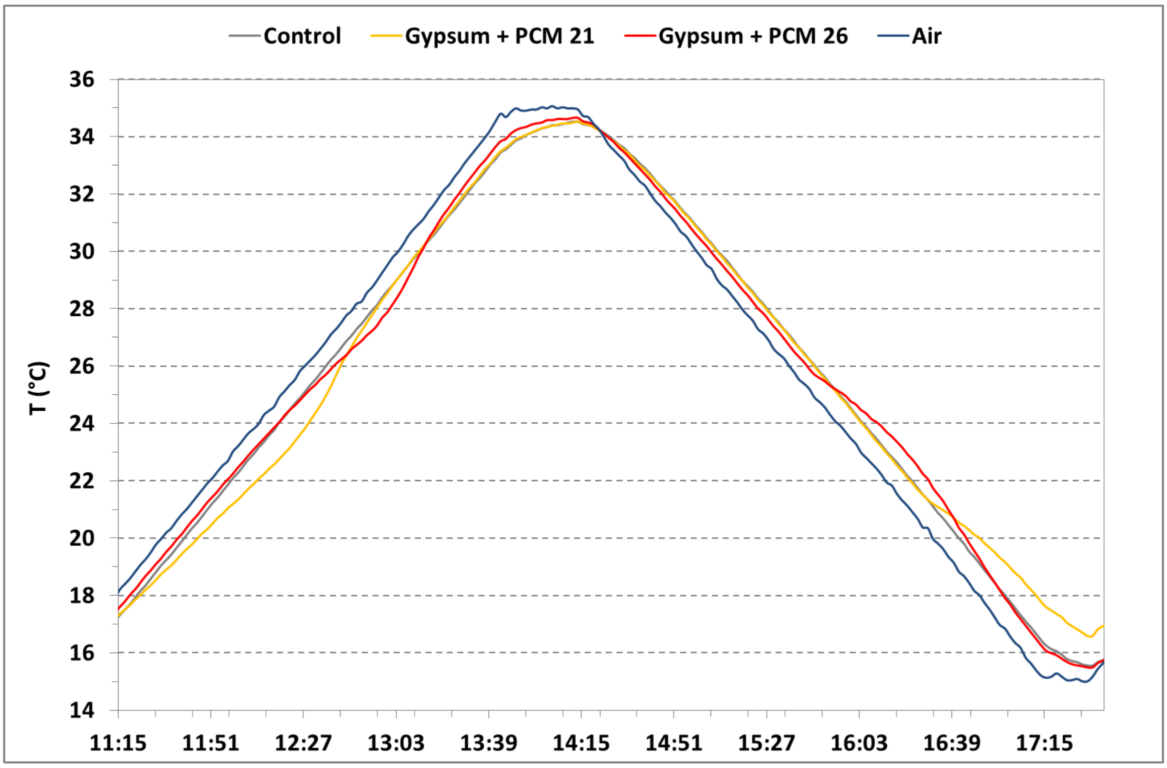

FIGURE 5 - THERMAL BEHAVIOUR OF GYPSUM SAMPLES CONTAINING PCM 21 AND 26 DURING A HEATING/COOLING CYCLE

Thermal behaviour of objects in contact with materials incorporating PCMs

In order to study a possible application of PCMs for the thermal stabilization of cultural heritage objects, several tests were performed in climatic chamber placing a wooden panel, simulating a painting, in contact with the gypsum panel containing 20% wt Micronal® DS 5001 X. A sandwich was composed as illustrated in Figure 6. Dimensions of the panels were 40 x 40 x 1.4 cm. The following temperatures were measured during different thermal cycles with platinum thermo-resistances previously calibrated (accuracy 0.1°C): air, wooden external surface (called wood ext), interface wood/gypsum (called wood int). The sandwich was placed within a polystyrene box inside the climatic chamber in order to reduce the disturbance of the ventilation of the device (Figure 6). Several preliminary cycles were run to define the best experimental set up and the proper parameters for the thermal cycles.

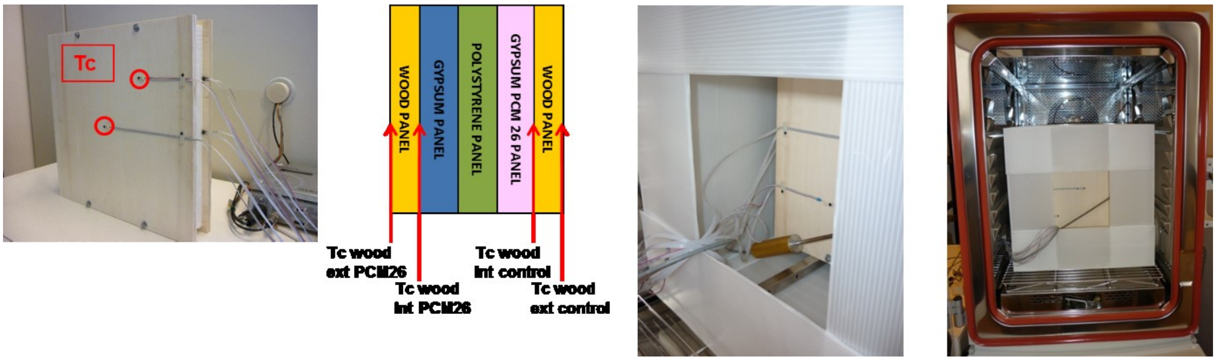

FIGURE 6 - EXPERIMENTAL SET UP TO STUDY THE THERMAL EFFECT OF PCM26 ON WOODEN PANELS DURING THERMAL CYCLES IN CLIMATIC CHAMBER

The results demonstrated the different thermal behaviour of the external and internal wooden surfaces, and of the same kind of surface (internal/external) in contact with the control gypsum panel or the gypsum panel with PCM 26 (Figure 7).

The maximum temperature reached by the internal and external wooden surfaces in contact with the gypsum panel with PCM 26 was 1.7°C lower than the temperature of the corresponding wood surface in contact with the control panel, due to the thermal storage capacity of PCMs. Moreover, the wooden panel in contact with the gypsum panel with PCM 26 took more time to reach the highest temperature with respect to the wooden panel in contact with the control panel: respectively, 40 and 70 minutes delay for the external and internal surfaces. Obviously, the thermal difference and the time delay strongly depends on the cycle set up. Similar conclusions can be drawn for the cooling process, which was slighter for the wood panel in contact with the gypsum panel with PCM 26.

The maximum difference between the external and internal wooden surfaces during the cycle was determined: 3.6°C for the wooden panel in contact with the gypsum panel with PCM 26, and 2.3°C for the wooden panel in contact with the control panel. This result confirmed the drawback already observed in laboratory, i.e. the increase of the thermal gradient between the heritage material surfaces when PCMs are used in contact with it, thus increasing the risk of mechanical damage (measured increase of 1.3°C).

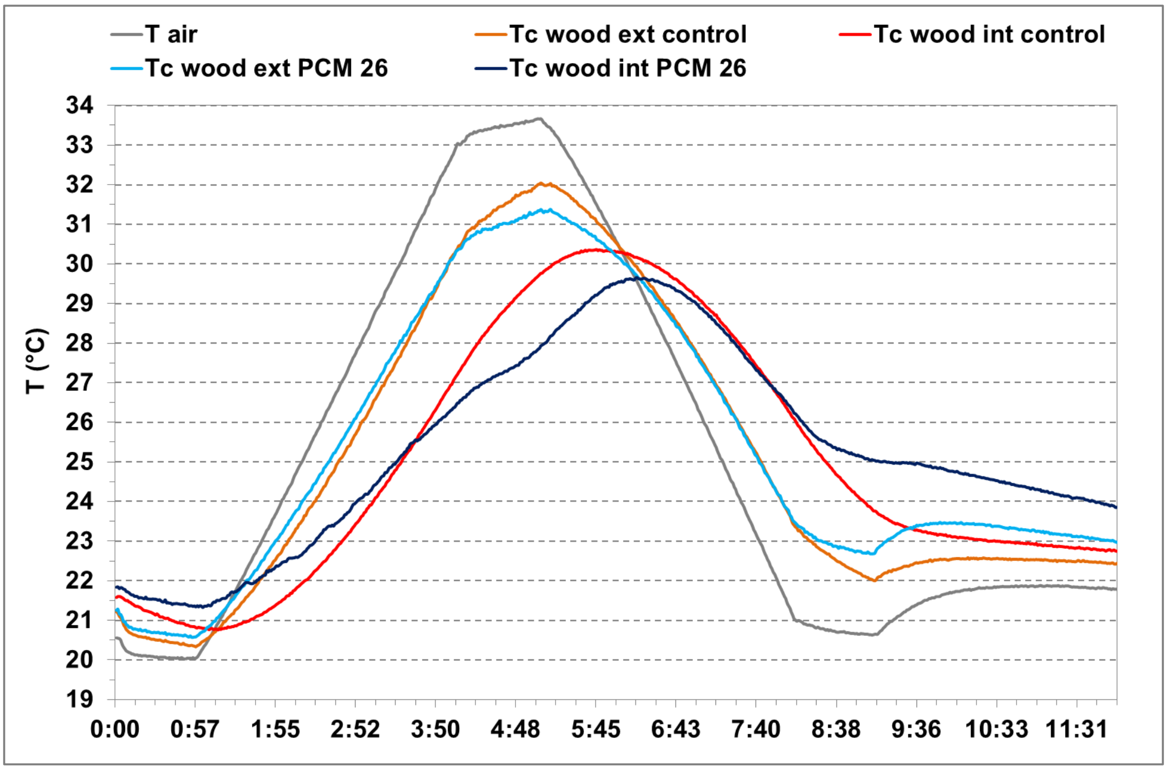

FIGURE 7 - TEMPERATURE TRENDS OF AIR AND OF THE DIFFERENT WOODEN SURFACES DURING THE FOLLOWING THERMAL CYCLE: 1HR AT 20°C, 3HRS FROM 20°C TO 35°C, 1HR AT 35°C, 3HRS FROM 35°C TO 20°C, 1HR AT 20°C

Similar thermal cycles, characterized by a small increase in the duration of the steps at steady temperature or by a slight increase/decrease of the maximum/minimum temperatures, indicated the same results (Figure 8). The duration of the steps at steady temperature was increased in order to achieve the following conditions:

- thermal equilibrium between all the materials at the beginning and at the end of the cycle;
- activation of as much PCM 26 as possible;
- to make the internal wooden surface reach maximum/minimum values as close as possible to the maximum/minimum air temperature.

It is worthwhile to compare in Figure 8 the temperatures at which the effect of the PCMs was notable at the external/internal wood surfaces with the declared melting point of 26°C.

During the cycle shown in Figure 8 the maximum thermal gradient between the external and internal wood surfaces in contact with gypsum panel was even higher than in the previous test, close to 2°C. At the same time, the surfaces in contact with the control panel and with the panels containing PCMs reached the same highest and lowest temperature because in this the cycle they were able to discharge completely the PCMs.

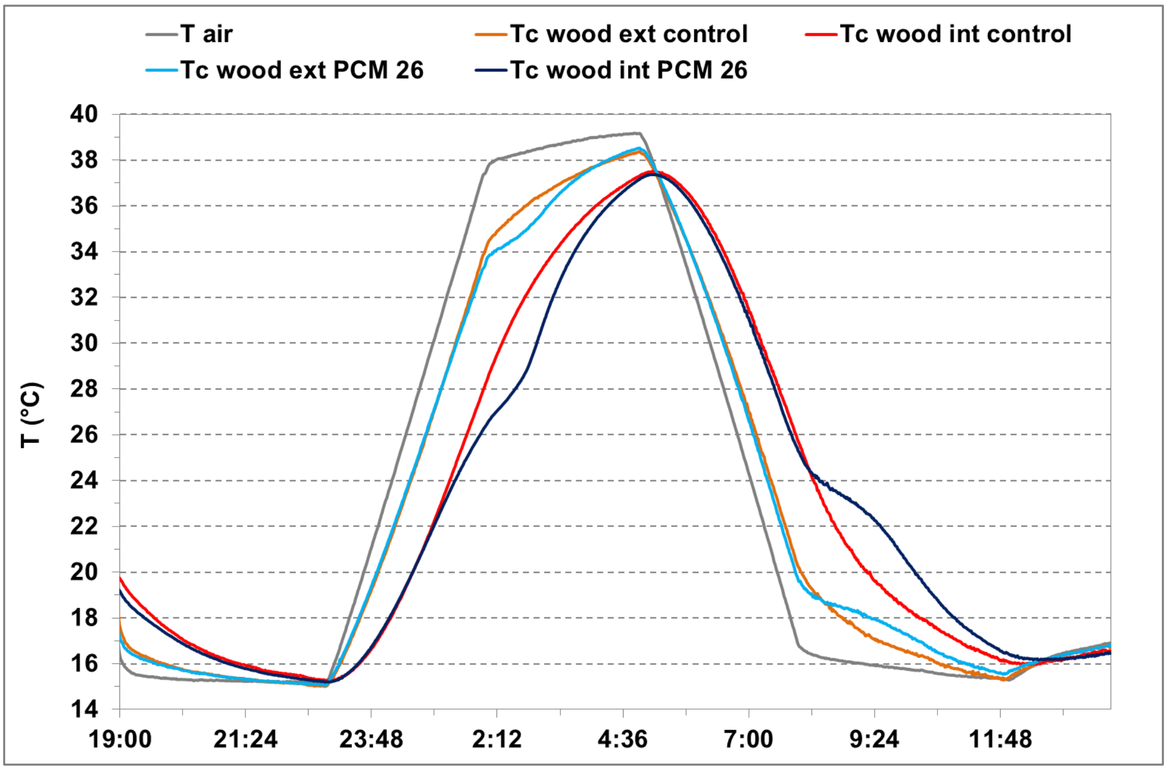

FIGURE 8 - TEMPERATURE TRENDS OF AIR AND OF THE DIFFERENT WOODEN SURFACES DURING THE FOLLOWING THERMAL CYCLE: 4HRS AT 15°C, 3HRS FROM 15°C TO 40°C, 3HRS AT 40°C, 3HRS FROM 40°C TO 15°C, 4HRS AT 15°C

Study of the influence of the distance between model samples and materials containing PCM

In order to analyse more in depth the limitation on the use of PCMs, pointed out in the previous paragraph, a new experiment was designed.

The gypsum samples 20 x 20 x 2 cm, containing 10% weight Micronal®DS 5029 X, were placed on a wall and canvas pieces simulating paintings were hung at different distances (d = 0, 1, 2 and 4 cm) from the gypsum panels. The effect of PCMs and the influence of the distance between the gypsum panels containing PCMs and the canvas were analysed. Temperature sensors were placed on the wall surface and on the back and front sides of the canvas. Samples have been exposed in an office room (approximately 35 m^2 with 4 people working inside) for several weeks.

The temperature of 22.5◦C was selected as reference (being the melting temperature of PCMs 21°C). The time required by the canvas (front side) to reach 22.5°C was higher for the canvas close to the gypsum panel containing PCMs compared to the canvas close to the control panel (30, 10, 5 and 5 min more, respectively, for distances of 0, 1, 2 and 4 cm). Hence, the shorter the distance between the panels containing PCMs and the painting, the higher the protection of the paintings from the exposure to high temperatures.

Results indicated also that the canvas close to the gypsum panel containing PCMs were subjected to temperatures higher than 22.5°C for shorter times than the canvas close to the gypsum control panel. As expected, this tendency depended on the distance between the canvas and the gypsum: the lower the distance, the shorter the time the canvas closest to the gypsum panel containing PCMs was subject to temperatures higher than 22.5°C. For 4 cm distance, there is no difference between the canvas respectively close to the control panel and the gypsum panel containing PCMs.

The thermal gradient between front and back sides of the canvas was also analysed at the different distances. The thermal gradient between both sides of the canvas was slightly increasing when it was placed at 0 cm distance from the gypsum panel containing PCMs compared to the thermal gradient of the canvas placed at the same distance from the control gypsum panel. However, when the distance was increased to 1 cm, the thermal gradient of the canvas close to the gypsum panel containing PCMs was the same to that of the canvas close to the control gypsum panel. Then, under those experimental conditions, the thermal gradient between the front and backsides of a painting placed on a wall containing PCMs can be neglected only by placing the painting at least at 1 cm distance from the wall.

1.2.2.2 FIELD TESTS

The thermal behaviour of PCMs was also evaluated directly in the field in one experimental site, the Santa Croce Museum in Florence (Italy).

The microclimate of the museum was previously studied within a national project aimed at monitoring and improving the conditions in relation to the conservation of the works of art and the human comfort (Bernardi A., 2010) (Bernardi A., 2011). Based on the results of this study, briefly described in the following, it was possible to select the most suitable rooms for testing PCM 21 and 26.

The measured values of temperature and relative humidity were acceptable on average, but they were not properly suitable for the preservation of the works of art, because of their sharp and sudden changes, and their minimum or maximum values sometimes too high or too low, at the limits of the tolerance range for the conservation of the materials. In fact, important thermo-hygrometric excursions were measured, such as daily maximum $\Delta T=7°C$ and $\Delta RH=50\%$ in winter. These are mainly due to the management of the museum: the opening of the doors; the heating by fan coils; the artificial lighting (halogen lamps pointed directly at the paintings); the natural light from the windows not properly shielded; the heating of the beams of the ceiling. Hence, the use of PCMs could be particularly effective in such variable environmental conditions.

The main effects on the works of art preserved in the museum are thermo-hygrometric stress and gradients between high/low level and front/back surfaces especially for the paintings on wooden panels, which may result in dimensional variations. The painted layers are also extremely sensitive to thermo-hygrometric variations, as they have different thermo-hygrometric behavior respect to the material underneath.

In order to select the most suitable rooms for the PCMs testing, among the 6 rooms of the museum, the annual number of air thermal cycles around 21°C and 26°C in each room was calculated. The results obtained (Table 2) showed that room I was the more suitable for the testing of PCM 21, while for room VI PCM 26 was preferred because of the importance of the works of art preserved (oils on wooden boards, a fresco and the famous Crucifix by Cimabue).

	Annual number of cycles around	
Room	**21°C**	**26°C**
I	681	397
II	332	177
III	133	450
IV	64	255
V	218	461
VI	45	285

TABLE 2 - ANNUAL NUMBER OF AIR THERMAL CYCLES AROUND 21°C AND 26°C IN EACH ROOM OF THE MUSEUM

Hence, the PCMs selected for testing were Micronal® DS 5001 X and DS 5029 X. 20% weight of PCMs was incorporated in gypsum panels of 40 x 40 x 1.4 cm. A wooden panel with a size of 40 x 40 x 0.3 cm was placed in contact with each gypsum panel, simulating a painting. The panels (with and without PCMs) were placed at 1 m above the floor, close to each other, in a corner of room I and close to a wall of room VI (Figure 9). Air temperature and relative humidity in proximity of each panel, and the surface temperature of the wood and of the gypsum panels were measured.

FIGURE 9 - PCMS TESTING IN ROOM I AND VI OF THE SANTA CROCE MUSEUM AND MICROCLIMATIC SENSORS INSTALLED ON EACH PANEL

As expected, according to the basic microclimatic conditions of the museum, the effect of PCM 21 was visible in winter, especially in room I (Figure 10), while the effect of PCM26 was visible in summer, in particular in room VI.

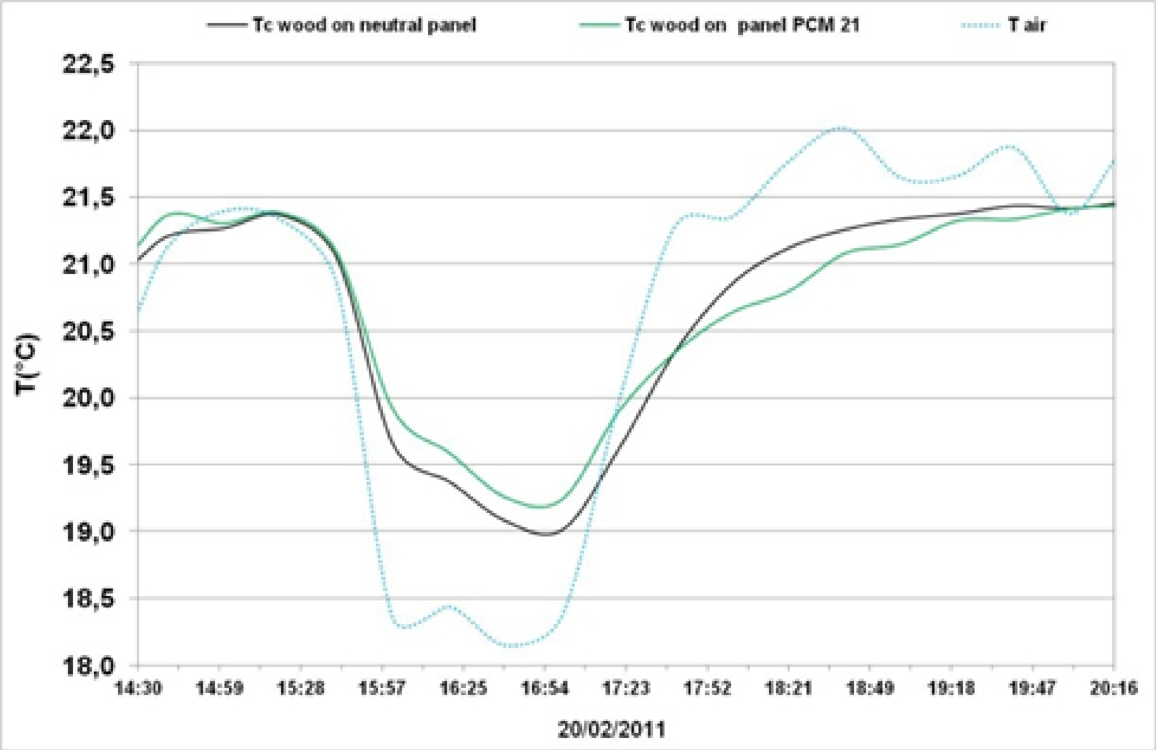

FIGURE 10 - TEMPERATURE OF AIR AND OF THE DIFFERENT GYPSUM AND WOODEN SURFACES IN ROOM I IN WINTER

The monitoring on site confirmed the results of the laboratory tests, even if in real environmental conditions the effect of PCMs was less evident than in controlled conditions. Data showed again the reduction of maximum temperatures of the gypsum panels incorporating PCMs and of the wood panels in contact with them, with respect to the control configurations and a delay in the time to get the maximum and minimum temperatures. Nevertheless, the effect was more notable in room I, because of the very big volume of room VI in relation to the dimension of the tested panels.

The risk of increasing the thermal gradients between the external and internal wooden surfaces – and consequently the risk of stress - was confirmed also in the field. This phenomenon was particularly evident in room VI were the maximum difference was respectively 0.6°C for the control configuration and around 1°C for both the PCM 21 and PCM 26 configurations.

2 NEW THERMAL INSULATING MATERIALS

2.1 PERFORMANCE INDICATORS FOR THERMAL COMFORT

The preliminary objective was the definition of indicators useful for the impact assessment of the implementation of new energetic retrofitting interventions in historic buildings (Bernardi A., 2013).

The starting point of the state-of-art was the definition of indicator. As stated in the UNI norm 11097:2003, "Indicators are qualitative and / or quantitative information associated to a phenomenon (or a process or a result) under observation, which allows you to investigate the changes during time, as well as to verify the accomplishment of a goal, in order to allow for proper decision-making" (UNI, 2003). Indicators can be quantitative or qualitative and can be compared to specific standards, thresholds, guided values or principles, in order to assess the performance of products, building components, buildings in relation to an objective (performance indicator) (Steskens P., 2010).

Thermal comfort is defined in the European Standard EN ISO 7730 and ASHRAE Standard 55-20044 as 'that condition of mind which expresses satisfaction with the thermal environment and is assessed by subjective evaluation' (ISO, 2005) (ASHRAE, 2004).

The thermal comfort assessment includes a part of objectively and measurable performance indicators and the other part of human's thermal sensation, mainly related to the thermal balance of the body as a whole, which is influenced by physical activity and clothing, as well as the environmental parameters.

Based on ASHRAE definition the zone of thermal comfort is the span of conditions where 80% of sedentary or slightly active persons find the environment thermally acceptable. In terms of climatic conditions, the acceptable ambient temperature of comfort would be slightly higher in the summer than in the winter, being 23–26°C and 20–24°C, respectively.

Thermal sensation and thermal comfort are bipolar phenomena ranging from "cold" to "hot" with comfort or neutral sensation in the middle. Several scales have described this continuum of sensations: the subjective ratings of discomfort and the corresponding physiological correlates are summarized in Table 3 (Epstein Y., 2006).

VOTE (A)	THERMAL SENSATION	COMFORT SENSATION
+3	Hot	Uncomfortable
+2	Warm	Slightly uncomfortable
+1	Slightly warm	
0	Neutral	Comfortable
-1	Slightly cool	
-2	Cool	Slightly uncomfortable
-3	Cold	Uncomfortable

(a) Thermal scale according to ASHRAE 55.

TABLE 3 - COMFORT VOTE AND THERMAL SENSATION, IN ASSOCIATION TO THE PHYSIOLOGICAL ZONE OF THERMAL EFFECT AND THE ASSOCIATED PERCENT SKIN WETNESS

Note that the original ASHRAE scale used numbers from 1 to 7, where 1 meant cold and 7 meant hot, but now the symmetrical scale with votes between -3 and +3 is used in most studies.

2.1.1 QUANTIFICATION OF THERMAL COMFORT

2.1.1.1 PREDICTED MEAN VOTE (PMV)

The predicted mean vote (PMV) integrates four environmental parameters with the effects of two personal parameters. In fact, it is determined by the measurement or prediction of the air temperature, mean radiant temperature, relative air velocity and air humidity, besides to the estimation of the metabolic rate and the clothing insulation. The PMV index is derived for steady-state conditions, but it can be applied also during minor fluctuations of one or more variables, using the time-weighted averages of the previous 1 hour period.

PMV is expressed as the general function (Steskens P., 2010):

$$PMV = f\,(M, W, p_a, t_a, f_{cl}, t_{cl}, t_r, h_c)$$

with

$f_{cl} = f\,(I_{cl})$

$t_{cl} = f\,(I_{cl}, f_{cl}, t_r, t_a)$

$h_c = f\,(t_{cl}, t_a, v_a)$

where

M is the metabolic rate [W/m^2],
W is the external work (zero for most indoor activities) [W/m^2],
p_a is the partial water vapour pressure [Pa],
t_a is the air temperature [°C],
f_{cl} is the ratio of the clothed surface area to the nude surface area [-],
I_{cl} is the thermal resistance of the clothing [(m^{2}K)/ W],
t_{cl} is the surface temperature of the clothing [°C],

t_r is the mean radiant temperature [°C],
h_c is the convective heat transfer coefficient [W/(m^{2}K)],
v_a is the air velocity relative to the human body [m/s].

In detail, PMV is calculated based on the equation developed by Fanger (Fanger P.O., 1982), as follows (ISO, 2005):

$$\mathrm{PMV} = [\,0.303 \cdot \exp(-0.036 \cdot M) + 0.028\,] \cdot$$

$$\left[\begin{array}{l} (M - W) - 3.05 \cdot 10^{-3} \cdot [\,5733 - 6.99 \cdot (M - W) - p_a\,] - 0.42 \cdot [\,(M - W) - 58.15\,] \\ -1.7 \cdot 10^{-5} \cdot M \cdot (5867 - p_a) - 0.0014 \cdot M \cdot (34 - t_a) \\ -3.96 \cdot 10^{-8} \cdot f_{cl} \cdot [\,(t_{cl} + 273)^4 - (\bar{t}_r + 273)^4\,] - f_{cl} \cdot h_c \cdot (t_{cl} - t_a) \end{array} \right]$$

with

$$t_{cl} = 35.7 - 0.028 \cdot (M - W) - I_{cl} \cdot \{3.96 \cdot 10^{-8} \cdot f_{cl} \cdot [\,(t_{cl} + 273)^4 - (\bar{t}_r + 273)^4\,] + f_{cl} \cdot h_c \cdot (t_{cl} - t_a)\}$$

$$h_c = \begin{cases} 2.38 \cdot |t_{cl} - t_a|^{0.25} & \text{for } 2.38 \cdot |t_{cl} - t_a|^{0.25} > 12.1 \cdot \sqrt{V_{ar}} \\ 12.1 \cdot \sqrt{V_{ar}} & \text{for } 2.38 \cdot |t_{cl} - t_a|^{0.25} < 12.1 \cdot \sqrt{V_{ar}} \end{cases}$$

$$f_{cl} = \begin{cases} 1.00 + 1.290\, I_{cl} & \text{for } I_{cl} \lesssim 0.078\ \mathrm{m^2 \cdot K/W} \\ 1.05 + 0.645\, I_{cl} & \text{for } I_{cl} > 0.078\ \mathrm{m^2 \cdot K/W} \end{cases}$$

where

M is the metabolic rate, in watts per square metre [W/m^2];
W is the effective mechanical power, in watts per square metre [W/m^2];
I_{cl} is the clothing insulation, in square metres kelvin per watt [m^2· K/W];
f_{cl} is the clothing surface area factor;
t_a is the air temperature, in degrees Celsius [°C];
t_r is the mean radiant temperature, in degrees Celsius [°C];
v_{ar} is the relative air velocity, in metres per second [m/s];
p_a is the water vapour partial pressure, in pascal [Pa];
h_c is the convective heat transfer coefficient, in watts per square metre kelvin [W/(m^2· K)];
t_{cl} is the clothing surface temperature, in Celsius degrees [°C].

The thermal parameters of the environment should be measured in the occupied zones of the building and at the centre of gravity, which is 0.6 m for sedentary occupants and 1.1 m for standing activity from the floor. Standard and guidelines like (ISO, 2005) and (ASHRAE, 2004) provide detailed descriptions of the requirements for the measuring instrumentation and for thermal comfort measurement procedures.

The metabolic rate (M) is the rate of energy production of the body by metabolism, which varies depending on the activity, the person and the conditions under which the activity is performed. The met unit can quantify it, where 1 met is defined as the metabolic rate of a sedentary person and it is equivalent to 58.2 W/m^2. The unit W/m^2 refers to the area of the nude body. A detailed description of the evaluation and measurement of metabolic rate as well as a comprehensive collection of metabolic rates for typical activities can be found in ISO8996 (ISO, 2004). Here the method has an accuracy of around 20% and involves observation of the activity and the use of tabulated values of metabolic rates (oxygen consumption) for specific activities.

Clothing insulation varies between occupants in a space, due to differences in clothing preferences, season, etc. The clothing insulation is measured in unit [clo]: 1 clo = 0.155 $m^2 \cdot °C/W$. It can be measured with a heated thermal manikin or with human subjects; otherwise information on the insulation provided by a wide variety of individual garments or clothing ensembles can be found in ISO 9920 (ISO, 2007).

The mean thermal sensation predicted by PMV is based on the seven-point scale of ASHRAE. It is recommended to use the index only for PMV values in the range -2 to +2, and the other parameters as follows (ISO, 2005).:

- metabolic rates from 0.8 met to 4 met;
- clothing insulation from 0 clo to 2 clo;
- air temperatures from 10 to 30 °C;
- mean radiant temperatures from 10 to 40 °C;
- relative air velocities from 0 to 1 m/s

The influence of humidity on thermal sensation is small at moderate temperature close to comfort and may usually be disregarded when determining PMV values. Anyway, it is recommended to limit the relative humidity to 30-70% (CEN, 1995).

2.1.1.2 PREDICTED PERCENTAGE DISSATISFIED (PPD)

The predicted percentage dissatisfied (PPD) index is derived from the PMV index and predicts the percentage of thermally dissatisfied persons among a large group of people, due to individual thermal sensation.

When the PMV value is known, the PPD index can be calculated (ISO, 2005):

$$\mathrm{PPD} = 100 - 95 \cdot \exp\left(-0.03353 \cdot \mathrm{PMV}^4 - 0.2179 \cdot \mathrm{PMV}^2\right)$$

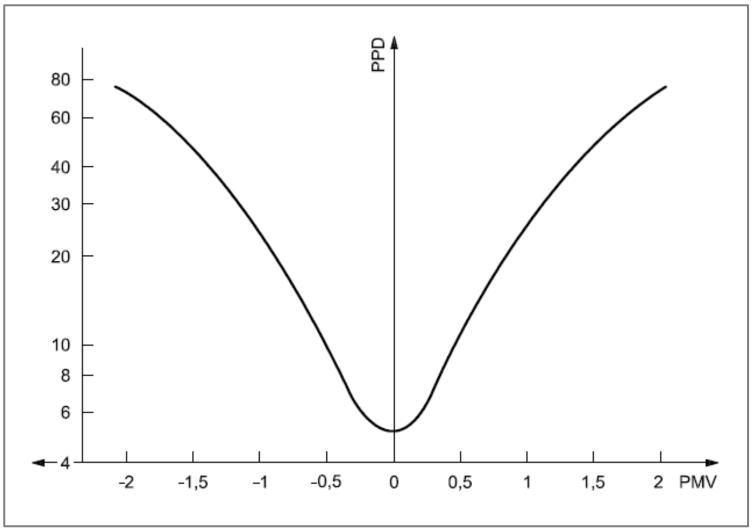

FIGURE 11 - PPD AS FUNCTION OF PMV

Typically, a 10% dissatisfaction criterion for whole-body thermal comfort is used for the determination of acceptable thermal conditions (ISO, 2005) (ASHRAE, 2004) and it corresponds to PMV in the range -0.5 to +0.5 (Figure 11). Note that the minimum attainable PPD is 5%, even when the result is a neutral thermal sensation (PMV = 0), because it is not possible to satisfy everyone.

2.1.1.3 LOCAL THERMAL DISCOMFORT

Thermal neutrality for the body as a whole is a necessary, but not sufficient, condition for thermal comfort. Local thermal discomfort due to draft, vertical temperature gradient, radiant asymmetry, warm/cool floors may cause occupants to find the thermal conditions unacceptable.

Regarding the discomfort due to draught, the percentage of people predicted to be bothered by draught is calculated by the draught rate (DR) equation (ISO, 2005), while the other types of local thermal discomfort are determined by calculation of the percentage dissatisfied (PD).

$$\mathrm{DR} = (34 - t_{a,l})\,(\bar{v}_{a,l} - 0.05)^{0,62}\,(0.37 \cdot \bar{v}_{a,l} \cdot \mathrm{Tu} + 3.14)$$

for $\bar{v}_{a,l} < 0.05$ m/s use $\bar{v}_{a,l} = 0.05$ m/s;

for DR > 100 % use DR = 100%

where

$t_{a,l}$ is the local air temperature [°C],

$\bar{v}_{a,l}$ is the local mean air velocity [m/s],
Tu is the local turbulence intensity [%]; if unknown 40% may be used.

The model applies to people at light, mainly sedentary activity with a thermal sensation for the whole body close to neutral and for prediction of draught at the neck. The model could overestimate the DR at the level of arms and feet, if activity is not sedentary or if people feel warmer than neutral.

For the other types of local thermal discomfort the following equations are used (ISO, 2005):

1) For vertical air temperature difference between head and ankles

$$\mathrm{PD} = \frac{100}{1 + \exp(5.76 - 0.856 \cdot \Delta t_{a,v})} \qquad \text{with } \Delta t_{a,v} < 8°\mathrm{C}$$

2) For warm or cool floors

$$\mathrm{PD} = 100 - 94 \cdot \exp\,(-1.387 + 0.118 \cdot t_f - 0.0025 \cdot t_f^2)$$

3) For radiant temperature asymmetry

in case of warm ceiling

$$\mathrm{PD} = \frac{100}{1 + \exp(2.84 - 0.174 \cdot \Delta t_{p,r})} - 5.5 \qquad \text{with } \Delta t_{p,r} < 23°\mathrm{C}$$

in case of cool wall

$$\mathrm{PD} = \frac{100}{1 + \exp(6.61 - 0.345 \cdot \Delta t_{p,r})} \qquad \text{with } \Delta t_{p,r} < 15°\mathrm{C}$$

in case of cool ceiling

$$\mathrm{PD} = \frac{100}{1 + \exp(9.93 - 0.50 \cdot \Delta t_{p,r})} \qquad \text{with } \Delta t_{p,r} < 15°\mathrm{C}$$

in case of warm wall

$$\mathrm{PD} = \frac{100}{1 + \exp(3.72 - 0.052 \cdot \Delta t_{p,r})} - 3.5 \qquad \text{with } \Delta t_{p,r} < 35°\mathrm{C}$$

2.1.1.4 CATEGORY OF THERMAL ENVIRONMENT

The desired thermal environment for a space may be selected from among three different categories defined by (ISO, 2005). Each category prescribes a maximum percentage dissatisfied for the body as a whole (PPD) and a PD for each of the four types of local discomfort (draft, vertical temperature gradient, radiant asymmetry, warm or cold floors). The categories of the thermal indoor environment are presented in Table 4.

CATEGORY	THERMAL STATE OF THE BODY		LOCAL DISCOMFORT			
	PPD [%]	PMV [%]	DR [%]	PD [%] caused by		
				vertical air temperature difference	warm or cool floor	radiant asymmetry
A	<6	-0.2<PMV<+0.2	<10	<3	<10	<5
B	<10	-0.5<PMV<+0.5	<20	<5	<10	<5
C	<15	-0.7<PMV<+0.7	<30	<10	<15	<10

TABLE 4 - CATEGORIES OF THE THERMAL INDOOR ENVIRONMENT

Category A: high level of expectation; recommended for space occupied by sensitive people or with special needs, such as disabled, sick, children and elderly.

Category B: normal level of expectation; it should be used in new or refurbished buildings.

Category C: moderately acceptable level of expectation; it could be used in existing buildings.

Table 5, Table 6, Table 7 give ranges for the four local thermal discomfort parameters for each of the three categories presented in Table 4 (ISO, 2005).

CATEGORY	VERTICAL AIR TEMPERATURE DIFFERENCE °C
A	< 2
B	< 3
C	< 4

TABLE 5 - VERTICAL AIR TEMPERATURE DIFFERENCE BETWEEN HEAD AND ANKLES

CATEGORY	FLOOR SURFACE TEMPERATURE RANGE °C
A	19 to 29
B	19 to 29
C	17 to 31

TABLE 6 - RANGE OF FLOOR TEMPERATURE

CATEGORY	WARM CEILING	COOL WALL	COOL CEILING	WARM WALL
A	< 5	< 10	< 14	< 23
B	< 5	< 10	< 14	< 23
C	< 7	< 13	< 18	< 35

TABLE 7 - RADIANT TEMPERATURE ASYMMETRY

2.1.2 RELATIVE HUMIDITY (RH)

The influence of humidity on the perception of an indoor environment can play a part in the perceived temperature and their thermal comfort. Actually, relative humidity affects the evaporation from the skin, which is the primary human mechanism to regulate temperature. At lower RH, more sweat is allowed to evaporate from the body, while at higher values it is harder for this process to happen, because the air's moisture content is already elevated. Because humans perceive the rate of heat transfer from the body rather than temperature itself, we feel warmer at a given temperature when the relative humidity is high than when it is low. Therefore, very humid environments (RH > 70-80%) are usually uncomfortable because the air is close to the saturation level, thus strongly reducing the possibility of heat loss through evaporation. On the other hand, very dry environments (RH < 20-30%) are also uncomfortable because of their effect on the mucous membranes. The recommended level of indoor humidity is in the range of 30-60% (Wolkoff P., 2007) (CEN, 1995).

For climate control in buildings using HVAC (heating, ventilation, air conditioning) systems, the key is to maintain the relative humidity at a comfortable range: low enough to be comfortable, but high enough to avoid problems associated with very dry air.

When the temperature is high and the relative humidity is low, evaporation of water is rapid, e.g. wooden furniture can shrink, causing the paint that covers these surfaces to fracture.

When the temperature is high and the relative humidity is high, evaporation of water is slow: when relative humidity approaches the saturation level (100%), condensation can occur on surfaces, leading to problems with mould, corrosion, decay, and other moisture-related deterioration.

2.1.3 ADAPTIVE COMFORT STANDARD (ACS)

According to the steady-state heat-balance theory, the PMV model does not take into account adaptations of the human body, which play a key role in determining subjective thermal sensation and perception. It has been claimed that the ISO 7730, which is based on the heat balance model, overestimates the occupant responses on the ASHRAE scale at high temperatures and underestimates them at low temperatures (Brager G.S., 1998) (de Dear R.J., 1998).

Thereafter, a new Adaptive Comfort Standard (ACS) has been updated to the ASHRAE Standard 55 (de Dear R.J., 2002) (ASHRAE, 2004): it is based on the analysis of 21000 sets of raw data compiled from field studies in 160 buildings, both air conditioned and naturally ventilated, located on four continents in varied climatic zones.

de Dear claimed that the adaptive and heat balance approaches to modelling thermal comfort are complementary rather than contradictory, since the static heat balance model takes into account clothing and activity level. Therefore, it is believed that only a combination of the features of both these modelling approaches will eventually be able to account for both the thermal and non-thermal influences on occupant response in real buildings (Runming Y., 2009).

The adaptive comfort theory was first proposed in the 1970s and it is based on the findings of surveys of thermal comfort conducted in the field. The fundamental assumption of the adaptive approach is expressed by the adaptive principle: if change occurs such as to produce discomfort, people react in ways that tend to restore their comfort (Nicol J.F., 2002). Therefore, self-regulatory actions will take place.

There are three main sorts of self-regulation: physiologically adaptive, psychologically adaptive and behaviourally adaptive (Brager G.S., 1998) (de Dear R.J., 1998).
A new physiological balance of the human body can be achieved because of the gradual diminution in the strain induced by such exposure. There are two sub-categories included in physiological adaptation: genetic adaptation (from generation to generation) and acclimatization (within one generation).
Psychological adaptation is usually mentioned as an altered perception of, and reaction to, sensory information due to subjective past thermal experiences and expectations (de Dear R.J., 2002).
Many behaviours carried out in daily life (such as putting on/taking off clothing, switching on/off a fan or heating and taking in hot/cold drinks), can be considered as behavioural adjustment, because these behaviours will consequently induce a change in the heat balance of the human body (de Dear R.J., 1998) (Brager G.S., 1998) (Wohlwill J.F., 1975).

Personal (e.g., removing an item of clothing), technological (e.g., turning on an air conditioner), and cultural (e.g., having a siesta in the heat of the day) responses are the three main sub-classifications.

However, there is general agreement that physiological acclimatization does not play a role in adaptive procedures; consequently, expectations and behavioural adjustments have a much greater influence (Brager G.S., 1998).

The adaptive model reveals also that the thermal comfort temperature is a function relating to the outdoor air temperature. Auliciems was the first to propose the adaptive control algorithm (ACA) in 1986 (Auliciems, 1981). Humphreys, Nicol, Auliciems, de Dear, CIBSE and other researchers have also presented several empirical equations for the indoor thermal comfort temperature based on the different surveys of free-running buildings (Runming Y., 2009).

2.2 AEROGEL FIBRE

2.2.1 SPACEFILL

A large number of historical buildings are solid walls construction with a small cavity between the wall and the internal lath and plaster internal finish. The insulating of these is problematic as insulating the solid wall internally or externally can lead to aesthetic damages, which is obviously not desirable in older buildings with historic significance. In Britain and Ireland, plaster-on-laths wall finishes have often been used as a historical interior wall finish, consisting of horizontal timber laths, fixed to vertical timber battens, in turn fix to the masonry. The laths are fitted so that gaps remain between them. Plaster is then applied from the room side keying to the laths and gaining particular adhesion due to some plaster being pressed through the gaps between the laths. This traditional wall finish leaves air cavities in between the battens and between the laths and the masonry. These cavities can be filled with insulation, by blowing an insulating from the room side into the cavity. The same application technique can also be used to fill cavities behind plasterboard dry lining, often used in late 20th century renovations of historic building. The installation process only requires few holes, is thereby fast and cost effective, and only causes minimal disruption to building fabric and occupants. One might consider that filling air cavities could be inappropriate where they are required for moisture evaporation from the masonry (Gouas, et al., 2015).

Aerogel is growing in popularity due to its unique set of properties that ensures high thermal performance, vapour permeability and water resistance. An application of advanced aerogel as blow-in insulation could allow optimising the insulation’s performance in terms of both used space as well as structural health and reversibility of intervention (Baglivo L., 2015).

Traditionally, monolithic aerogels are fragile, breaking down easily under pressure, such as exercised by blow applications. Previous knowledge on successfully blown-in insulation suggested a fibrous aerogel product with the possible addition of another insulating medium, such as cork, EPS (expanded polystyrene), polyester fibre, or aerogel dust. The fibrous polyester material was selected for its robustness, high thermal performance (l-value of 0.014 W/mK), low vapour yet high water resistance. The medium was impregnated with silica aerogel for improving its thermal performance. This aerogel blanket was cut into 0.005 m cubes that resulted in the best fibre size for the installation process (Lucchi E., 2017).

The advantages of this form of Spacefill installation are:

- significant thermal improvement with thin insulation material
- use in cavity behind wall finishes, such as existing laths and plaster
- no reduction of room space
- use of the same installation techniques and methods as other cavity fill insulation products
- simple and cost-effectiveness installation techniques without the removal of the internal wall finishes
- minimal redecoration
- vapour permeable
- use of recycled materials

The main disadvantages are the creation of dust during production and installation, and high production cost.

The material was characterized in laboratory and the following technical data were obtained (Table 8) (Lucchi E., 2017).

MATERIAL PROPERTIES	VALUE
λ-value	0.0255 W/(m·K) with density of 70 kg/m^3
Reaction to fire	Class E
Water absorption	0.11344 kg/m^2
Water vapour transmission	Assumed 1, as for mineral wool products

TABLE 8 – MATERIAL PROPERTIES OF SPACEFILL BLOW-IN AEROGEL

2.2.2 GLASGOW CASE STUDY

2.2.2.1 CASE STUDY BUILDING

The property identified for the demonstration is within a traditional, four-storey tenement flat in Yoker district (a western suburb of Glasgow, approximately 8 km west of the city centre). It is owned by a local housing association (Yoker Housing Association) and part of a U-shaped building ensemble along Blawarthill Street and Dumbarton Road. The building ensemble appears to date from the first decade of the 20th century, possibly the 1910s or 1920s, judging by geo-referenced maps; it is not included in heritage protection lists, nor is it located within conservation areas (Vivarelli A., 2015). The property is on the 2nd floor (i.e. third storey), surrounded by other flats to the left, right, above and below (Figure 12). The street elevation faces north and the rear elevation south.

FIGURE 12 - AERIAL VIEW OF BLAWARTHILL STREET AND NEIGHBOURHOOD IN YOKER DISTRICT, WITH THE CASE STUDY BUILDING IN RED (LEFT); NORTH-FACING STREET ELEVATION WITH POSITION OF PROPERTY IN RED (RIGHT) (IMAGE COURTESY OF HISTORIC ENVIRONMENT SCOTLAND)

The external walls of the property are traditional stone masonry, made from sandstone bedded in mortar. The walls are approximately 60 cm thick, including internal wall finishes. The property has three bedrooms (1 north facing, 2 south facing), living room (north facing), kitchen (south facing) and bathroom (internal) as well as three storage rooms (internal). The property contains 10 windows (6 north facing, 4 south facing). Most of these have recessed window breasts, i.e. stone areas below the windows where the masonry is thinner than at normal walls. The property was refurbished, presumably during the 1980s. The interior wall finishes are plasterboard on dry lining with no or only minimal insulation behind. The window breasts are finished with timber sheeting, possibly ply board, otherwise plasterboard (Casado M., 2016).

2.2.2.2 MATERIAL APPLICATION AND MONITORING SYSTEM INSTALLATION

The north-facing wall of the tenement flat was identified as fabric suitable for the monitoring. The aerogel was applied in one of the three bedrooms, whilst the living room was used as control room (Figure 13). The areas below the windows, the window breast, were identified for the measurements (Table 9). The window breasts are thinner wall sections (ca. 25 cm thick), finished internally with ply board on battens. As wall finishes would normally be in the form of plaster, ply boarding was replaced with conventional plasterboard in the control room and on the left window in the demonstration room; and with traditional plaster on laths finish (three coat lime plaster with hair reinforcement and softwood timber laths) on the mid window in the demonstration room. In addition, also the performance between the mid- and the right window in the demonstration room was measured, using the existing plasterboard finish as is (plasterboard dry lining with foam insulation backing, ca. 10 + 15 mm thick) (Figure 14).

In February 2015, Spacefill was successfully installed at the Glasgow case study flat, using a conventional cavity-fill blowing method.

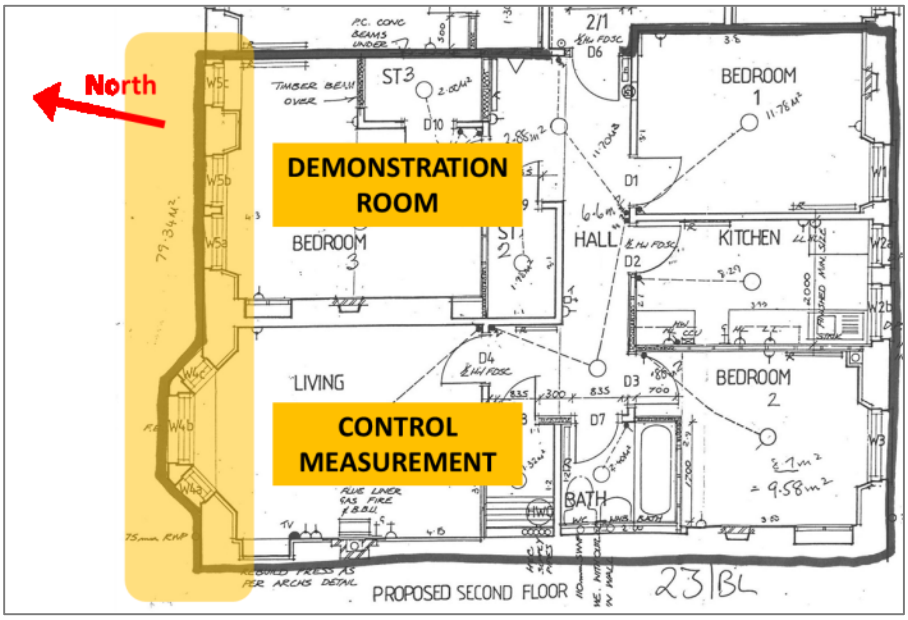

FIGURE 13 - FLOOR PLAN OF CASE STUDY FLAT: SENSORS INSTALLED ON THE NORTH-FACING EXTERNAL WALL (LIGHT YELLOW SHADING) IN A DEMONSTRATION AND CONTROL ROOM (IMAGE COURTESY OF HISTORIC ENVIRONMENT SCOTLAND)

FIGURE 14 - EXTERIOR WALL IN THE DEMONSTRATION ROOM, PRIOR TO PREPARATORY AND RETROFIT WORKS, WITH PROPOSED WALL FINISHED INDICATED IN RED, REPLACING THE EXISTING PLY BOARD

ROOM	LOCATION	MASONRY THICKNESS	INTERNAL FINISH
Control	breast of mid window	thin (ca. 20 cm)	new plasterboard
Demonstration	breast of left window	thin (ca. 20 cm)	new plasterboard
Demonstration	breast of mid window	thin (ca. 20 cm)	new lime plaster on timber laths
Demonstration	between mid- and right window	thick (ca. 50 cm)	existing plasterboard with foam insulation backing

TABLE 9 - MONITORING LOCATIONS (AS SEEN FROM THE ROOM SIDE)

In April 2015, thermo-hygrometric monitoring equipment was installed in the demonstration and control rooms at each of the four locations listed in the table above. Externally, sensors were fitted measuring relative humidity and temperature at the masonry surface. The same sensors were fitted at the internal surface of the wall finish and at the interface between insulation and masonry. In addition, heat flux plates were installed to the internal wall faces (Figure 15). Data on indoor / outdoor air temperature and humidity were also recorded.

The rooms were heated with electric heaters placed further down in the room to achieve a stable indoor temperature of about 20 °C. The radiators near the windows were shut down to avoid their convective and radiative impact on the heat flow plates.

FIGURE 15 - PICTURES OF THE INSTALLATION: EXTERNAL SURFACE CONTACT SENSORS (LEFT), HEAT FLOW METER AND SURFACE CONTACT SENSORS IN THE REFERENCE ROOM (CENTER), HEAT FLOW METER AND SURFACE CONTACT SENSORS AT THE THREE LOCATIONS IN THE DEMONSTRATION ROOM (RIGHT)

2.2.2.3 DATA ANALYSIS AND RESULTS

The thermal performance of the blow-in aerogel was evaluated by analysing the data recorded during both a continuous monitoring (period 09/04/2015 – 07/02/2016) and a manual campaign (carried out on 16/02/2016) in the control and demonstration rooms of the apartment building to calculate the internal thermal comfort. During these manual campaigns, the thermographic measurements were carried out.

The values of both air and surface temperatures of the exterior wall, measured outdoors and indoors, were analysed by comparing their temporal trend, as well as their absolute differences between in and out, in the test vs. reference room.

The thermal comfort was evaluated by means of a “fangerometer” composed by air temperature and relative humidity sensors, a globe-thermometer and an air velocity transducer. Air temperature data were firstly analysed in order to verify the applicability of Ref. (ISO, 2005), i.e. steady-state thermal environmental conditions. Then the PMV and PPD indices were calculated accordingly. A metabolic rate of 1.0 met was set in the Fanger equation, which corresponds to a seated, relaxed condition (ISO, 2004) and a clothing combination of 0,96 was applied in winter season (ISO, 2007). The evaluation of the thermal comfort conditions both in the reference and test rooms was carried out according to Method A described in Annex H of (ISO, 2005).

The thermal conductance (C) of the west wall was calculated using the progressive average method (ISO, 2014), starting from the measured values of the thermal flux, the internal and external surface temperatures during 13 stationary days chosen when the fluctuation of the temperature was small.

The thermal transmittance (U) was calculated from the thermal conductance considering also the resistance of the internal air (Ri) and external air (Re), respectively 0.125 and 0.04 for a vertical wall:

$$U = \frac{1}{R_i + \frac{1}{C} + R_e}$$

These values were calculated for both rooms to verify the improvement of thermal transmittance and conductance due to the blown-in aerogel.

Air and surface temperature of exterior wall

Table 10, Figure 16, Figure 17, Figure 18 report the maximum, minimum and average temperature values recorded by the air and surface sensors placed outdoors and indoors of the exterior wall in the test and reference rooms.

		Ref. Tc in	Ref. Tc out	Ref. Ta in	Ta out	Test Tc in	Test Tc out	Test Ta in
April 2015	max	19.3	19.6	20.0	20.2	20.4	20.0	21.2
	min	14.3	3.3	15.5	0.7	15.6	3.1	16.5
	average	16.3	10.8	17.4	10.1	17.6	10.6	18.6
May 2015	max	20.4	20.3	21.4	21.6	20.9	20.5	21.7
	min	12.9	4.3	14.0	1.8	14.9	4.3	16.6
	average	17.3	11.7	18.3	11.0	18.3	11.5	19.2
June 2015	max	23.5	24.8	24.3	26.4	24.4	25.3	24.9
	min	17.3	7.0	18.3	5.6	18.2	6.9	18.9
	average	19.8	15.7	20.6	14.9	20.8	15.6	21.3
July 2015	max	24.4	28.4	25.7	29.2	25.5	28.1	26.2
	min	17.9	10.6	18.9	8.5	19.3	10.4	20.0
	average	20.5	16.7	21.3	15.9	21.5	16.5	22.1
August 2015	max	22.2	23.7	23.0	26.4	23.1	24.6	23.7
	min	18.3	11.2	19.1	9.1	19.5	11.1	20.0
	average	20.5	17.1	21.2	16.4	21.5	17.0	22.0
September 2015	max	20.2	19.9	21.2	22.5	21.3	19.7	22.2
	min	17.5	8.1	18.5	6.0	18.3	7.8	19.0
	average	18.5	13.8	19.4	13.2	19.2	13.5	20.0
October 2015	max	18.6	17.5	20.5	17.9	19.1	16.9	20.9
	min	16.3	5.4	17.7	3.3	17.4	4.8	18.5
	average	17.6	11.3	19.0	10.7	18.3	10.8	19.3
November 2015	max	18.1	14.0	20.3	14.7	18.8	13.5	21.0
	min	14.7	1.4	16.7	-0.4	16.4	1.2	18.0
	average	16.9	8.4	18.8	8.0	17.9	7.8	19.3
December 2015	max	18.1	14.1	20.4	14.3	18.8	13.6	20.9
	min	14.2	0.4	15.9	-1.6	15.5	0.0	17.5
	average	16.6	7.9	18.7	7.6	17.7	7.3	19.3
January 2016	max	17.9	13.5	20.5	13.6	18.7	12.9	21.0
	min	13.4	0.0	15.7	-2.8	15.3	0.0	17.3
	average	15.9	5.6	18.4	5.0	17.2	4.9	19.2
February 2016	max	17.1	10.0	20.3	10.4	18.1	9.3	20.8
	min	10.1	0.5	11.8	-2.1	11.3	0.0	12.9
	average	13.1	5.4	14.6	4.8	14.1	4.8	15.6

TABLE 10 - MAXIMUM, AVERAGE AND MINIMUM VALUES OF AIR (TA) AND CONTACT (TC) TEMPERATURE OUTDOORS AND INDOORS IN THE TEST AND REFERENCE ROOMS IN THE WHOLE MONITORING PERIOD

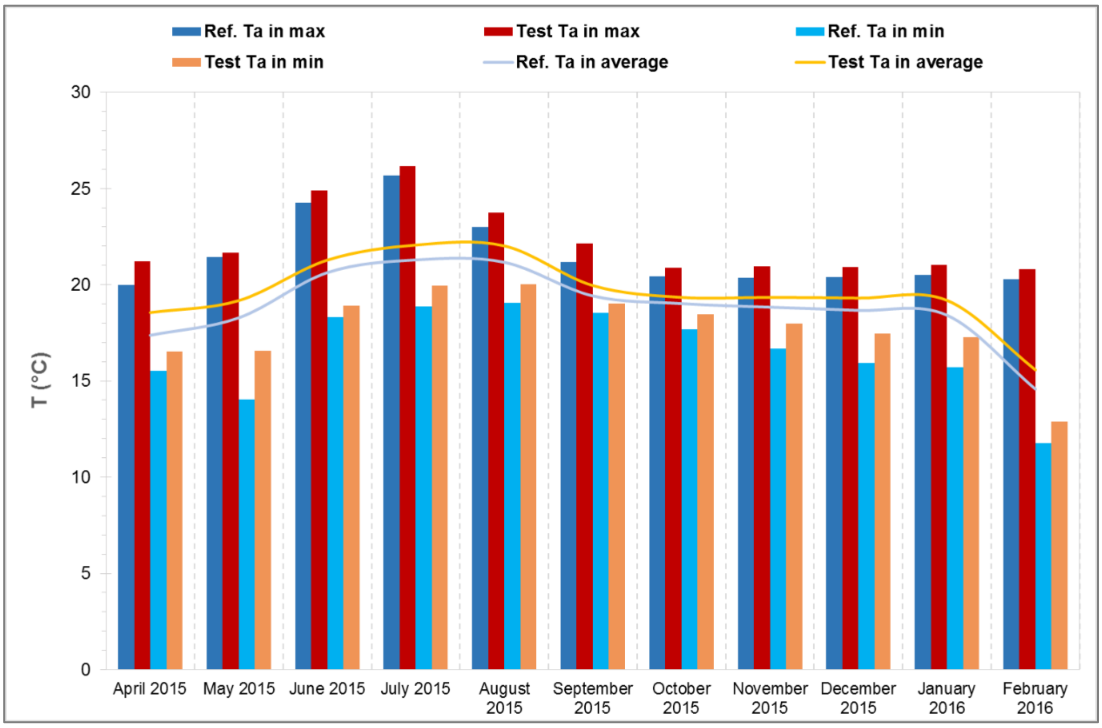

FIGURE 16 - MAXIMUM, MINIMUM (COLUMNS) AND AVERAGE (LINES) VALUES OF AIR (TA) TEMPERATURE INDOORS IN THE TEST (RED COLOURS) AND REFERENCE (BLUE COLOURS) ROOMS IN THE WHOLE MONITORING PERIOD

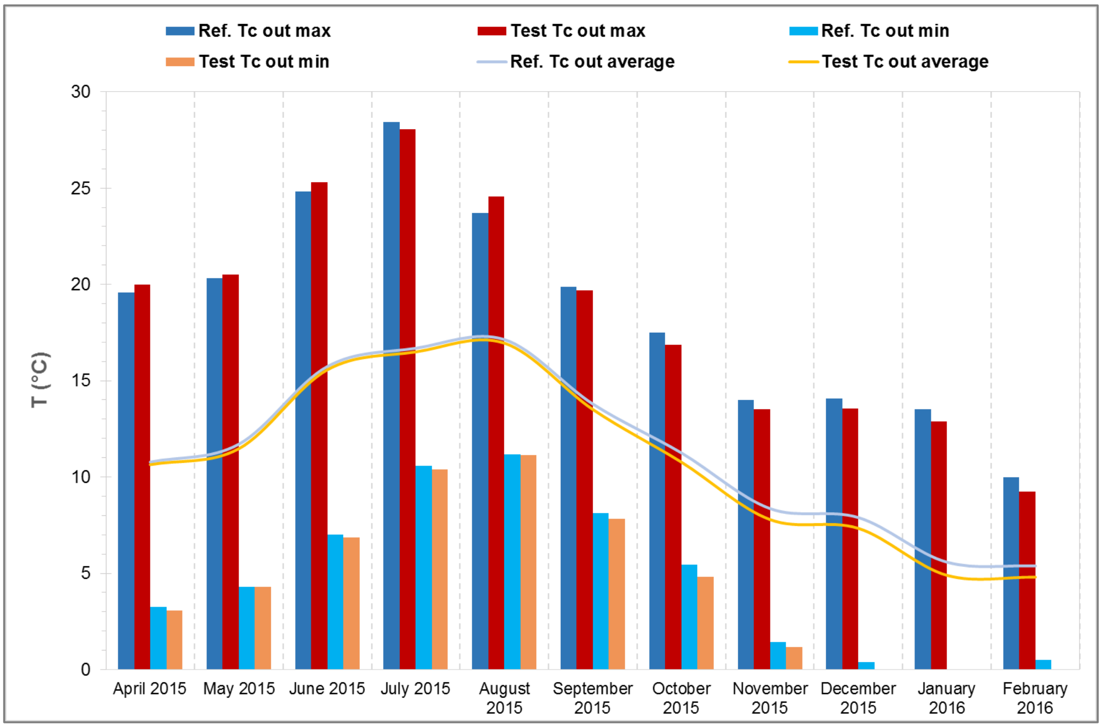

FIGURE 17 - MAXIMUM, MINIMUM (COLUMNS) AND AVERAGE (LINES) VALUES OF CONTACT (TC) TEMPERATURE OUTDOORS IN THE TEST (RED COLOURS) AND REFERENCE (BLUE COLOURS) ROOMS IN THE WHOLE MONITORING PERIOD

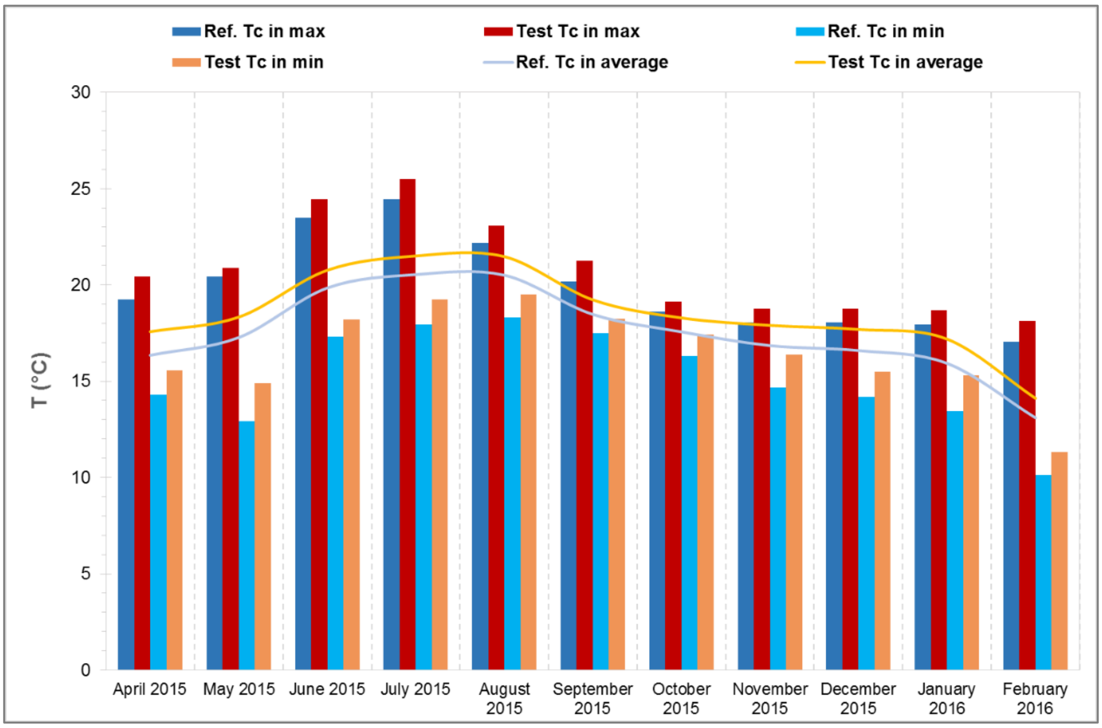

FIGURE 18 - MAXIMUM, MINIMUM (COLUMNS) AND AVERAGE (LINES) VALUES OF CONTACT (TC) TEMPERATURE INDOORS IN THE TEST (RED COLOURS) AND REFERENCE (BLUE COLOURS) ROOMS IN THE WHOLE MONITORING PERIOD

As it is clearly visible from the above graphs, both air and contact temperatures are higher of about 1°C inside the test room than in the reference room in the maximum, minimum and average values (Figure 16, Figure 18).

This trend occurs in all months, despite that the contact temperatures outdoors are quite similar, even slightly higher in the maximum and average values out of the exterior wall of the reference room (Figure 17), in particular from September 2015 to February 2016.

Therefore, the analysis of the absolute difference – calculated between the temperatures recorded outdoors and indoors both in air and on the surface of the exterior wall - shows again higher values in the test than in the reference room all over the year, demonstrating the thermal insulation of the aerogel. In detail, the temperature difference between in and out is higher in the test room of about 1°C in air and 1.5-2°C on the surface, especially in the cold season in the average and maximum values.

Table 11, Figure 19, Figure 20, report the maximum, minimum and average values of the absolute difference recorded by the air and surface sensors placed outdoors and indoors in the test and reference rooms.

		Ref. Tc out-in	**Ref. Ta out-in**	**Test Tc out-in**	**Test Ta out-in**
April 2015	max	12.0	17.2	13.9	18.2
	min	0.0	0.0	0.1	0.2
	average	5.6	7.3	6.9	8.5
May 2015	max	10.3	14.7	11.8	15.4
	min	0.0	0.0	0.3	0.1
	average	5.6	7.3	6.9	8.2
June 2015	max	10.6	14.4	11.8	14.4
	min	0.0	0.0	0.0	0.0
	average	4.2	5.8	5.2	6.4
July 2015	max	9.5	12.5	10.4	13.4
	min	0.0	0.0	0.0	0.0
	average	4.0	5.5	5.1	6.3
August 2015	max	7.8	10.7	9.0	11.7
	min	0.0	0.0	0.0	0.0
	average	3.4	4.8	4.5	5.6
September 2015	max	6.3	9.2	7.4	9.6
	min	0.0	0.0	0.1	0.0
	average	4.7	6.2	5.7	6.8
October 2015	max	11.4	16.6	13.0	17.0
	min	0.8	1.3	2.0	1.7
	average	6.3	8.3	7.5	8.6
November 2015	max	14.3	20.0	16.1	20.7
	min	3.6	4.1	4.9	4.6
	average	8.5	10.9	10.1	11.4
December 2015	max	15.1	21.3	17.3	21.8
	min	3.8	4.4	4.9	5.0
	average	8.7	11.1	10.4	11.7
January 2016	max	15.4	22.2	17.2	23.3
	min	4.1	4.8	5.6	5.5
	average	10.4	13.4	12.3	14.2
February 2016	max	12.7	18.0	14.6	18.9
	min	4.3	5.2	5.7	6.1
	average	7.8	9.7	9.4	10.7

TABLE 11 - MAXIMUM, AVERAGE AND MINIMUM VALUES OF THE ABSOLUTE DIFFERENCE OF AIR (TA) AND CONTACT (TC) TEMPERATURE BETWEEN OUTDOORS AND INDOORS IN THE TEST AND REFERENCE ROOMS IN THE WHOLE MONITORING PERIOD

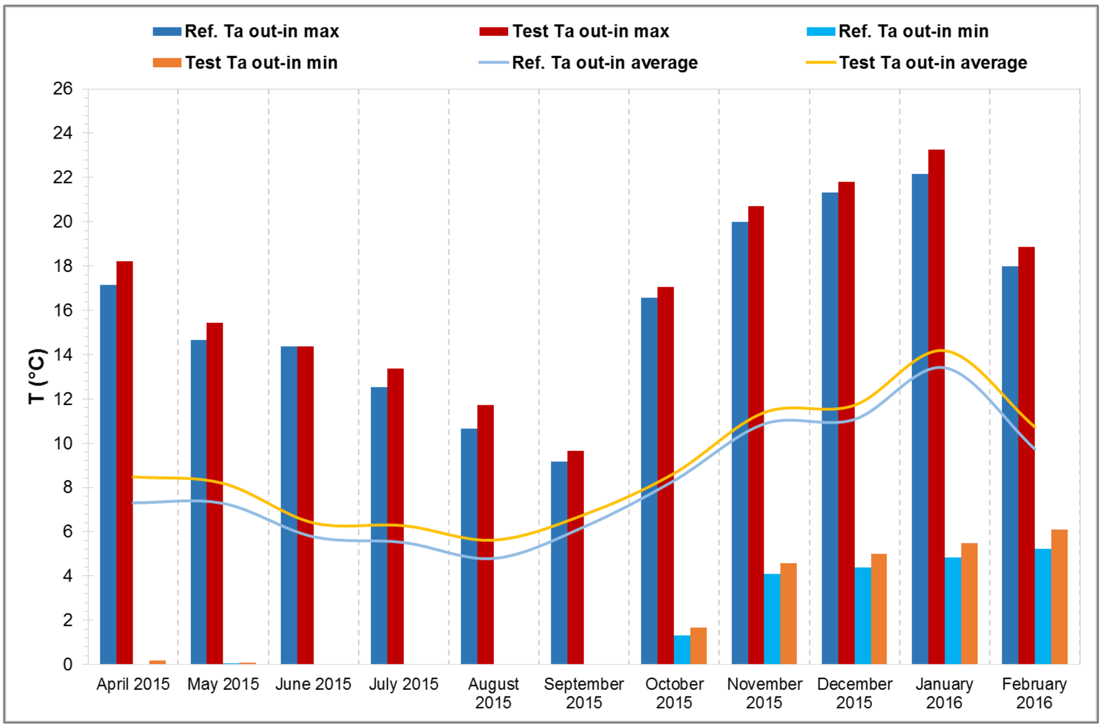

FIGURE 19 - MAXIMUM, MINIMUM (COLUMNS) AND AVERAGE (LINES) VALUES OF THE ABSOLUTE DIFFERENCE OF AIR (TA) TEMPERATURE BETWEEN OUTDOORS AND INDOORS IN THE TEST (RED COLOURS) AND REFERENCE (BLUE COLOURS) ROOMS IN THE WHOLE MONITORING PERIOD

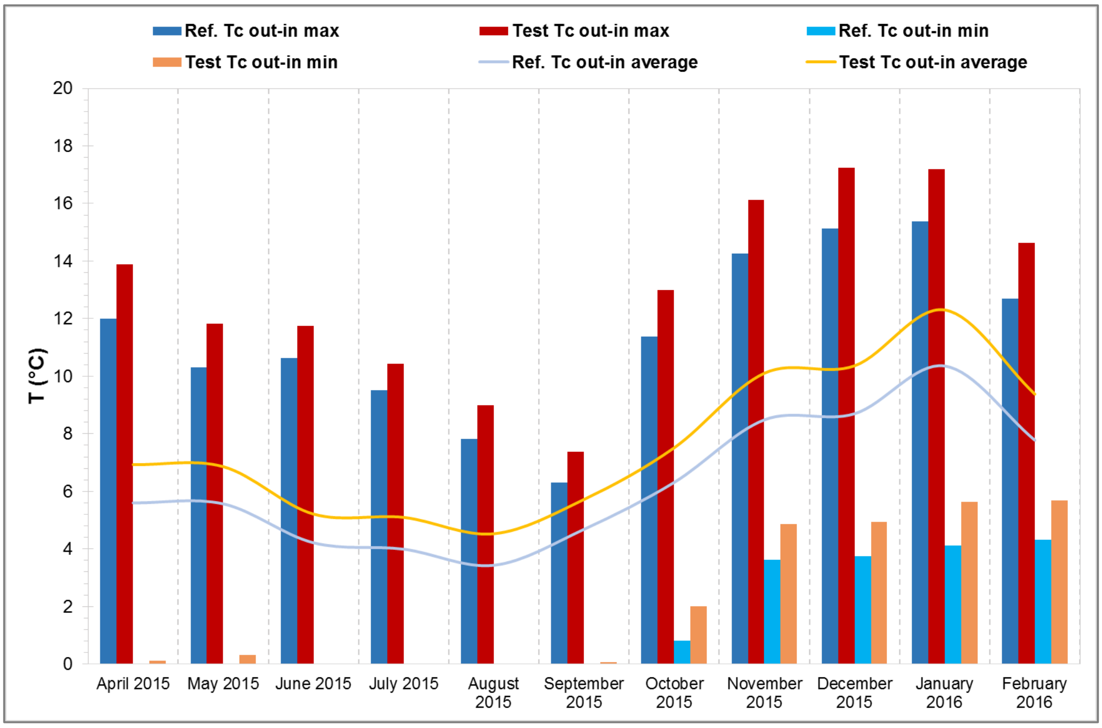

FIGURE 20 - MAXIMUM, MINIMUM (COLUMNS) AND AVERAGE (LINES) VALUES OF THE ABSOLUTE DIFFERENCE OF CONTACT (TC) TEMPERATURE BETWEEN OUTDOORS AND INDOORS IN THE TEST (RED COLOURS) AND REFERENCE (BLUE COLOURS) ROOMS IN THE WHOLE MONITORING PERIOD

Thermal comfort

Figure 21 shows the PMV trend both in the reference and test rooms, compared with ISO 7730 thermal sensation scale (Table 3).

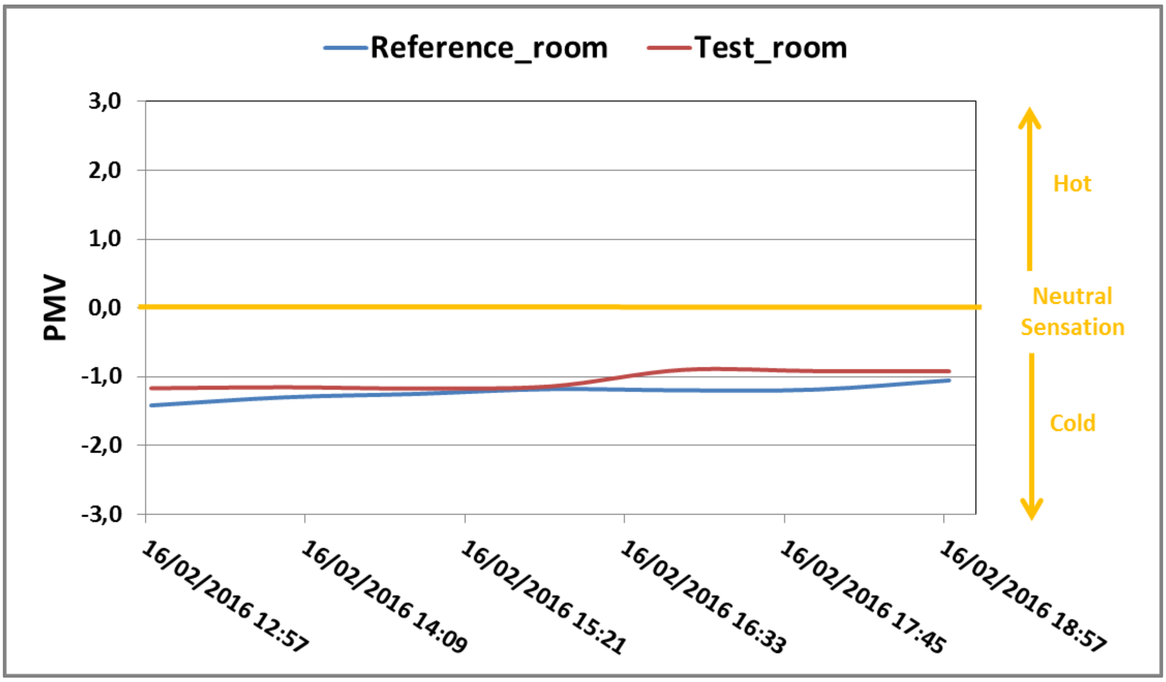

FIGURE 21 - COMPARISON OF THE PMV TREND IN BOTH REFERENCE AND TEST ROOMS DURING THE MANUAL CAMPAIGN IN FEBRUARY 2016

According to the results, the calculated PMV value is far away from the neutral sensation zone both in the reference and test rooms, demonstrating that the internal condition of the rooms included in the Glasgow case study are not optimal. Nevertheless, the installation of the aerogel resulted in an improvement of the internal conditions of about 40%. In Table 12, the percentage of hours, with occupied building and PMV included in a specific range, is reported. The reference room was always characterized by a PMV value between -2 and -1, whilst in the test room this PMV range was covered only for the 57% of the occupancy hours. The PPD values are 37 % and 33 % in the reference and test rooms respectively.

	REFERENCE ROOM		**TEST ROOM**	
	% hours	**PPD (%)**	**% hours**	**PPD (%)**
-1 < PMV < -0,7	0	0	43	23
-2 < PMV < -1	100	37	57	33

TABLE 12 - PMV AND PPD RESULTS FOR THE REFERENCE AND TEST ROOMS DURING THE MANUAL CAMPAIGN IN FEBRUARY 2016

Thermographic measurements

The thermographic measurements were carried out by means of a FLIR T400 Western thermal camera operating in the spectral range between 7.5 - 13 μm with an accuracy of ± 2°C. The temperature range of the thermal camera was set to -20, + 120°C. The thermographic results are completely in agreement with the results obtained from the continuous monitoring.

Figure 22 and Figure 23 show the infrared images of both the test and reference rooms respectively. Figure 24 shows the visual and infrared images recorded on the main facade of the building; the reference and test rooms are included in the red circle.

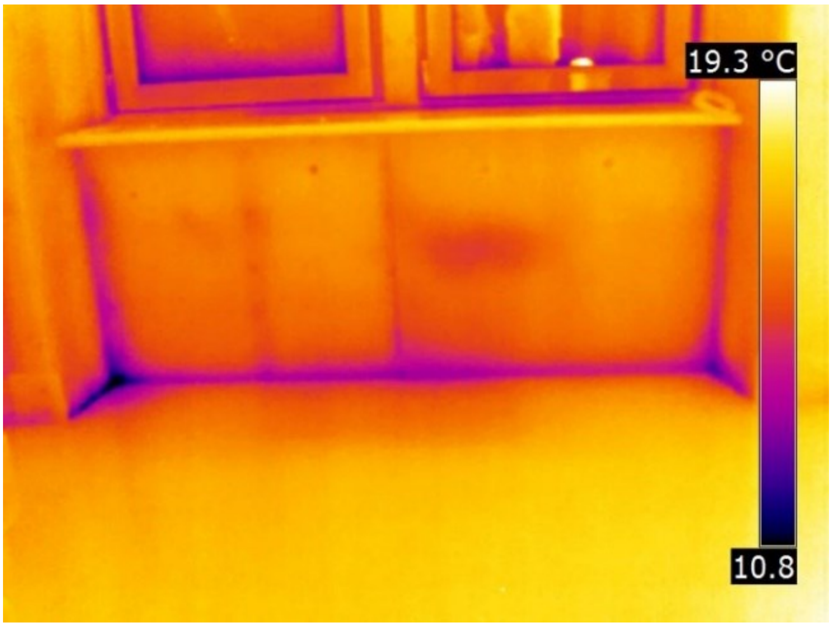

FIGURE 22 - INFRARED IMAGES OF THE TEST ROOM

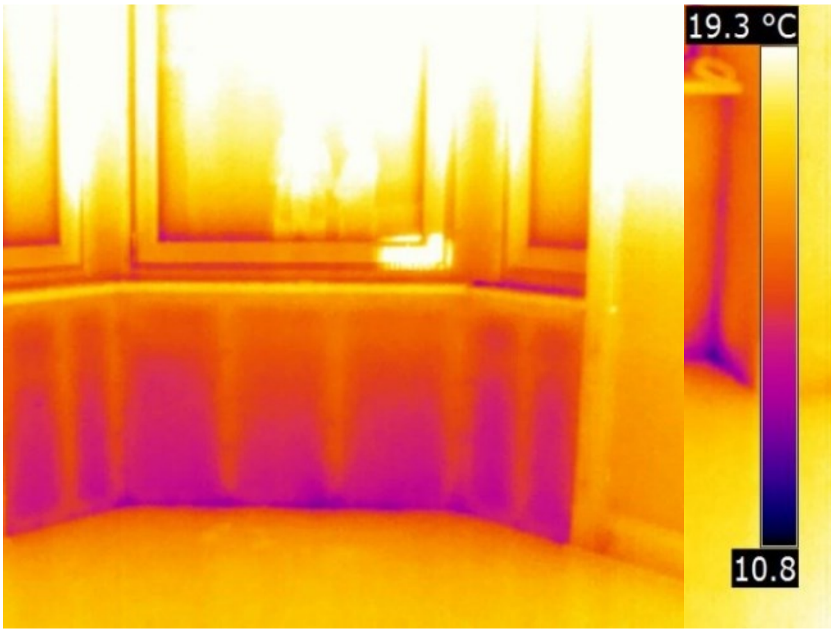

FIGURE 23 - INFRARED IMAGES OF THE REFERENCE ROOM

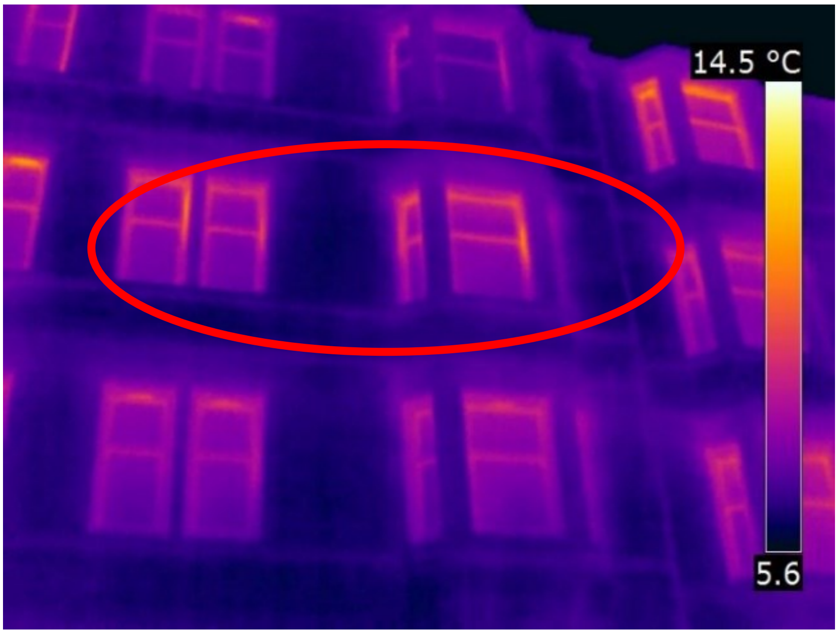

FIGURE 24 - INFRARED IMAGES OF THE BUILDING TAKEN FROM OUTSIDE

The temperature of the internal surface of the test room (Figure 22) is about 1°C higher in the maximum, minimum and average values than in the reference room (Figure 23). The temperatures of the external surface of the reference and test rooms, measured in correspondence of the indoor area (Figure 24) are quite similar. The thermal difference between the two external surfaces is about 0.2 °C, with the average value slightly higher in the reference room than in the test one. Furthermore, the temperature difference between in and out is higher in the test room of about 1.5 °C respect to the reference one.

The thermographic measurements, along with yearly campaign, confirm the thermal insulation capacity of the aerogel.

Thermal Conductance and Transmittance

The heat flux was lower in the test room with a value of Q = 7.91 W/m^2 in comparison to Q = 29.66 W/m^2 in the reference room.

In the reference room, the value of the thermal conductance was 2.452 Wm^{-2}K^{-1}; in the test room was 0.523 Wm^{-2}K^{-1} with an improvement of 80%.

The thermal transmittance in the reference room was 1.746 Wm^{-2}K^{-1}; in the test room was 0.482 Wm^{-2}K^{-1} with an improvement of 70%.

Reversibility

Reversibility trials were undertaken in order to demonstrate the impact on conservational issues of historic building fabric. The removal was a relatively simple process: Spacefill was sucked out and came out very dry. The bay below the window only took approximately 30 minutes to empty, whilst the tall wall, due to the presence of horizontal studs took approximately 1 hour and a half to empty. The removal did not cause any apparent damage to the wall finishes, the dust creation was minimal and nearly all material was removed with this method (Figure 25). This demonstration proved that the installation of the insulation material can easily be reversed.

FIGURE 25 - REVERSIBILITY TRIALS IN GLASGOW CASE STUDY
(IMAGE COURTESY OF A. PROCTOR GROUP LTD.)

2.3 THERMAL INSULATING MORTAR

2.3.1 ISOCAL

The majority of the building-stock with a construction year before 1900 are built with natural hydraulic lime-based mortars in massive masonry. Due to their low elastic modulus, there has never been a need for dilation joints in old masonry structures, since they are able to accommodate small-scale movements resulting from shrink and expansion due to hot-cold cycles. Moreover, lime-based mortars have a high vapour transmission rate, beneficial to the breathing capacity of monolithic historic masonry. This specific quality of lime allows the render to be used for inside as well as outside applications due to its resistance against mechanical and environmental influences (Strikolith B.V.).

The development of ISOCAL started in laboratory with the selection of the most suitable binding agent and insulating filler material. Preferably binder should be a natural hydraulic lime (NHL), as it is compatible with historic substrates. Several commercial lime-based mortars were evaluated with respect to their mechanical properties and thermal conductivity, and finally NHL5 was identified as the most suitable due to its good strength development to bind a high ratio of insulating filler.

To optimize the insulating value of the mortar, several fillers were tested in different ratios, granulometry and mixing proportions (mineral granulates, aerogel particles, cork) and finally EPS beads were selected. EPS has the advantage of an easy use in mortar formulation together with a good cohesion/coherence with the mortar binder. EPS beads incorporated in a reversible/removable mortar layer would not harm historic substrates, and would not be visible when a NHL-based 100% mineral finishing layer is applied. To optimize its insulating value, the new mortar contained up to 80% EPS filler. Additives like cellulose fibres, air entraining agents and stearates were used to improve the mortar formulation in terms of workability, applicability and final weathering resistance characteristic.

The obtained product ISOCAL is a dry premixed formulated mortar to be mixed with 0.9 l/kg ± 0.02 l/kg tap water during the application in-situ by hand or spray as an uninterrupted light weight skin on the substrate (1-3 cm layer thickness in one application), thus eliminating thermal bridges. A compatible thin finishing plaster (2-5 mm) is needed to be applied, after drying of ISOCAL, for aesthetical function, particularly important for heritage buildings, but it also acts as a protection against environmental factors in outdoor applications. In case the historical substrate is (partly) fragile, inhomogeneous, continuously damp and/or contaminated with salts, it is recommended to prior consolidate it with a compatible product, after adequate cleaning.

This mortar is compatible with a wide range of historic buildings typology, mainly characterized by a porous mineral substrate, as natural stone and brick masonry, ceramic block, old intact mineral render/plaster and concrete (Brocken H., 2014).

Table 13 resumes the main properties of ISOCAL as characterized in laboratory following the specific standard procedures (series of UNI EN 1015).

MATERIAL PROPERTIES	**VALUE**
Colour	Light beige/grey
Density dry mortar powder/ mixed paste	0.24/0.50 kg/l
pH-value	>10.5
Compressive strength after 28/90 days	0.3/0.4 MPa
Flexural strength after 28/90 days	0.2/0.3 MPa
Capillarity	0.07 kg/m²/30 sec
Modulus of elasticity after 28 days	164 MPa
Thermal conductivity (λ-value) after 28 days	0.0627 W/m K

TABLE 13 – MATERIAL PROPERTIES OF ISOCAL MORTAR

2.3.2 BENEDIKTBEUERN CASE STUDY

2.3.2.1 CASE STUDY BUILDING

Benediktbeuern Monastery is one of the oldest in upper Bavaria, its roots going back to 8th century AD. The selected building called “Alte Schäfflerei” (“old cooperage”) (Figure 26), dated around 1760, belongs to the former craftsmen court of the monastery and it is heritage protected by being classed as a listed building. The building was originally used as a cooperage, later as abbeys workshop and smithy, and since 2010, it is used as the Fraunhofer Centre for Conservation and Energy Performance of Historic Buildings, a research and demonstration building dealing with topics related to renovation and preservation of historic buildings and monuments (Vivarelli A., 2015).

It has four small non-used rooms (about 15m²-20m²), with two outside walls not exposed to South. The masonry is made from a mixture of stone and lime or clay bricks without cement and plaster. The external layers are made of soft white lime-plaster with blisters partially empty and partially filled with sand. The internal layers are mainly made of lime plaster, partially coated with very solid plaster (possibly cement-based) and originally covered with different coloured layers. Both external and internal layers underwent to several construction and renovation works in successive phases leading to various corrections and over-plastering from different periods, thus the precise structure of the walls is unknown.

The insulation is restricted to the floor and ceiling with traditional materials, respectively Glassfoam pellets (30 cm) and EPS board (10 cm). The windows are from the 90s, have double-glazing and gaps sealed with silicone (Gouas, et al., 2015).

For the specific demonstration, one room on the ground floor in the northern part of the building was selected, which has a surface of about 16 m^2, one outer wall 60 cm thick and a window in the west side (Figure 26).

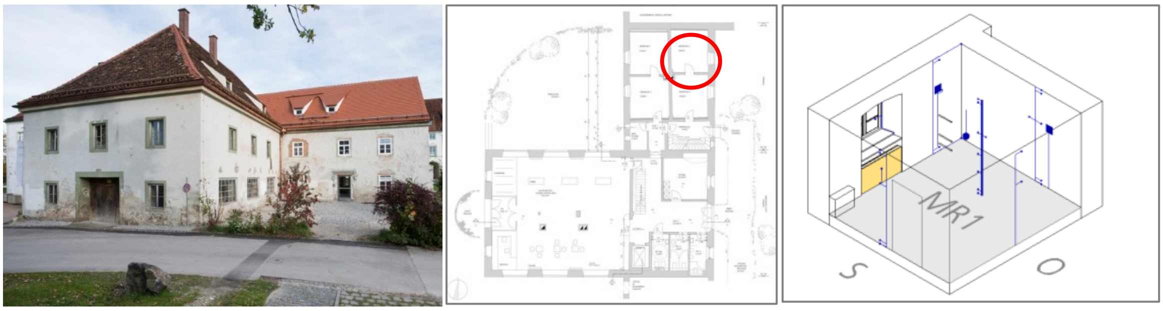

FIGURE 26 - VIEW OF THE SELECTED BUILDING AND DETAILS OF THE ROOM USED AS DEMONSTRATION (IMAGE COURTESY OF FRAUNHOFER)

2.3.2.2 MATERIAL APPLICATION AND MONITORING SYSTEM INSTALLATION

As the evaluation of the new mortar was done by comparing the environmental conditions and the energy consumption before and after the intervention, the monitoring program started in June 2013, whilst ISOCAL was applied one year later (June 2014) on the inner surface of the west wall. A layer of NHL2 lime with water was previously applied in order to protect the support and to remove easily ISOCAL at the end of the testing period, without damaging the substrate. ISOCAL was applied in two layers of about 1.5 cm thick each. After 7 days a finishing NHL5-based plaster was also applied over ISOCAL.

The wall temperature (Ts) was measured by means of thermistors placed: a) on the internal surface of the wall; b) in the transient layer (between the internal surface of the wall and the ISOCAL layer); c) on the external surface of the wall. Air temperature (T) and relative humidity (RH) were measured outside and inside the room by means of thermo-hygrometric sensors (Combi-sensors); the inside sensors were positioned at about 150 cm distance from the wall where also the thermal vertical distribution of the indoor air was investigated (3 points: 10, 110 and 170 cm above the floor level) (Figure 27, Figure 28, Figure 29, Figure 30).

The thermal transmittance of the new lime-based mortar was measured using a heat flow sensor in accordance with Ref. (ISO, 2014). The heat flux pad was affixed on the west wall, 90 cm right of the window at 170 cm from the floor.

A globe thermometer was placed inside the room close to the T-RH sensor.

The electric power consumption meter was placed on the heating devices.

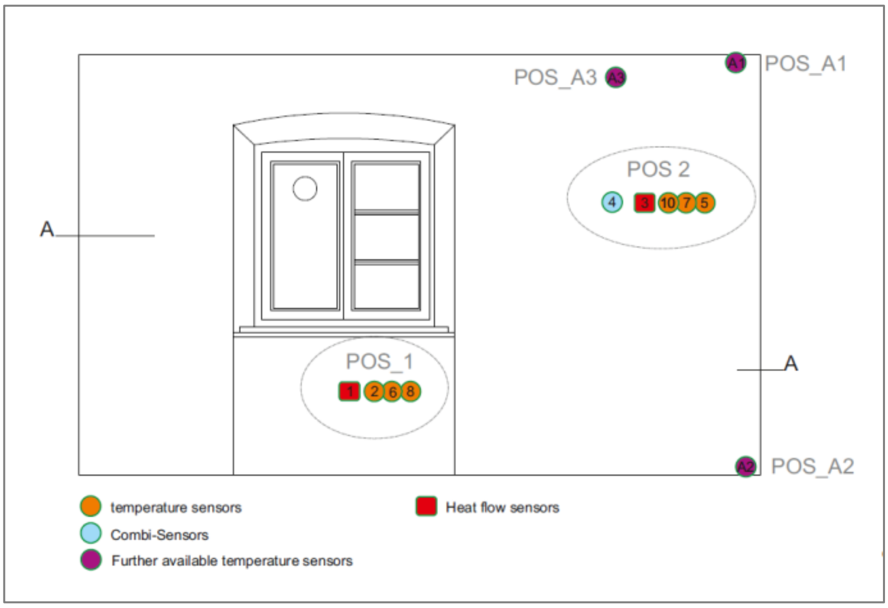

FIGURE 27 – VERTICAL SLICE OF THE WESTERN WALL AND SENSOR POSITIONS AT DIFFERENT HEIGHTS (IMAGE COURTESY OF FRAUNHOFER)

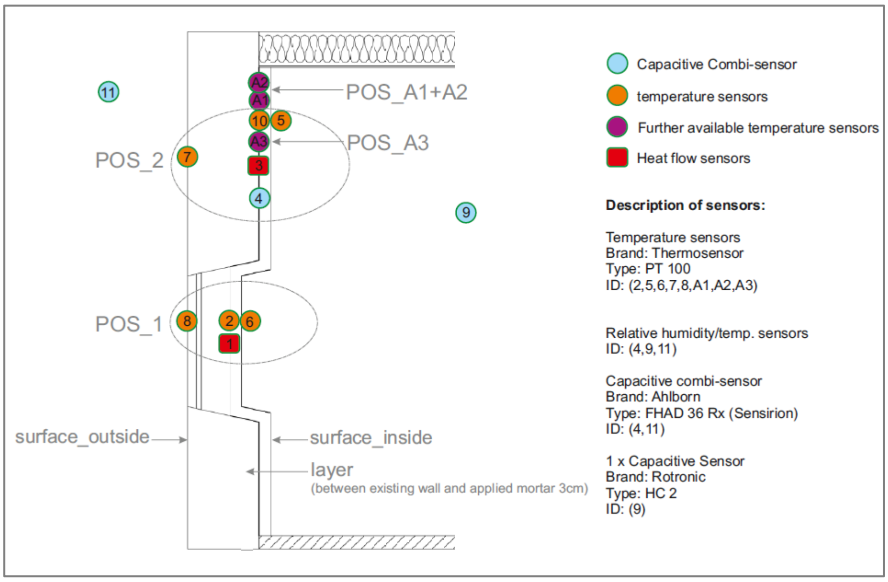

FIGURE 28 - HORIZONTAL SLICE OF THE WESTERN WALL AND SENSOR POSITIONS IN THE DIFFERENT LAYERS (IMAGE COURTESY OF FRAUNHOFER)

FIGURE 29 - SENSOR SET UP ON THE TRANSIENT LAYER, RIGHT OF THE WINDOW REVEALS: CAPACITIVE SENSOR, HEAT FLOW METER AND TEMPERATURE SENSOR (IMAGE COURTESY OF FRAUNHOFER)

FIGURE 30 - SENSOR SET UP ON THE INNER SURFACE AFTER THE APPLICATION OF THE MORTAR (IMAGE COURTESY OF FRAUNHOFER)

2.3.2.3 DATA ANALYSIS AND RESULTS

In order to evaluate the thermal performance of the new insulating mortar, the data recorded before the intervention were compared with the ones collected after the application of the mortar.

Two periods of the same duration (about 2 weeks) were selected in summer and in winter, in order to include in the evaluation the two extreme seasons, the latter characterized by the activation of the heating system. The choice was based on the analysis of temporal trend and daily variations of temperature inside and outside, as average values depend strongly on the specific climatic conditions in the year under examination.

The following periods were identified for comparison:

1) 31st July – 17th August 2013 (before intervention) vs. 2014 (after intervention);
2) 14th – 31st January 2014 (before intervention) vs. 2015 (after intervention) when the heating system was active.

In addition, as winter is the most suitable season for the evaluation of the performance of an insulating material in Central Europe, 3 months (December-February) in 2014 were also compared to the same months in 2015.

The measured values of both air and surface temperatures of the west wall outdoors and indoors were analysed in their distribution and temporal trend, as well as in their differences before and after the intervention.

The same periods were compared to analyse the indoor thermal comfort, as well as the local thermal discomfort. The thermo-hygrometric data collected by the Combi-sensors, as well as the operative temperature measured by the globe-thermometer, were used to calculate PMV and PPD, setting air velocity at 0.1 m/s. A metabolic rate of 1.6 met was included in the Fanger equation, which corresponds to a standing, light activity (ISO, 2004). Two different clothing combinations were applied in the different seasons, namely 0.67 in summer and 0.96 in winter (ISO, 2007). The local discomfort due to vertical air temperature difference between head and ankles was calculated according to Ref. (ISO, 2005). A local turbulence intensity of 40% was used.

The thermal conductance (C) and transmittance (U-value) of the west wall were calculated using the same method used in the Glasgow test field. The comparison was made considering a 14 days period when external surface temperature were stable and external temperature where similar in the two different years.

Finally, the electric input power of the heating devices was used to estimate the energy consumption. In this case, two periods characterized by similar boundary conditions (i.e. outdoor temperature) were selected for a reliable comparison: 28/02 – 07/03/2014 before the application of the mortar and 13/12 – 20/12/2014 after the intervention.

Air and surface temperature of insulated wall

In Table 14, the maximum, minimum and average temperature values recorded by the air and surface sensors placed outdoors and indoors before/after intervention are reported, as well as their difference in both the seasons.

		SUMMER		**WINTER (HEATING ON)**			
		1-17/08		**14-31/01**		**Dec-Jan-Feb**	
		Before (2013)	**After (2014)**	**Before (2014)**	**After (2015)**	**Before (2013-14)**	**After (2014-15)**
T out	average	20.1	17.1	2.4	1.0	3.1	1.2
	max	36.7	30.5	8.5	12.1	15.8	17.9
	min	9.8	8.9	-4.8	-5.8	-7.9	-11.0
T in	average	22.1	21.0	20.2	19.9	20.1	20.0
	max	23.3	21.6	20.7	20.6	20.8	20.7
	min	20.3	20.0	19.5	19.4	19.3	19.4
T in - Tout	average	1.9	3.9	17.8	19.0	17.0	18.8
	max	10.7	11.1	25.4	25.8	27.9	31.0
	min	-13.7	-9.0	11.6	7.9	4.3	2.1
Ts out	average	21.1	17.9	3.0	1.2	3.3	1.2
	max	44.2	37.1	7.5	8.5	14.0	16.6
	min	11.7	10.3	-2.5	-3.8	-6.9	-8.4
Ts in	average	21.6	20.3	17.1	17.7	17.0	17.7
	max	23.0	20.9	17.5	18.1	17.8	18.4
	min	19.7	19.1	13.8	17.3	13.8	17.2
Ts in - Ts out	average	0.6	2.4	14.1	16.5	13.7	16.4
	max	8.2	9.0	19.5	21.4	22.9	25.8
	min	-21.8	-16.4	9.6	9.4	3.2	0.8

TABLE 14 - MAXIMUM, AVERAGE AND MINIMUM VALUES OF AIR (T) AND SURFACE (TS) TEMPERATURE OUTDOORS AND INDOORS AND THEIR DIFFERENCE IN THE PERIODS SELECTED FOR COMPARISON BEFORE AND AFTER INTERVENTION

Analysing the data reported in Table 14 the effect of the climatology is evident: as an example, the highest temperature recorded outside in the summer period was 36.7°C in 2013, whilst it was 30.5°C in 2014. Hence, the evaluation of the conditions after the intervention should be based on the differences between the corresponding parameters related to the same period of the two years and not on their absolute values.

After the intervention, the difference between air and surface temperatures measured outside and inside increased in the average and maximum values in both summer and winter, giving evidence to a better thermal insulation due to the application of the new mortar. In fact, the average difference between air T measured inside and outside passed from 1.9°C to 3.9°C in August, and from 17.8°C 19.0°C in January (from 17.0°C to 18.8°C taking into account three winter months).

Concerning the difference between the surface temperatures measured outside and inside, in August 2013 it was 0.6°C on average, and in 2014 it increased up to 2.4°C. In particular, the increasing of the total difference is the result of two contributions: the increase of 1.4°C between the external surface and the mortar layer, and a further increase of 1.0°C between the mortar layer and the internal surface. One may note that the increase of 1.0°C on average was obtained with a mortar layer very thin (3 cm) respect to the total thickness of the wall.

The average difference between the external and internal surface temperatures measured in January increased from the value of 14.1°C in 2013, to 16.5°C in 2014 (from 13.7°C to 16.6°C considering 3 winter months period). Again, the total difference measured after the intervention is the result of the increase of 10.5°C between the external wall surface and the mortar layer, combined with a further increase of 6.0°C between the mortar layer and the internal surface. In conclusion, the application of the mortar layer resulted in an increase of the average temperature difference between the external and internal wall surface of 4 and 1.2 times respectively in summer and winter.

Thermal comfort

The desired thermal environment may be selected among three different categories defined by the standard (ISO, 2005), as described in Table 4.

Figure 31 and Figure 32 show the PMV trend in January and in August respectively; in each graph, the values before and after the intervention are compared. The comparison between the PPD values (%) calculated before and after the intervention in the same periods are reported in Table 15.

Based on the three categories indicated in Table 4, the Güttinger room in winter period could be ascribed to category B before the application of the mortar, being the PVM in the range ±0.5 and the PPD of 6 % for the 100 % of occupancy hours. After the intervention, the conditions inside the room changed to category A, with a PMV in the range ±0.2 and PPD of 5% (Table 15).

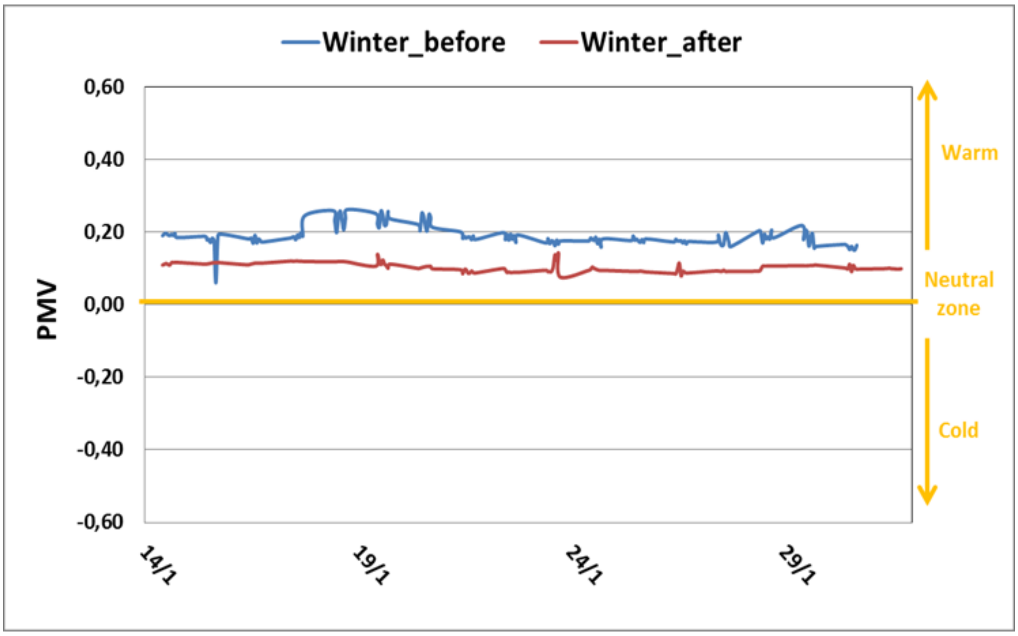

FIGURE 31 - PMV TREND BEFORE AND AFTER THE INTERVENTION DURING WINTER

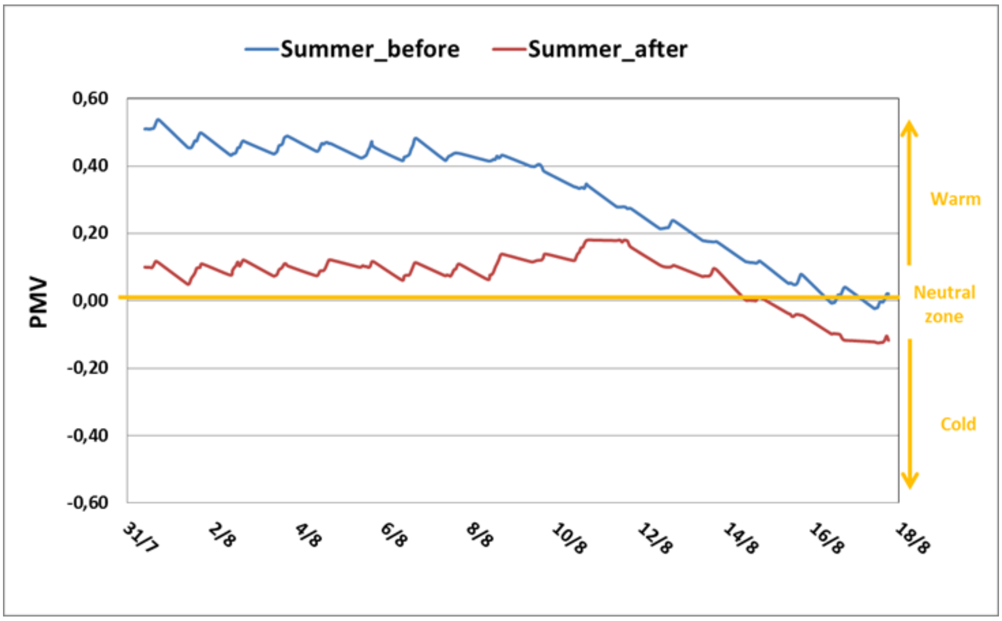

FIGURE 32 - PMV TREND IN AUGUST BEFORE AND AFTER THE INTERVENTION

CATEGORY	WINTER BEFORE		WINTER AFTER	
	% hours	% hours	% hours	PPD (%)
A	78	100	100	5
B	100	0	0	0
C	0	0	0	0

TABLE 15 - PMV AND PPD RESULTS IN WINTER BEFORE AND AFTER THE INTERVENTION

If the analysis of the winter period is extended to three months (December-January-February), the PMV and PPD are included in category A both before (91% of occupancy hours) and after the intervention (100 % occupancy hours). These results indicated a high indoor thermal stability in winter due to the activation of the heating system.

A greater difference was found before and after the intervention in August, because according to PMV and PPD values, the room condition changed from category C to A (Table 16). In fact, the PVM value was in the range ±0.7 and the PPD was 8 % before the intervention, whilst a PMV of ±0.2 and a PPD value of 5% were calculated after the mortar application, both for the total time of occupancy.

CATEGORY	SUMMER BEFORE		SUMMER AFTER	
	% hours	% hours	% hours	PPD (%)
A	28	5	100	5
B	95	8	0	0
C	100	8	0	0

TABLE 16 - PMV AND PPD RESULTS IN SUMMER BEFORE AND AFTER THE INTERVENTION

Local thermal discomfort conditions were not observed in the Güttinger room neither before nor after the intervention. In fact, the index value of the discomfort due to draught (DR) was less than 10 % both before and after the intervention, in the two seasons; hence, it can be referred to category A (Table 4). In winter, the average value of DR is 2.5% before the intervention and about 2.6% after the intervention. The same difference was calculated in summer, with a DR average value of about 2.3% before and about 2.4% after the intervention. Furthermore, very small temperature differences were measured between head and ankles, resulting in a very low DP (about 1%).

Thermal conduction and transmittance

Two similar external temperature profiles were chosen to compare the trend of the heat flux and of the inner surface temperature. The presence of the insulating ISOCAL mortar produced an increase of the internal surface temperature and a decrease of the heat flux.
Before the intervention, the value of the thermal conductance was 1.146 $Wm^{-2}K^{-1}$; after the intervention, it was 0.656 $Wm^{-2}K^{-1}$ with an improvement of 40%.
Before the intervention, the thermal transmittance was 0.964 $Wm^{-2}K^{-1}$; after the intervention, it was 0.608 $Wm^{-2}K^{-1}$ with an improvement of 37%.

Energy consumption for heating system

The energy consumption was measured in relation to the working of the heating devices during one week (28/02 – 07/03/2014 before the application of the mortar and 13/12 – 20/12/2014 after the intervention). Before the intervention, the weekly average level of electrical demand was around 341 W, with maximum peak of 404 W; after the intervention, it was reduced to 278 W on average, with maximum peaks up to 334 W. Moreover, in the weeks selected for comparison, the data collected by the energy metering indicated a consumption of 61.33 kWh before the intervention, which decreased up to 50.1 kWh after the application. A reduction of the 18% energy consumption in one week was achieved due to the presence of the insulating ISOCAL mortar.

2.4 RADIANT COATING

2.4.1 RADIATION SELECTIVE COATINGS

Two different types of radiation selective coatings, both mainly based on semi- and metal oxides, were developed (Becherini F., 2018) (Casado M., 2014):

- Coating 1: Infrared absorbing coatings, synthetized via sol-gel methodology, which nanoparticles mainly absorb and rarely diffusely reflect the IR radiation
- Coating 2: Infrared reflective coatings, synthetized on water base solution and/or ethanol solution, which nanoparticles have high reflectivity properties, thus the coating repels most of the thermal radiation, avoiding the transmission of the heat to the substrates (walls, roofs…).

The primer selected to ensure the reversibility of both coatings was Paraloid B-72: it is a thermoplastic acrylic resin (ethyl-methacrylate copolymer), with excellent adhesive properties, durable and non-yellowing.

2.4.2 ISTANBUL CASE STUDY

2.4.2.1 CASE STUDY BUILDING

The building selected for the demonstration is located in Kallavi Street (Figure 33), in Beyoglu District and is owned by Beyoglu Municipality. It consists of five floor and was refurbished recently (2014/2015).

FIGURE 33 - ISTANBUL CASE STUDY: BUILDING IN İSTIKLAL CAD. KALLAVI SOK. NO.5
(IMAGE COURTESY OF ACCIONA INFRASTRUCTURES S.A.)

Initially, it was planned to apply the coating on the main façade of the building facing North. Later, as a result of a deeper knowledge of the building features, two main objections to the initial plan were found. Firstly, despite the reversibility of the coating demonstrated in laboratory, it was pointed out that due to the quality of the substrate of the case study building (its porosity, roughness and the ageing of the top surface), it seemed impossible to apply any coating on its façade, as complete removal cannot be guaranteed. Secondly, the demonstration building has large window openings so the wall surface area is limited and interior walls are very thick, hindering the proper performance of the coating (Gouas, et al., 2015).

For all the above reasons, it was agreed to place samples of coated and uncoated substrates (Istanbul stones, lime mortar and metal plates) on the roof of the demo building.

2.4.2.2 MATERIAL APPLICATION AND MONITORING SYSTEM INSTALLATION

Eight lime mortar samples and eight Istanbul stones were mounted in two timber frames. The timber frames were primed, painted white and weather sealed. Samples were glued with epoxy resin to the frame and then covered all the gaps with silicone to avoid water penetration. Also, five metal plates were prepared.

The samples were treated as follows (Figure 34):

- **R1 , R2:** two reference samples, non-coated
- **P1, P2:** two samples both painted with Paraloid B72 only
- **S1.1, S1.2:** two samples painted with Paraloid B72 and two layers of coating 1
- **S2.1 , S2.2**: two samples painted with Paraloid B72 and two layers of coating 2

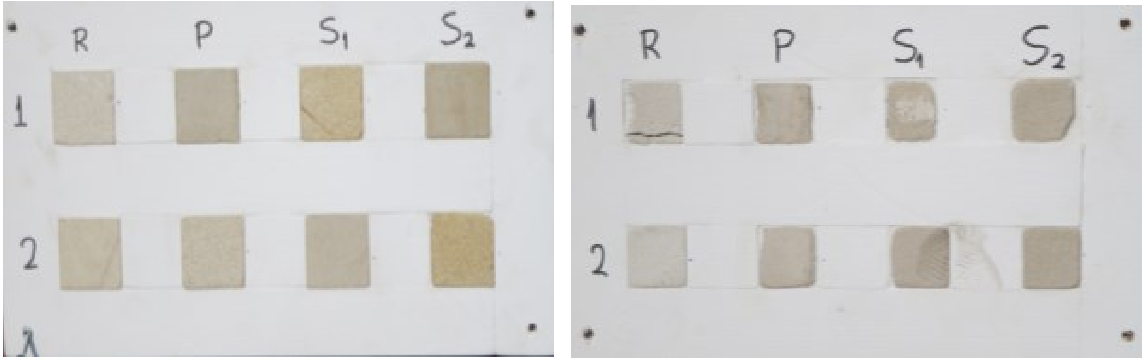

FIGURE 34 – ISTANBUL STONES (LEFT) AND LIME MORTAR SAMPLES (RIGHT)
(IMAGE COURTESY OF ACCIONA INFRASTRUCTURES S.A.)

The five metal plate samples were treated as follows (Figure 35):

- **S_1 white:** white primer, Paraloid B72 and two layers of coating 1
- **S_2 white**: white primer, Paraloid B72 and two layers of coating 2
- **R white:** reference white primer and one layer of Paraloid B72
- **R grey**: reference grey primer and one layer of Paraloid B72
- **S_1 grey**: grey primer, Paraloid B72 and two layers of coating 1

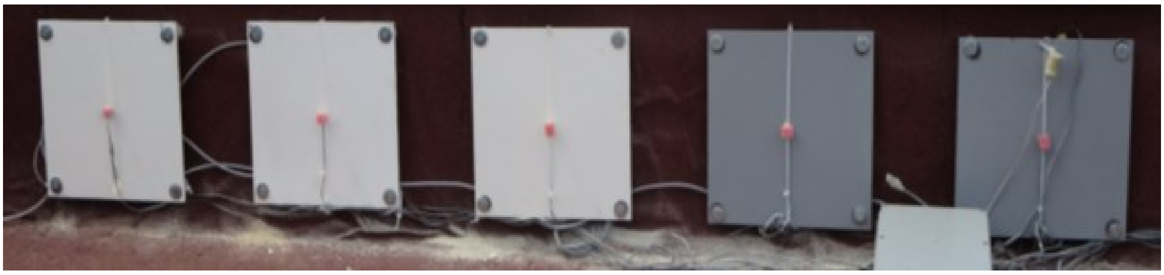

FIGURE 35 – METAL PLATE SAMPLES WITH SENSORS INSTALLED
(IMAGE COURTESY OF ACCIONA INFRASTRUCTURES S.A.)

Samples and sensors installation was made in parallel in August 2015. Metal plates and wooden frames were fixed in the roof, in the parapet wall facing East.

The monitoring system consisted of air temperature, relative humidity and about 24 surface contact temperature sensors. Contact temperature sensors were mounted on the front and the back of each metal plate and on the backside of the Istanbul stones and lime mortar samples. The relative humidity and air temperature sensor was installed on one of the metal plates. The sensors were protected from extreme temperature changes with insulation foam.

Additionally, a weather station was installed on a pole located in the roof of the building to measure wind velocity and direction, solar radiation, precipitation, relative humidity and temperature.

2.4.2.3 DATA ANALYSIS AND RESULTS

The following features were evaluated:

- Thermal performance
- Durability
- Reversibility

The thermal performance of the coatings was evaluated by analysing the data of surface temperature and solar radiation recorded during the continuous monitoring campaign (22/08/2015 - 12/01/2016).

The durability of the coatings was assessed by visual and scanning electron microscopy (SEM) inspections before and after 9 months of exposure (Casado M., 2016). Please note that although the monitoring system was shut down at the beginning of January 2016, the samples continued to be exposed outdoors until the end of May 2016.

The reversibility of the samples was validated through scanning electron microscopy with energy dispersive X-ray spectroscopy (SEM/EDX) analysis of all the samples before and after being cleaned (Casado M., 2016).

Thermal performance

Analysing the data obtained at the front of the metal plates, it resulted that the temperature depended on the colour shade of the metal plate. Indeed, the samples painted with grey primer reached a maximum temperature of 41.5°C, while the white ones reached 50.6°C at the highest.

Looking at the back of the metal plates, the temperature of Cool 1 white was lower than Reference white. Similar trend was observed at the back of Cool 1 grey, which temperature was less than Reference grey, especially during medium-low irradiated days. On the contrary, the back of Cool 2 white showed higher temperatures than the Reference white.

To get a better picture of the thermal performance of the coatings compared to the references, the difference of temperature (ΔT) between the front and backside of the sample and reference plates was evaluated. It resulted that ΔT of Cool 2 white was lower than ΔT of Reference white, which means that Cool 2 behaved as an absorbing coating. On the contrary, ΔT of Cool 1, both white and grey, was higher than ΔT of Reference, which means that Cool 1 behaved as a reflective coating. The same was observed by analysing the difference between the $\Delta T_{reference}$ and the ΔT_{sample} in summer, autumn and winter: the coating with IR reflective performance should give y values <0, which means $\Delta T_{reference} < \Delta T_{sample}$. According to the results, Cool 1 (both grey and white) behaved as a reflective coating while Cool 2 white behaved as an adsorbing coating. Moreover, Cool 1 white showed the best performance during summer (high irradiated days), while Cool 1 grey showed the best performance during winter (low irradiated days).

- Cool 1 white temperature reduction: - 4.8°C − -1°C
- Cool 1 grey temperature reduction: -3°C − -0.5°C

It is confirmed that the reflectance depends heavily on the colour shade of the substrate.

Concerning the Istanbul stones, the difference between the backside of the sample and the reference was calculated to get an overview of the thermal performance and to calculate the reduction of temperature due to the reflective property of the coatings.

All the samples studied showed a similar trend. The range (maximum and minimum) of the temperature reduction of each sample, due to the reflectivity, is exposed below:

- Paraloid temperature reduction : -1.3°C − -0.5°C
- S1 temperature reduction: -1.6°C − -0.5°C
- S2 temperature reduction: -2.7°C − -0.5°C

The thermal performance of the coatings on the lime mortar substrates was evaluated following the same approach as the Istanbul stones samples. In this case, the range of the temperature reduction (maximum and minimum) of each sample was the following:

- Paraloid temperature reduction : - 1.5°C − -0.5°C
- S1 temperature reduction: -2.0°C − -0.5°C
- S2 temperature reduction: -3.0°C − -0.6°C

The results obtained for the Istanbul stones and the lime mortar samples are very similar. In both cases the coatings behave as reflective coating and the temperature reduction ranges from -0.5°C to -3.0°C approximately.

2.4.2.4 DURABILITY

Figure 36 shows the aspect of samples at month 0 (M0) and after 9 months (M9) of outdoor exposure: no signs of deterioration were observed with the visual inspection. This result was confirmed by SEM analysis (Casado M., 2016).

FIGURE 36 - PHOTOGRAPHS OF ALL THE SAMPLES AT M0 (TOP) AND M9 (BOTTOM)
(IMAGE COURTESY OF ACCIONA INFRASTRUCTURES S.A.)

2.4.2.5 REVERSIBILITY

In order to evaluate the reversibility of the coatings, the surface topography of all the samples was analysed by SEM before and after the cleaning/removal of the coatings from the substrates, taking into account the different composition of substrates, white/grey primer, Paraloid B72 and coatings S1 and S2 (Table 17). The cleaning was done with acetone using a brush and tissue, with the aim to remove only the transparent coatings and not the white/grey primer.

	Carbon (C)	**Oxigen (O)**	**Calcium (Ca)**	**Titanium (Ti)**	**Silica (Si)**	**Indium (In)**
Metal plate	X				X	
Istanbul stones	X	X	X			
Lime mortar samples	X	X	X			
White/grey primer				X		
Paraloid B72	X					
Coating S1, S2	X					X

TABLE 17 - MAIN REPRESENTATIVE CONSTITUENTS FOR EACH SUBSTRATE AND COATING

The results can be summarised as follows:

- Metal plates: the coating is removed if the concentration of C and In decreases and the amount of Ti and Si increases. The coatings were removed from all the samples, except Cool 2 which were only removed partially, maybe due to a poor cleaning;
- Istanbul stones: the coating is removed if the concentration of C and In decreases and the amount of Ca and O increases. The coatings were removed from all the samples;
- Lime mortar samples: similarly to the Istanbul stones, the coating is removed if the concentration of C and In decreases and the amount of Ca and O increases. The coatings were removed from all the samples, except S2, which probably needed a second cleaning.

CONCLUSION OF SECTION A

The first important results achieved was related to the practical application of phase change materials embedded in construction materials as a possible solution to decrease the thermal stresses on old paintings and canvas in presence of temperature variation.

The PCMs potential of storing thermal energy and thus of buffering thermal fluctuations when incorporated in gypsum panels and silicon coatings was investigated both in laboratory and in the field; PCMs in different forms (powder and emulsion) and with different melting points (21°C and 26°C) were considered.

Laboratory tests showed in general a reduction of the highest temperature and an increase of the lowest temperature reached by the materials containing PCMs, as well as a delay in the time to get to these values both in the heating and cooling processes. Similar results were obtained in the many thermal cycles performed, concluding that the thermal behavior of the samples is reproducible. This is an important advantage in order to increase the durability of Cultural Heritage.

However, the most interesting and innovative result of the research performed was an important drawback related to the use of PCMs when applied to heritage objects.

In fact, the application methodology tested - PCMs incorporated in gypsum panels placed in contact with a wooden panel used as test material simulating a painting – has revealed not sustainable for CH conservation, as it increases the thermal gradient between the internal and external surfaces of the wooden panel. Even if the measured gradients were not so important in their absolute values, we have to take into account that heritage objects are more sensible to thermal shocks and that the effects are strongly dependent on the time scale. In fact, even if a phenomenon is not particularly important in the daily timescale, it will certainly bring about notable and irreversible dangerous effects over the centuries.

All the results obtained in laboratory were confirmed by the monitoring of model samples in a heritage building, the S. Croce Museum in Florence (Italy). In both cases, the effectiveness of PCMs as thermal energy storage materials was confirmed as well as the drawback of increasing the thermal gradients between the front and back (in contact with the PCMs) surfaces of the objects monitored.

Further tests on the field showed that this drawback can be avoided by increasing the distance between the object and the panel containing PCMs.

In conclusion, the effectiveness of the PCMs in decreasing the heating rate, the time during which the object is subjected to high temperatures and the maximum thermal value reached by the object was confirmed. These effects strongly depend on the experimental conditions, such as % of PCMs to be included in the substrate, typology and size of the substrate and of the object, microclimatic conditions and volume of the environment, and so forth.

In the Cultural Heritage field, different methods of application of PCMs should be evaluated, but particular care has to be taken in the use of materials with PCMs incorporated in direct contact with heritage objects. This application is in general not recommended, because of the risk of thermal stresses at the front and back surface of the object and consequently of mechanical damage.

In order to overcome this drawback, the object should be placed at a certain distance from the material containing PCMs. Then, the relation between the heat storage of the PCMs and the thermal gradient between the front and the back sides of the object should be studied in order to find the distance corresponding to the best compromise to get maximum heat storage and less thermal gradient. Parameters that could be optimized are the weight percentage of PCMs or the thermal conductivity of the substrate containing the PCMs.

Another important topic addressed was the testing in field of new insulating materials and the evaluation of their impact on energy saving and indoor thermal comfort. The results demonstrated the applicability of new effective solutions for building envelope retrofitting that properly fit into the current background of energy efficiency and environmental sustainability needs, next to the respect of all those aspects connected to the conservation of ancient buildings.

Every innovation developed and tested at laboratory scale should be further demonstrated in practical case studies. Thus, the importance of the validation of these new products in real-world conditions and the evaluation of the related improvement over time through monitoring activities. Finally, in the specific case of historical buildings, also the reversibility should be guaranteed, along with the criteria of compatibility.

In this thesis, the applicability and performance of three innovations were demonstrated in as many demonstration sites:

- Blown-in aerogel for use in cavities behind existing wall finishes in a traditional tenement building located in the Yorker district of Glasgow (United Kingdom);
- New thermal insulation mortars for indoor use as plaster and outdoor use as render in the Benediktbeuern Monastery (Germany);
- Radiant reflective coatings for external application in a historic building located in Kallavi St, Beyoglu District, Istanbul (Turkey).

First of all, a comparison between the conditions with and without the innovation was performed in order to understand qualitatively and quantitatively the improvements. The comparison was carried out in two ways:

- By monitoring the parameters simultaneously in a test area and in an equivalent unmodified reference area, with the same boundary conditions and physical characteristics, to enabling the analysis of data in the same period of time;

- By monitoring the parameters in the same area but before and after the intervention. In this case, it was necessary to compare the data from the two different periods with similarly outdoor weather conditions.

All the variables that can influence the behavior of the materials constituting the building envelope were carefully analyzed: climate, location in the urban settlement, orientation, direct impact of solar radiation, shape of the building ensemble, typology and constructional materials of the walls, thickness of the walls, percentage of area covered by windows, and type of windows.

Afterwards, the performance of innovations was proved in terms of improvements to indoor comfort and reduction of energy consumption. On one side, energy consumption could be easily monitored by measuring the electric input power, while energy saving could be calculated from the associated costs. On the other side, the evaluation of people thermal comfort includes several indicators: some objectively and measurable performance indicators, as well as human thermal sensations related to the thermal balance of the body, which are influenced by physical activity and clothing as well as the environmental parameters. These aspects are summed up in the predicted mean vote (PMV) indicator and in the maximum percentage of persons dissatisfied (PPD) for the human body as a whole, and for local thermal discomfort conditions due to draught, vertical temperature gradient, radiant asymmetry, warm/cool floors. For the determination of PMV and PPD, the following parameters were measured: air temperature, relative humidity, surface temperature of walls, air velocity, and mean radiant temperature or operative temperature (measured by a globe-thermometer).

In the following, the main conclusions drawn from each case study are given.

Glasgow

Thermal performance	The results demonstrated the thermal insulation ability of the aerogel. The difference of temperature between in and out in the test room was about 1°C higher in air and 1.5-2°C on the surface than the reference room. This behavior was also confirmed by the thermographic measurements. In addition, an improvement from 79% to 82% was found for the thermal conductance and from 72% to 76% for the transmittance.
Thermal comfort	The calculated PMV value was far away from the neutral sensation zone both in the reference and the test rooms. Nevertheless, the installation of the aerogel resulted in an improvement of the internal conditions of about 40%. The PPD values were 37% and 33% in the reference and test rooms respectively.
Reversibility	The cavities of the walls were clean after the reversibility trial, probing that the Spacefill aerogel can be sucked out easily.

Benediktbeuern

Thermal performance	The thermal insulation of ISOCAL mortar resulted in the warmer temperature of the wall surface, the improvement of the conductance and transmittance (40% and 37% respectively), as well as a reduction of the energy consumption (60 kWh before intervention vs. 50 kWh after intervention).
Thermal comfort	A higher indoor thermal stability was found in winter due to the activation of the heating system. In August, the PMV and PPD values indicated that the room condition changed from category C to A after the mortar application. Local thermal discomfort conditions were observed neither before nor after the intervention.

Istanbul

Thermal performance	The results obtained for the Istanbul stones and lime mortar samples were very similar. In both cases, the coating behaved as a reflective coating and the temperature reduction ranged from -0.5°C to -3.0°C.
Durability	No signs of deterioration of the coated samples were found after 9 months of outdoor exposure.
Reversibility	Most of the coatings were easily removed with acetone in all the substrates under study.

SECTION B – APPLICATION OF ARCHAEOMETRICAL IMAGE TECHNIQUES TO OTHER DISCIPLINES

Schlieren technique for full-scale ventilation studies

The patterns of airflow are central to almost everything associated with HVAC. However, since these patterns are normally invisible, it is difficult to know how the airflow is behaving and the possibility of error is significant. Most traditional flow viewing methods involve seeding the air with tracer particles, which are not keyed to thermal differences in the flow, so what one observes often depends upon the way the particles were introduced. However, there is another approach that is keyed to thermal differences in the flow. Optical flow viewing involves no tracer particles, but passes a light beam through the flow and then examines this beam for distortions caused by temperature differences. This works because the optical refractive index of air varies linearly with temperature.

The Schlieren technique is not normally used in routine HVAC airflow studies because of the scale of the test area: it requires a precise lens or mirror of the same size as the flow-field under study, which is impractical for full-scale ventilation flows.

For example, Figure 37 shows a schlieren photograph of the warm air rising from the body of a teenage girl, made visible using a parabolic telescope mirror 1 m in diameter. Although this mirror is part of one of the largest conventional schlieren optical systems available, it is obviously still too small and not portable enough for full-scale ventilation work. Scale-model schlieren studies have been done, but are of limited use due to concerns about modelling and scale-up accuracy (Settles G.S., 1997).

FIGURE 37 - SCHLIEREN PHOTOGRAPH OF THE HUMAN THERMAL BOUNDARY LAYER OF A TEENAGE GIRL ACQUIRED WITH A PARABOLIC TELESCOPE MIRROR 1 M IN DIAMETER (SETTLES G.S., 1997)

An important improvement on the original concept was the complementary grid-focusing schlieren system, originally described by R.A. Burton in 1949 (Burton, 1949). Burton's technique relied on the same edge filtering concept but instead of using collimated light, it images a background grid pattern onto a complementary opaque cut-off filter such that the filter edges lie along the edges of a light-dark edges of the pattern, while the target object is imaged in a different plane by the camera objective.

As diagrammed in Figure 38, one wall of a large room is covered with a uniform "source" grid made of parallel black and white lines. At the other end of the room, a lens forms an image of this grid on a sheet of photographic film placed in the cut-off position. When the film is exposed, developed, and placed precisely back in position, it is an exact negative of the image of the source grid, with dark lines matching the white lines of the source, so little light gets past it.

If one now heats the air locally in the test area, halfway between the lens and source grid, some light rays are refracted or bent by thermal gradients in the air. The exact correspondence between the negative cut-off grid and the image of the source grid is now spoiled. This causes some gridlines to shift so that light gets past the cut-off grid to form a schlieren image of the test area, which can be observed in real time. The light, which thus gets past the cut-off grid, corresponds to zones in the test area where temperature differences occur (Settles G.S., 1997).

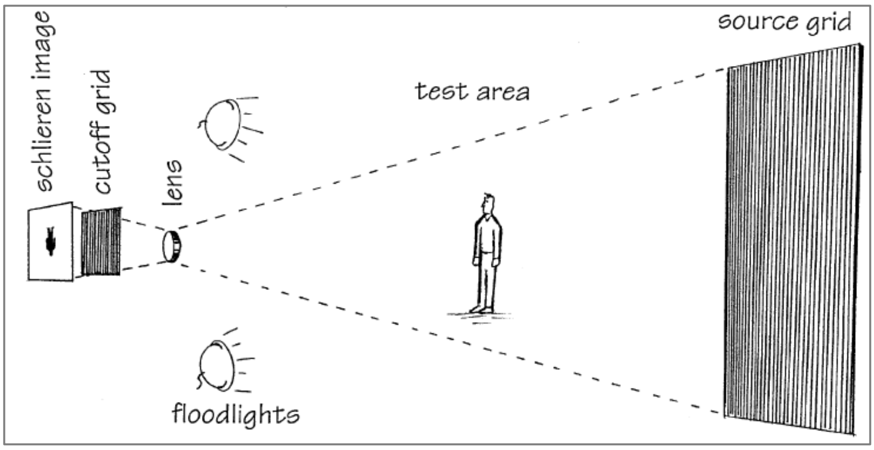

FIGURE 38 - DIAGRAM OF FULL-SCALE SCHLIEREN OPTICAL SYSTEM (SETTLES G.S., 1997)

The focusing approach generally allows for obtaining schlieren imaging through much larger areas without using the excessively large optics that make classical schlieren prohibitively expensive and difficult for large fields of view. Focusing schlieren approaches thus generally require less expensive equipment than traditional collimated-light schlieren systems and can more easily be scaled up to cover large areas, though previous approaches have still tended to be difficult to set up and align.

The main challenge with focusing schlieren lies in the fact that the cut-off grid and the background grid have to be very precisely matched to get good sensitivity. This makes the system very sensitive to misalignment and aberrations in the optical system.

Several trials have been performed to study the airflows associated to: commercial kitchen ventilation, indoor ventilation and air distribution, thermal boundary layer of the human body and linked IAQ researches (Figure 39) (Settles G.S., 1997).

Further interest in this technique can be found to study laboratory fume hoods, refrigerated grocery display cases. Moreover, hospital ventilation schemes, like the flow recirculations caused by large overhead lights, could benefit from schlieren technique. Similar ventilation problems occurring in cleanrooms have already been studied using conventional schlieren optics (Settles G.S. and Via G., 1986).

Figure 39 - Full-scale schlieren photograph trials. a) A shopper removing a frozen pizza from a chest-type grocery store freezer; b) a domestic room with person, lamp and electric space heater; c) a commercial kitchen griddle and exhaust hood in use with cooking fumes (Settles G.S., 1997)

Finally, the Schlieren technique could be helpful to validate computational simulations to predict complex airflow patterns. Indeed, since HVAC airflows are mainly turbulent, such computations remain approximate. Local validation by way of checking a few points with a velocity probe can be misleading. Global validation, in terms of the realism of the overall computed flow pattern, can now be done by direct comparison with full-scale airflows displayed by the schlieren technique.

In the late 2000s, NASA scientist Dr. Leonard Weinstein developed a new concept for generating the background grid wherein it was projected onto a screen through a grid and optical system identical to the cut-off grid and camera optical system (Weinstein L.M., 2010). This pair of identical optical trains ensures that the projected grid and cut-off grid experience the same optical aberrations (Figure 40).

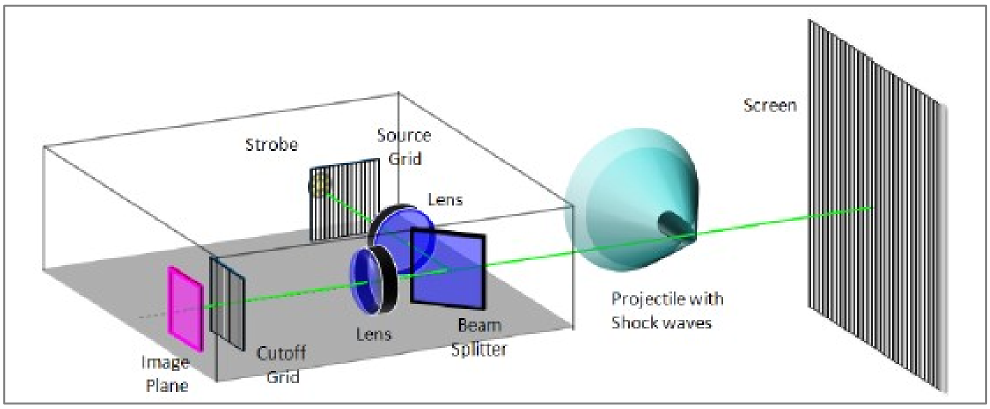

FIGURE 40 - DIAGRAM OF A FOCUSING SCHLIEREN SYSTEM (SPECTABIT OPTICS LLC.)

One of Spectabit Optics LLCs founding scientists, Dr. Drew L'Esperance, led an effort at MetroLaser Inc. to develop and test Dr. Weinstein's design concept, which led to the original Analog Schlierenscope, now a product available from Spectabit Optics LLC (Spectabit Optics LLC).

While at MetroLaser, Spectabit cofounders Dr. L'Esperance and Dr. Ben Buckner developed a new digital variant of Burton's focusing schlieren approach, Digital Focusing Schlieren, which retains one analogue cut-off grid, allowing for high sensitivity, but replacing the background grid with a digitally generated image, from either a digital projector system or a digital display system (Spectabit Optics LLC.). This patented approach (US 9-232-117-B2) allows software control to take over the task of aligning the grids and compensating for aberrations, resulting focusing schlieren system far less complex and more flexible than the analogue system.

Based on this patent, the Spectabit’s Portable Projection Schlieren System was developed, which employs a digital projector to project a pattern of lines onto a screen behind the object. The screen reflects the light back into the sTube™ optical system, where it passes through a cut-off filter before it reaches the camera sensor.

Notwithstanding the large literature and the equipment developments related to such a system, and considering the optical theory at the basis as explained in the dedicated chapter of this thesis, this approach can be more properly linked to shadowgraph rather than Schlieren technique.

Schlieren technique for particle bearing and human airflows studies

Previous studies on the display of airflow patterns have used techniques involving the use of tracer particles or gas with laser light illumination. As these methods are hazardous to humans, they have been applied to various types of manikins rather than human volunteers. Whilst the conclusion from these models have been useful, there is always the remaining question of how these airflows behave when generated by actual human volunteers. Airflow patterns of coughing human volunteers of different ages, with and without the wearing of various face masks, have been investigated elsewhere using this schlieren principle with a large 1 m-diameter, modified, parabolic mirror (Tang J.W., 2009) (Tang J.W., 2009). However, the paper by Tang et al. (Tang J.W., 2011) is the first description of a modern, large, spherical, concave mirror, specifically designed and constructed for this specific purpose of displaying exhaled human airflows.

In this study, from qualitative schlieren and shadowgraph imaging experiments, airflow patterns were displayed that were associated with common, everyday respiratory activities (such as quiet breathing, whistling, laughing, talking and sneezing) to demonstrate the generated exhalation flows. The effectiveness of various interventions (e.g. putting hands and tissues across the mouth and nose) to limit the spread of potentially infectious droplets in coughs and sneezes, thus to reduce the potential transmission of airborne infection were also investigated thanks to these imaging techniques.

Another interesting field of application of schlieren imaging is well represented by the study of airflow patterns in clean rooms. Contamination resulting from airborne particulates is one of the largest contributors to yield loss in microelectronics manufacturing. In order to reduce such contamination and thus promote reasonable yields, vertical laminar flow (VLF) clean rooms are used. In such installations, filtered air enters through the entire ceiling and it is then exhausted through a perforated, raised floor, whence it is recirculated through the ceiling HEPA (high efficiency particulate air) filters. With proper design, the particle count in the air entering the room from the ceiling can be kept below 1 μm-range particle/cubic meter/minute. We remind that such small particles are especially susceptible to Brownian motion and motion due to thermal and electrical gradients (whereas gravitational settling is a key deposition mechanism for large particles).

Notwithstanding, clean room flows are transitional or turbulent rather than laminar, except under ideal conditions. The human body is a prime contamination source, whilst tool-induced secondary flows may cause additional problems to airflow distribution, possibly allowing the trapping of contamination generated by the tools themselves or by human operators. Despite this, the proper integration of such strong secondary flows with the overall airflow balance of the room does not happen automatically upon tool installation.

The paper by G.S. Settles and G. G. Via (Settles G.S. and Via G.G., 1989) examines such airflows problems in VLF clean rooms. With the aid of the schlieren observations, the problems in the clean room under test were traced and the criterion for a proper airflow balance was established, leading to a modification in the tool installation.

On the basis of this premise, the archaeometric laboratory was asked to build a traditional Schlieren system to monitor the air movements due to the functioning of the air conditioning systems, in order to enhance their operating conditions to have no impact of the airflow on the human body, in particular in hospital recovery.

Spectroscopy applied to the study of oils

As a result of the greater technological development, the field of spectroscopy applications has also expanded to the field of food research and in particular has become a powerful analytical tool in the study of edible oils and fats. Spectroscopy is a non-destructive technique that allows the qualitative determination of organic compounds; in fact, as the nature and the composition of the sample vary, the absorption bands in the electromagnetic spectrum differ in intensity and frequency values.

The absorption spectra of extra virgin olive oils have a common profile (Figure 41), determined by the presence of the components optically active in the visible region, namely β-carotene (480 nm), chlorophyll *a* (670 nm), chlorophyll *b* (645 nm). The carotenoid and chlorophyll levels depend not only on the type of cultivation and the place of production, but also on climatic conditions. Therefore, the absorption bands show slight differences in form and intensity due to the different quantity of the compounds mentioned above, and/or to the presence of sealing agents.

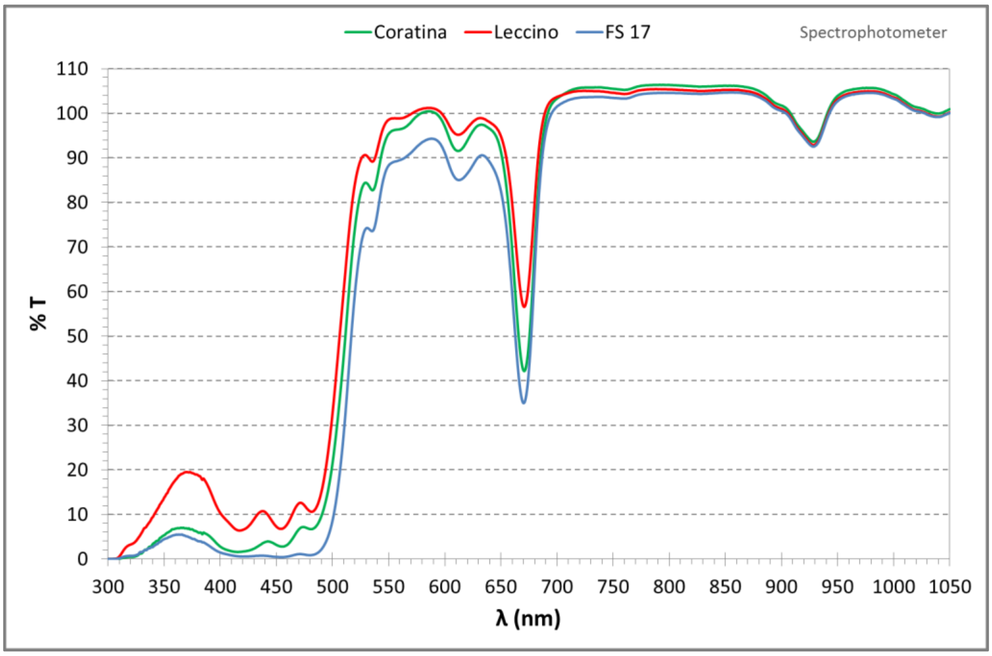

FIGURE 41 – COMMON PROFILE OF REFLECTANCE SPECTRA OF EXTRA VIRGIN OILS (MEASUREMENTS OBTAINED WITH SPECTROPHOTOMETER)

Among virgin and refined oils (e.g. oil of pomace, maize and grapeseed), there are important differences in the absorption spectra (Figure 42), particularly in the region of the spectrum within about 500 nm and in correspondence of the absorption peak at 670 nm.

Indeed, the extra virgin olive oils do not have components that absorb into the UV region, unlike refined oils. In contrast, refined oils do not have chlorophyll, responsible for the highest absorption peak at 670 nm. This distinctive, but non-discriminatory, trait identifies an extra virgin olive oil compared to a refined "pure" one. In fact, this peak can also be found in the case of olive oils, i.e. mixtures of refined oils with modest quantities of virgin oils (not necessarily extra-virgin oils). Moreover, even among the different varieties of extra virgin olive oils, there are also considerable differences, mainly due to the different composition and place of production. For example, the chlorophyll absorption is higher in oils of Tuscan and Umbrian origin than in those from Puglia or Sicily[1].

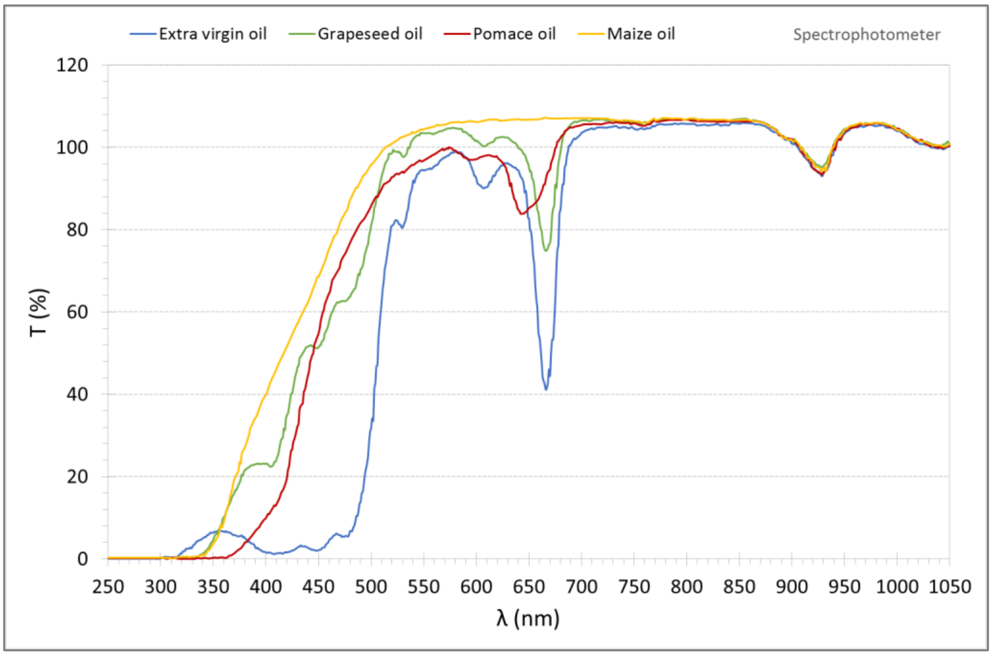

FIGURE 42 – REFLECTANCE SPECTRA OF AN EXTRA VIRGIN OIL AND REFINED OILS (MEASUREMENTS OBTAINED WITH SPECTROPHOTOMETER)

Notwithstanding the consolidate techniques to analyse oils and other foodstuffs available in literature, the archaeometric laboratory was asked to understand if also image spectroscopy could be a reliable technique to evaluate edible oils, being able to distinguish among different varieties of extra virgin oils or even to identify any adulteration with refined oils.

---

[1] Prof. Pasquale Catalano, Full Professor at Agricultural and Forestry Sciences and Technologies / Food Science and Technology at the University of Molise – Private communication

3 SCHLIEREN INTERFEROMETRY

3.1 HISTORICAL BACKGROUND

Schlieren imaging provide a powerful technique to view changes or non-uniformities in refractive index of air or other transparent media. The word *schlieren* itself derives from the German word *Schliere*, or *striae*, and refers to the streak-like appearance of fluid flow displayed through the system. As a dynamic and straightforward viewing tool, these systems are primarily applied to conduct qualitative visual studies. It is beneficial to use them in fluid dynamics studies because they are sensitive to changes and do not interfere with flow.

Proposed on 1672 by Robert Hooke, for over two centuries schlieren systems were typically implemented for a wide variety of non-intrusive real-time studies. Since the early 1800's, these techniques were used to study optical components in telescopes and microscopes. The first to officially recognize and present the schlieren imaging technique was August Toepler, who devised a functional apparatus for schlieren imaging as well as an in-depth procedure on how to design a simple schlieren system. During the early 20th century, Hubert Schardin conducted extensive research on the applications of schlieren imaging systems, developing numerous new techniques. Exploration within the field of schlieren imaging stagnated in the 1900's, largely due to the precise nature of constructing a Schlieren system, the exorbitant cost of creating a system large enough to study everyday objects, and the stationary nature of the system. With the rise of digital cameras and computing that are more powerful, new methodologies for studying refractive media based on schlieren optics have developed (Schardin H., 1942) (Settles G.S., 2004) (Settles G.S., 2006). Many physicists and fluid dynamics engineers applied the techniques to study striations in blown glass, inhalation in humans and animals, shock waves from aircraft, the mixing of liquids and gases, heat emanating from a system. Innovations such as background-oriented schlieren, rainbow schlieren interferometry, and synthetic schlieren imaging have built upon the fundamentals of schlieren imaging to provide less ambiguous, quantifiable studies of schlieren systems (Meier G.E.A., 2002) (Vogel A., 2006) (Atcheson B., 2009) (Hargather M. and Settles G.S., 2010) (Wetzstein G., 2011). These new applications of schlieren imaging systems have value in the fields of computer vision, biology, physics, and environmental engineering.

3.2 OPTICAL THEORY

The physical basis for schlieren imaging emerges from Snell's Law. If media is homogeneous, such as in a vacuum, or space, light travels uniformly, at a constant velocity. When encountering inhomogeneous media, such as fluids in motion, light rays refract and deflect from their continuous path, resulting in streak.

Snell's law describes how the direction of light propagation is diverted when passing through a medium to another one (Figure 43). It states that if the ray comes from a region with refractive index n_1 and enters into another medium with index n_2, the angles of incidence α and refraction β are bound by the expression:

$$n_1 sen\, \alpha = n_2 sen\, \beta$$

where

n_1 and n_2 are the refractive indices respectively of the optical medium 1 and of the optical medium 2,
α and β are the angles that the rays form in the optical means 1 and 2 with the perpendicular to the separation line between the two optical means.

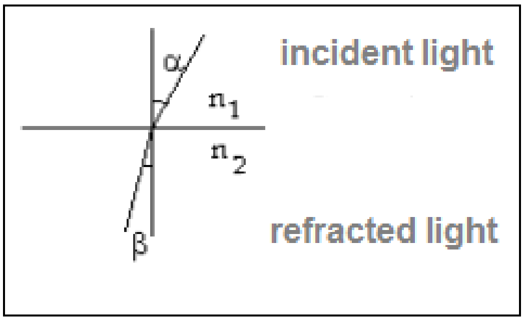

FIGURE 43 - THE REFRACTIVE INDEX

The index of refraction (n) is a dimensionless quantity which quantifies the decrease in the propagation speed of the electromagnetic radiation when it passes through a material. The decrease in the propagation speed is accompanied by the variation of its direction, according to the phenomenon of refraction.

The index of refraction (n) of an optical medium represents the ratio between the velocity of light in vacuum (c^*) and that in the medium itself (c).

$$n = \frac{c^*}{c}$$

The optical techniques used to display the flows are based on the variation of the refractive index of the fluid medium with its variation of density, as consequence of temperature/speed/compositional variations.

The index of refraction of a transparent medium is linked to the density of the substance by the equation of Lorenz-Lorentz:

$$\frac{n^2-1}{n^2+2} = \rho R(\lambda)$$

Where

$R(\lambda)$ is function of the wave length of the incident light for each substance.

The basic reason for using these techniques is their non-intrusiveness, thus obviating the problem of disturbing the flow to allow analysis.

Consider a beam of parallel rays (A) that crosses a transparent medium (B) and ends up illuminating a screen (C). In the absence of any density variation in B (air at rest, no temperature gradient), a ray of light would arrive at point P on the screen at time t with an inclination θ on the horizontal. If, on the other hand, there were variations in the density in B, the air refraction index of the test section would also vary (Figure 44).

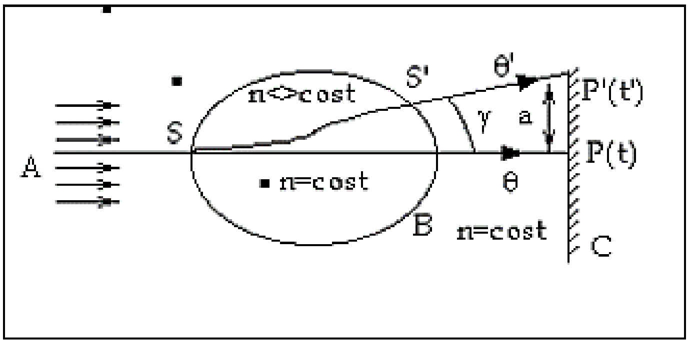

FIGURE 44 - GENERIC TRAJECTORY OF INCIDENT RAYS

In particular for the air it is:

$$n = 1 + 3 \times 10^{-4} \frac{\rho}{\rho_1}$$

Where

ρ is the punctual density of the air
ρ_1 the reference density at the pressure of 1 atm and temperature of 0°C
n the index of refraction.

The ray of light would begin to be deviated at point *S*, and follow a different trajectory, until it exits the region affected by the density variations at point *S’* with an inclination on the horizontal. The ray would then continue to go along a straight line from *S′* until it hits the screen at point *P′* at time *t′*.

The effect on the ray that passes through the gaseous medium subject to specific variations in density is threefold:

1. A variation γ of the angle of incidence of the ray on the screen equal to the difference between θ’ and θ. The technique called Schlieren is based on the detection and interpretation of this variation;
2. A variation of the point where the ray hits the screen: the ray moves from *P* to *P′* by a distance *a*. The technique called Shadowgraph is based on the detection and interpretation of this shift;
3. A difference in the optical path travelled by the ray (and therefore the time delay of the ray) from the source to the screen. The accumulated delay is equal to the difference between *t′* and *t*:
    a. The speed with which the ray of light passes through the region *B* changes due to the density gradients;
    b. The optical path that the ray of light must travel changes.

   The difference in optical path is the basis of interferometric techniques.

Schlieren technique exploits the deflection of light rays with respect to them departure direction due to density gradients (or, which is the same, to gradients of refractive index) perpendicular to the direction itself. The most rudimentary schlieren system implements a straight-line arrangement of lenses to display streak, as shown in Figure 45. A first lens focuses a parallel beam of light, emanating from a light source and passing through a slit. This parallel beam is then deflected by the subject in the test chamber and passed through a second lens, where it is focused on the knife-edge cut-off. The schlieren image is then depicted onto a screen or photographic sensor.

Figure 46 shows an example of Schlieren imaging application. The photo reveals the pattern of waves generated by a bullet passing through the plume of a candle: the different densities in the heated plume refracted the lower set of shock waves.

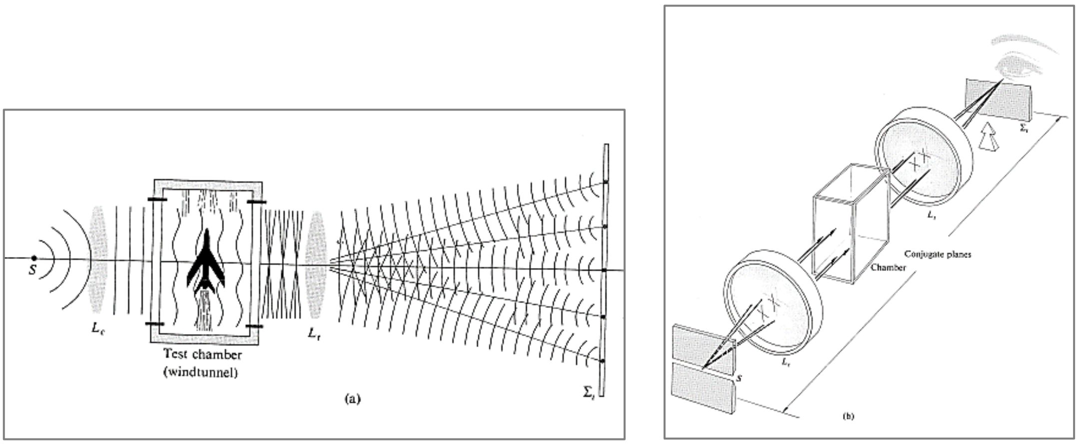

Figure 45 - A typical lens-based schlieren optics system
(Hecht E. and Zajac A., 1979)

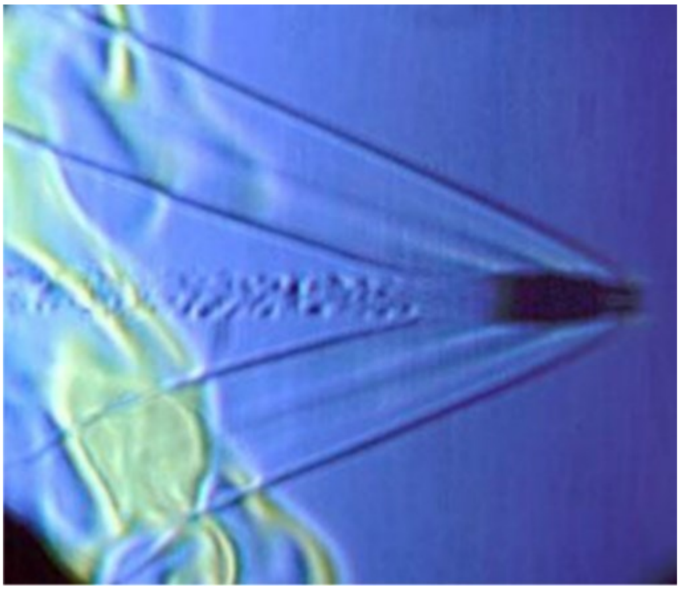

Figure 46 – Example of application of Schlieren technique to reveal the refraction of shock waves generated by a bullet passing though the plume of a candle (http://www.eng.vt.edu/fluids/msc/gallery/shocks).

Two notable methods have developed as a result of slight deviations in a conventional schlieren set-up, namely shadowgraphy and interferometry.

Shadowgraphy is an optical technique, which projects the shadow of an optical image onto a viewing plane for image capture. What is detected are the displacements of the rays with respect to the position that they would have if there were no density variations in the test section. A basic shadowgraphy system consists of a light source and a flat screen to project shadowgrams onto for observation, as shown in Figure 47. An example of shadowgraph image is given in Figure 48. Because shadowgrams are simply shadows of a schliere object, they can be magnified in accordance to their distance from the screen.

Because schlieren techniques produce actual images of the schlieren object rather than a shadow, they may seem to be more desirable to implement. Shadowgrams, however, have proven useful in that they are more easily observable and collectible. In addition, the size and flexibility of a shadowgraphy system's construction is desirable in displaying large-scale or extremely sensitive schlieren objects (Settles G.S., 2006).

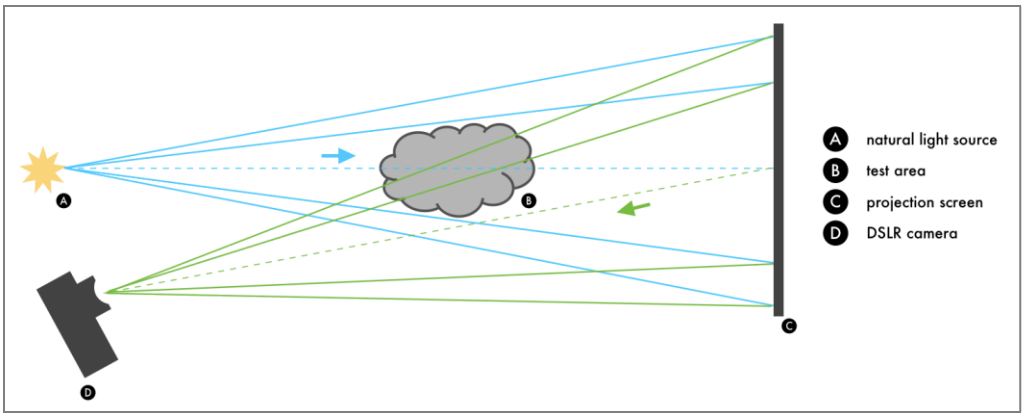

FIGURE 47 - A BASIC SHADOWGRAPHY SET-UP (MAZUMDAR, 2013)

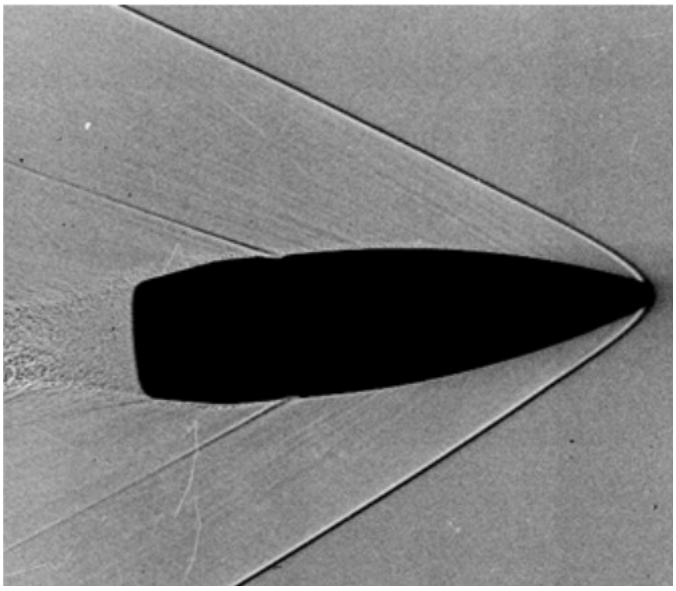

FIGURE 48 – EXAMPLE OF APPLICATION OF SHADOWGRAPH TECHNIQUE TO REVEAL THE SHOCK WAVES GENERATED BY A BULLET (HTTP://WWW.ENG.VT.EDU/FLUIDS/MSC/GALLERY/SHOCKS).

Schlieren interferometry techniques, although bearing closer ties to interferometry than schlieren imaging, does utilize some basics of the viewing technique, and should be accounted for. Schlieren interferometry was introduced and is most commonly used as a means to apply some form of quantitative analysis, thus has given rise to more efficient and informative methods of measurement. The typical schlieren interferometry system is set up like a basic two-lens schlieren system, but with the replacement of the knife-edge cut-off with some sort of prism or fine wire to induce interference or diffraction in the schlieren pattern, which can then be analysed.

3.2.1 THE IMPORTANCE OF THE KNIFE-EDGE IN SCHLIEREN SYSTEMS

Figure 49 represents a point light source S positioned in the focus of a first lens that on its right produces a beam of parallel light that crosses the test section. A second lens collects the rays coming out of the test chamber on its focal plane, showing the image of S.

In the absence of any refractive index gradient the ray hitting point A does not undergo deviations of trajectory and hits the screen at point A'. If at point A there is a variation in density and, therefore, in index of refraction, the ray will be deflected by an angle ε in the direction of the positive gradient of density, in this case in the direction of the air. This deflected ray hits the screen at the same point A'. Until now, uniform illumination is shown on the screen, even in presence of a density gradient in the test section.

Otherwise, as shown in Figure 49, a flat knife is used and positioned with the blade exactly at the focus to the right of the second lens, the screen illuminated by the point source S will be completely obscure except at point A'. In fact, the ray that hits the point A, in its deflected path exceeds the knife and reaches the screen, differently from all other undisturbed rays that find it on their path.

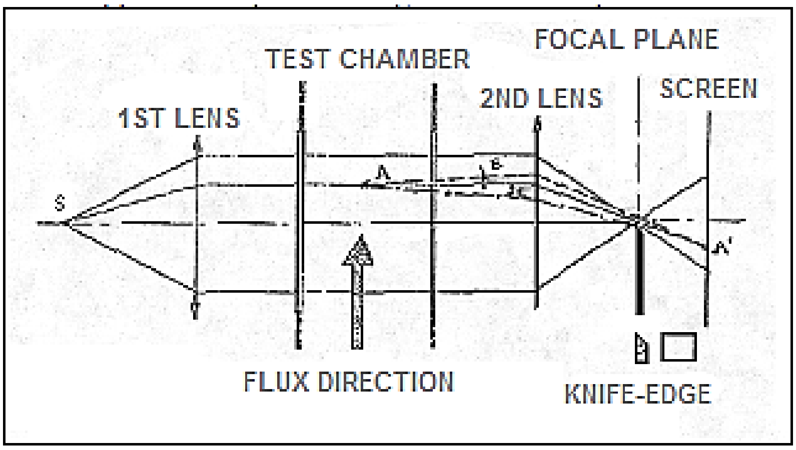

FIGURE 49 - KNIFE-EDGE EFFECT IN THE CASE OF A POINT SOURCE

Now suppose that the density gradient at point A is negative. In this case, the ray will find the obstacle of the knife before reaching the screen, as all the other undisturbed rays. The screen, then, will be completely dark.

To overcome the problem, the light source used is no longer point-like, but of finite extension (Figure 50). Every point of the new source can be thought as a point source whose rays are slightly inclined with respect to the direction of the midpoint of the source S. In this way, any point of the AB section will receive light from all the points of the source. All the rays that will hit A will illuminate A' on the screen.

Now introduce the opaque knife with the blade in correspondence of the focal plane to the right of the second lens (Figure 50). This cuts part of the incident light on the screen causing a decrease in light intensity on the screen and a variation of the luminous figure on it.

The knife-edge in the focal plane subtracts the same light intensity at all points of the screen, if there is no density variation in the test section. If instead the density gradient is present in the test section, the refraction through A will cause a deflection (equal to ε for all the rays of the source *S*) of the corresponding ray and, therefore, an increase in light intensity at point *A'*.

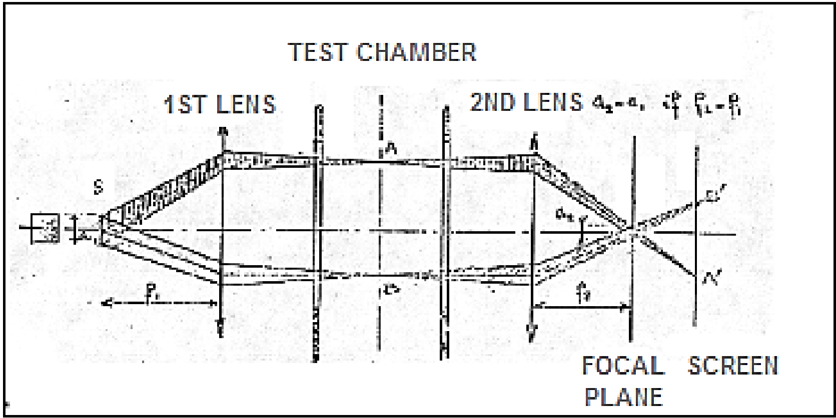

FIGURE 50 - KNIFE-EDGE EFFECT IN THE CASE OF A LIGHT SOURCE WITH FINITE EXTENSION

If you rotate the knife 180° around the focal axis of the right lens, the point *A'* will be less illuminated. If the ray, after the deflection, reaches the knife-edge, the system becomes saturated, i.e. it will no longer be possible to verify further density variations at point *A*. The saturation of the system depends on the dimension of the light source.

In conclusion, in the Schlieren technique it is important the variation of the inclination of the light rays due to the variation of the refraction index of the medium in the test section. Moreover, the technique is sensitive only to gradients that are perpendicular to the knife-edge.

3.2.2 LIMITATIONS

The most obvious limitation of the traditional Schlieren system is the size, which is dependent on the dimensions and focal length of the mirror, meaning a smaller mirror would be more compact; a compact system, however, sacrifices image size, as the image captured is dependent on the size of the mirror reflecting it. Additionally, with a system of this design, all subjects must be stationary, or small enough to move within the field of view of the system, as the system itself is not significantly flexible or portable.

Another considerable limitation is the cost of constructing a basic schlieren system. Although most of the parts can be found in any physics or optics lab, schlieren systems require high quality, polished field mirrors and lenses, as any defects in optical components can result in aberrations and distortions in the schlieren images.

3.3 SET UP AND TESTS IN LABORATORY

3.3.1 OBJECTIVE

The objective of the work was to set up a Schlieren optical system, for laboratory experiments, able to view the airflow, that is slight changes in the refraction index of the air. The final goal would be to build up a portable device to monitor the air movements due to the functioning of HVAC plants, in order to enhance their operating conditions in such a way to have no impact on the human body, in particular in hospital recovery. Indeed, it is a matter of fact that microbiological aerosol is transported within air drafts. Therefore, if HVAC systems are regulated so that the airflow hits the body of the patients, also the microbial loads affect them to a greater extent, increasing the risk of infections. On the contrary, if HVAC installations are set up in order to displace the air movements from the patients lying in bed, the risk of infections is reduced, with consequent benefits both on people health and costs of medical care. The advantage of the use of the Schlieren technique, instead of traditional fluid-dynamic studies, consists precisely in the return of an image that immediately indicates the direction of the airflow. For example, it allows to set differently the operating parameters of HVAC plants in real time, displaying immediately the effect of the change, without the need for post-date data collection and analysis or modelling.

In this thesis, the experimental work was focused to understand the potentiality of the system constructed in laboratory, i.e. to qualitatively analyse the volume of the test area and the sensitivity to thermal and density variations of air. The goal was to understand the basic conditions to work in real environments.

3.3.2 MATERIALS AND SET UP

The first trials were performed with a Helium-Neon Laser (Melles Griot, 15 mW max output, Class IIIb) as light source equipped with a pinhole, two optical lenses to collimate the light beam on a white projection screen shot by the camera. A sort of dotted effect, due to the speckle interference generated by the laser, affected the resulting images (Figure 51). Therefore, the laser as light source was discarded and substituted by a white LED light.

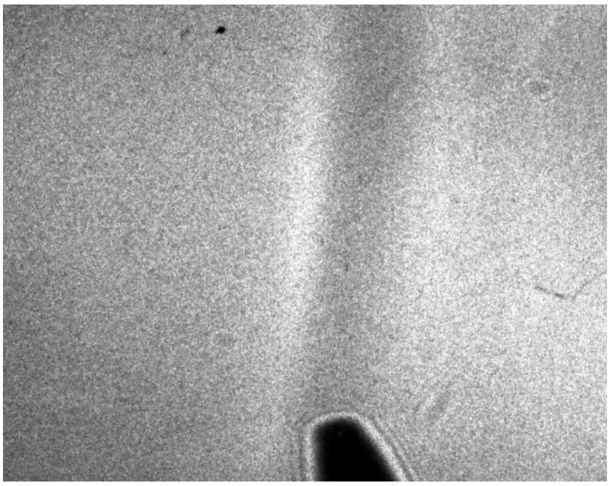

FIGURE 51 –SCHLIEREN IMAGE OF A PLUME FROM A WELDER WITH A LASER AS LIGHT SOURCE. THE SPECKLE INTERFERENCE OF THE LASER IS VISIBLE IN THE WHOLE IMAGE BACKGROUND

Since the Schlieren effect was still not so evident, the second step was to change the configurations by removing the projection screen and acquiring the images directly from the lenses with the camera, after adjusting the knife-edge position and the focus of the camera.

Finally, the ultimate set up was constructed as a single-mirror coincident schlieren system, instead of the lenses, mounted on an optical bench to ensure static positioning of the components. The system implemented the white LED light (Cree LED Bailong, 500 lm, Luxeon 3 Watt LED bulb), the pinhole to create a point light source and a parabolic mirror (10.8 cm diameter, 86.4 cm focal length, coated with protected Aluminium) provided by Edmund Optics (for the specific features, see Table 18). Images were captured by a Thorlabs digital camera (model SC1280 G23 MCPNIR) equipped with a Nikon lens (zoom 75-150 mm, f/32-3.5).

Type	Parabolic Mirror	**Effective Focal Length (mm)**	863.60
Substrate	BOROFLOAT®	**Focal Length Tolerance (%)**	±1.5
Surface Quality	60-40	**Aperture (f/#)**	f/8
Surface Accuracy	λ/8	**Coating**	Protected Aluminium (400-2000nm)
Diameter (mm)	108.00 +1.5/-0	**Coating Specification**	R_{avg} >85% at 400 - 700nm R_{avg} >90% at 400 - 2000nm
Thickness (mm)	19.10	**Back Surface**	Ground

TABLE 18 – SPECIFICATIONS OF THE MIRROR PROVIDED BY EDMUND OPTICS (EDMUND OPTICS LTD.)

The system was assembled by first arranging the components, as outlined in Figure 54 and Figure 53. The mirror was positioned at about two times its focal length far from the light source (i.e. 172 cm). The camera was positioned on the focus reflected by the mirror, mounted on a separate tripod next to the light source. The knife-edge was a razor blade positioned exactly in front of the camera lens to “cut” half of the light at the focus point and it was mounted on a parallel and smaller optical bench to be independently adjustable.

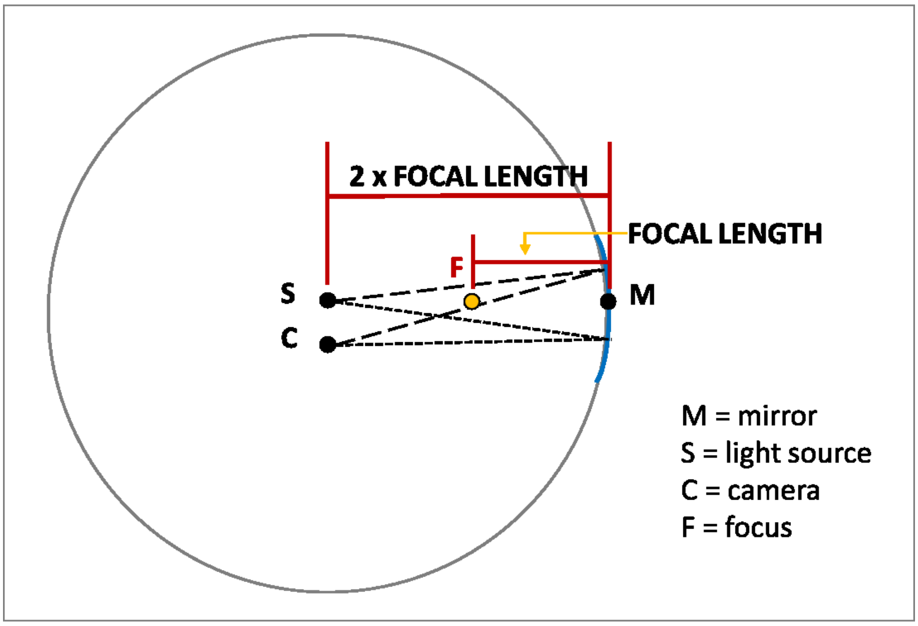

FIGURE 52 – OUTLINE OF THE POSITION OF THE COMPONENTS OF THE SCHLIEREN OPTICAL SYSTEM

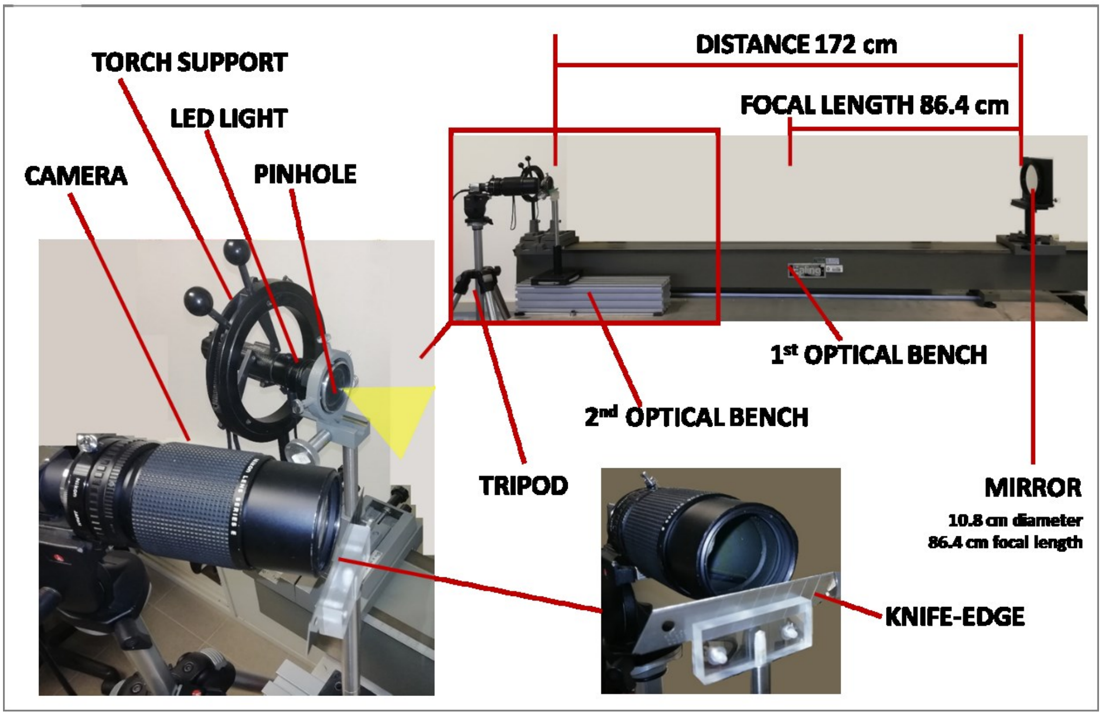

FIGURE 53 – LABORATORY SET UP OF THE SCHLIEREN OPTICAL SYSTEM

After positioning all of the components, they were then precisely adjusted for optimal results. The light was focused to avoid aberrations and misalignment of the optical components, and each of the components was carefully aligned to pass the light without interference or distortion. A test object was then introduced to the system to adjust the focus and zoom of the camera in order to ensure a proper exposure of the mirror, before introducing the knife-edge, which was last installed.

In order to obtain a uniform background and proper distribution of light, it was imperative the knife-edge be positioned exactly at the focus of the reflected light. If the knife-edge were a few millimetres closer or further from the focus, dark shadows would obscure the schlieren image, rather than uniformly reducing or increasing the intensity of the background.
Finally, by adjusting the height of the knife-edge in the image plane in order to cut the maximum zero order of diffraction, the number of schlieren rays deflected from the image increase, emphasizing the contrast between streaks in the image. This regulation was guaranteed by the mirror mount, which provided highly stable kinematic movement with two-axis tilt (pitch and roll) provided by a precise ball pivot adjustment and an orthogonal three-point suspension equipped with three pitch screws.

The acquisitions were driven by ThorCam software, which allowed changing some parameters to enhance the quality and appreciate much better the schlieren effect. The list of set parameters next to a short description (THORLABS, 2016) is given in Appendix 1.

The images were later elaborated with ImageJ software, to intensify brightness/contrast and to convert the original Multipage TIFF file into an AVI video.

3.3.3 RESULTS

The first tests were performed to display the heat “plume” from the tip of a welder (set at 150°C, the minimum temperature possible) and from the hand (Figure 54 and Figure 55 respectively).

The volume of the working area was estimated: the display of the Schlieren effect decreased considerably over 50-60 cm away from the mirror and then got lost when the focal length of 86 cm was exceeded. The maximum yield was very close to the mirror, especially when the temperature gradient with respect to air room temperature was low, i.e. in the case of the heat from the hand.

FIGURE 54 – DISPLAY OF THE HEAT “PLUME” FROM THE TIP OF A WELDER. EACH PLUME IS DOUBLE BECAUSE OF ITS REFLECTION ON THE MIRROR

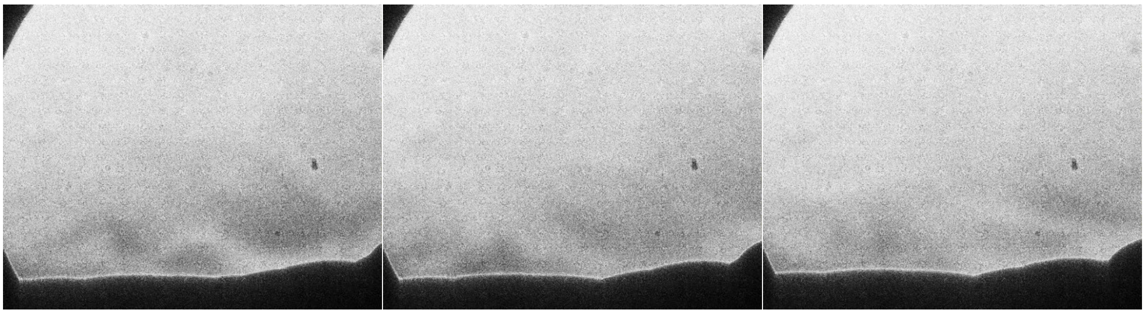

FIGURE 55 – DISPLAY OF THE HEAT TURBULENCE FROM THE HAND

You may note that the images were affected by several spots, still evident after cleaning the mirror and lenses of the camera (Figure 56, A and B respectively). Therefore, they were probably due to dust, dirt or degradation of some internal parts of the camera (CCD or inner surface of the lenses).

Then, the only possible removal of these spots was by software, by correcting the original images with the subtraction of the “white field” (Figure 57). The algorithm operates pixel by pixel, thus to eliminate field unevenness.

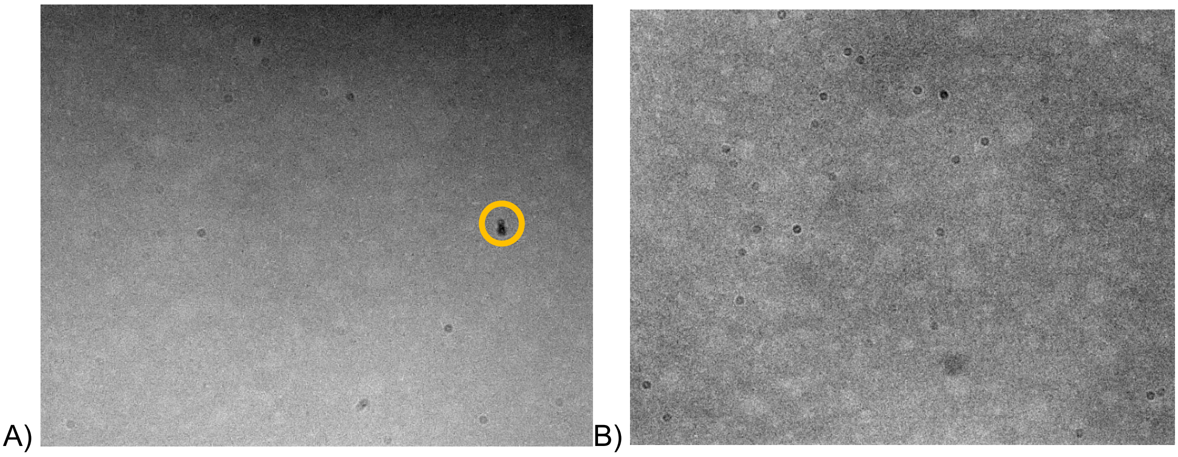

FIGURE 56 – SPOTS AFFECTING THE QUALITY OF IMAGES BEFORE (A) AND AFTER (B) CLEANING OPERATIONS. THE ONLY DEFECT ELIMINATED IS THE ONE INDICATED WITH A YELLOW CIRCLE (LEFT IMAGE)

FIGURE 57 – IMAGE OF THE HEAT TURBULENCE FROM THE HAND, ELABORATED BY SUBTRACTING THE BACKGROUND (“WHITE FIELD”, FIGURE 56-B) TO REMOVE THE SPOTS AND ADJUSTING BRIGHTNESS/CONTRAST TO EMPHASIZE THE STRIKES

In order to quantify the sensitivity to variations of the refraction index (n), a helium gas flow was used. The gas flow, from turbulent to stable "plume", was clearly displayed (Figure 58), demonstrating that a change from 1.000293 (n of air) to 1.000036 (n of helium) is visible.

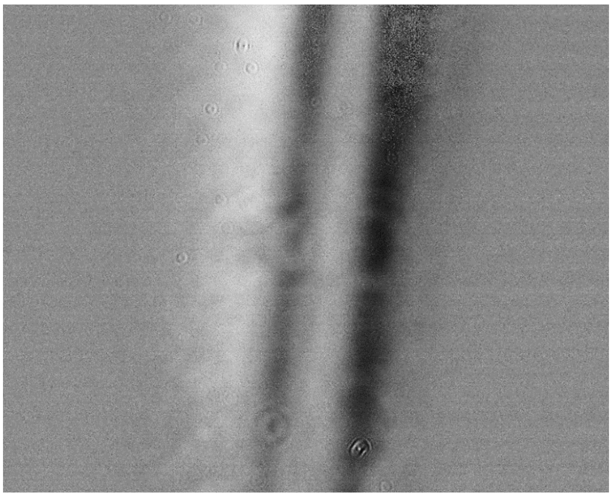

FIGURE 58 – DISPLAY OF THE HELIUM FLOW. IMAGE ELABORATED WITH WHITE FIELD CORRECTION AND BRIGHTNESS/CONTRAST ADJUSTMENTS. THE FLOW IS DOUBLE BECAUSE OF ITS REFLECTION ON THE MIRROR.

Further tests were performed with compressed air, by varying the pressure and perturbing the flux with both an object and the welder (Figure 59, Figure 60). The Schlieren effect was more evident with higher pressure (2 atmosphere instead of 1) and if the flow was subjected to movements (in case of 1 atm, this was the only possible way to see the strikes).

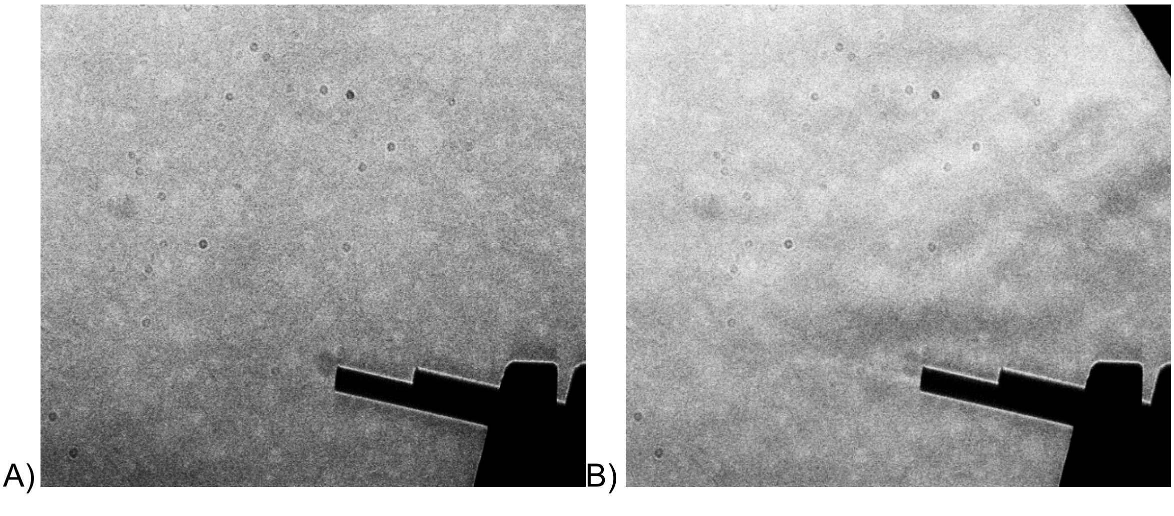

FIGURE 59 – DISPLAY OF COMPRESSED AIR FLOW WITH PRESSURE OF 1 ATM IN STEADY CONDITIONS (A) AND WITH AN OBJECT PERTURBING THE FLUX (B). BOTH IMAGES WERE ELABORATED WITH BRIGHTNESS/CONTRAST ADJUSTMENTS

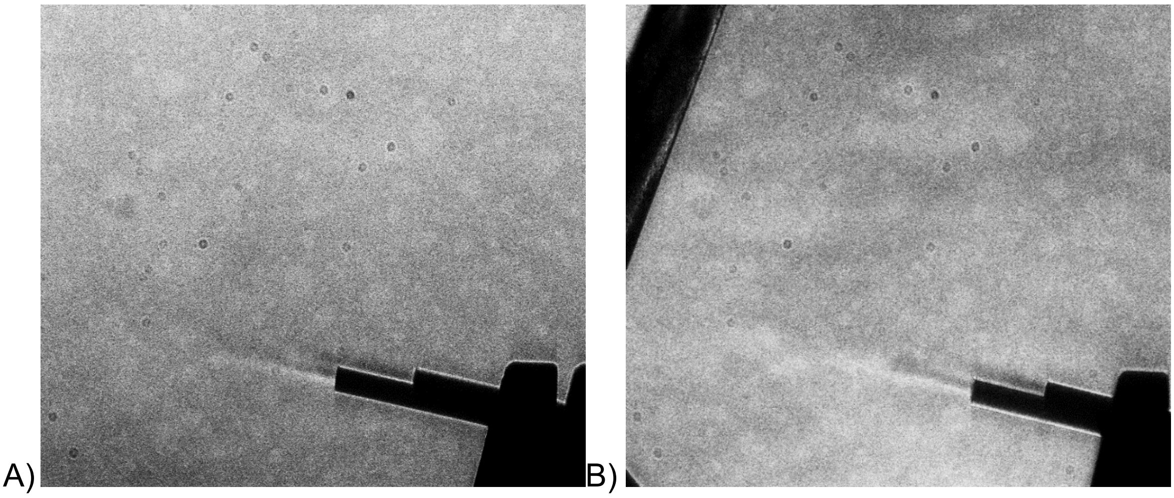

FIGURE 60 – DISPLAY OF COMPRESSED AIR FLOW WITH PRESSURE OF 2 ATM IN STEADY CONDITIONS (A) AND WITH AN OBJECT PERTURBING THE FLUX (B). BOTH IMAGES WERE ELABORATED WITH BRIGHTNESS/CONTRAST ADJUSTMENTS

4 REFLECTANCE IMAGE SPECTROSCOPY

4.1 GENERAL PRINCIPLES

Spectroscopic techniques are based on the energy exchange that occurs between the radiant energy and the matter under examination.
In particular, the spectroscopy used here is concerned with the phenomena generated by the radiations of the electromagnetic spectrum belonging to the visible and near infrared field.
The absorption of these types of radiations by the molecules is able to produce energetic transitions of the external electrons of the molecules.

When a beam of monochromatic light of intensity I_0 passes through a layer of thickness l of a medium, a part of it is absorbed by the medium itself and a part of it is transmitted with residual intensity I (Figure 61).

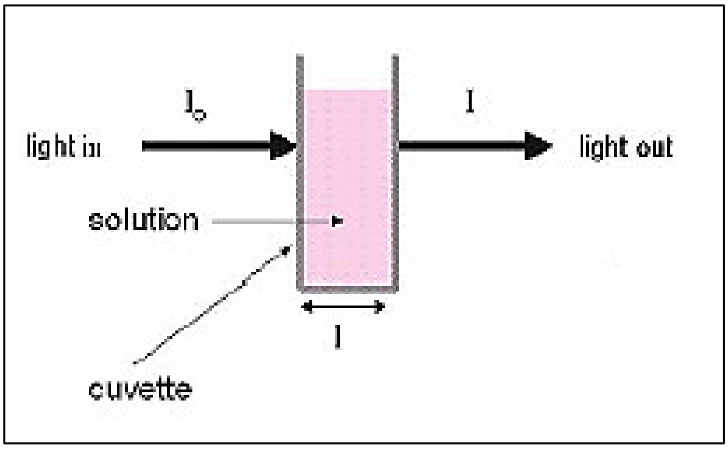

FIGURE 61 - REPRESENTATION OF ABSORPTION AND TRANSMISSION OF INCIDENT LIGHT THROUGH A CUVETTE FILLED OF LIQUID MEDIUM

The ratio between the intensity of transmitted and incident light on the crossed medium is expressed by the following relation:

$$T = \frac{I}{I_0} = e^{-k_\lambda l} = e^{-A}$$

where k_λ is the attenuation coefficient (which is a typical constant of the medium crossed and depends on the wavelength (λ) and l is the thickness of solution crossed.

Therefore, the transmittance (*T*) is defined as the ratio between the energy of the transmitted light (I) and of the incident light (I_0). Multiplying this ratio by 100 gives the percentage of transmittance.

$$\mathrm{T}_{\%} = \left(\frac{I}{I_0}\right) \times 100$$

If there is no scattering, the absorbance (*A*) is defined as the opposite of the natural logarithm of the transmittance, thus the law assumes an even more simplified form:

$$A = k_\lambda l$$

The instrument used to measure the properties of light according to its wavelength has the general name of spectrometer. The majority of spectrometers decomposes the light radiation in its wavelengths and measure its intensity with a detector.

To perform qualitative analyses, continuous spectrum polychromatic beams are used. The single monochromatic radiations of this ray pass through the test substance, which will absorb the radiations with different intensity. By reporting the values recorded in a wavelength-absorption graph, the absorption spectrum of the examined substance is obtained. Since each substance has its characteristic absorption spectrum, the examination of such spectra allows its identification.

4.2 REFLECTANCE SPECTROSCOPY TECHNIQUES

Reflectance spectroscopy is the optical investigation technique based on the measurement of the reflected light from a surface. The measurement can be performed by two different techniques: spectrophotometry and image spectroscopy.

For its accuracy and repeatability, spectrophotometry is often used as reference technique for image spectroscopy reflectance spectra in the visible spectral range.

The relevant physical observable is the diffuse reflectance factor, defined as a percentage ratio between the intensity of the light reflected from the sample in a non-specular way and the intensity of the incident light (Figure 62):

$$R_D = \frac{I_{RD}}{I_0}$$

where

R_D is the diffuse reflectance factor

I_{RD} is the irradiance of the light reflected diffusively

I_0 is the incident irradiance.

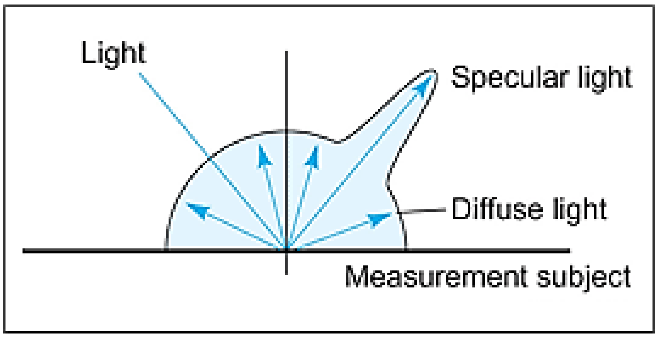

FIGURE 62 - REPRESENTATION OF SURFACE REFLECTANCE WITH SPECULAR AND DIFFUSE COMPONENTS

The measurement of the optical properties of the materials depends on the geometry of the instrument.

The incident beam and the observed beam can be of two types: directional or hemispherical. The geometrical conditions that must be indicated are the following, further explained in detail:

- angles of incidence, ε_1 and φ_1, and of observation, ε_2 and φ_2
- angles of opening of the incident beam, $2\sigma_1$, and of the observed beam, $2\sigma_2$

The measurement geometry is specified by means of polar coordinates system, centred at the point 0 on the specimen surface and with azimuthal angles referred to an appropriate direction on the specimen (Figure 63) (Rossi G., 1998):

- ε_1 is the angle between the perpendicular to the specimen (axis z) and the direction of incidence;
- ε_2 is the angle between the perpendicular to the specimen (axis z) and the direction of observation;
- φ_1 is the angle between a reference axis (axis x) and the plane of incidence;
- φ_2 is the angle between a reference axis (axis z) and the plane of observation.

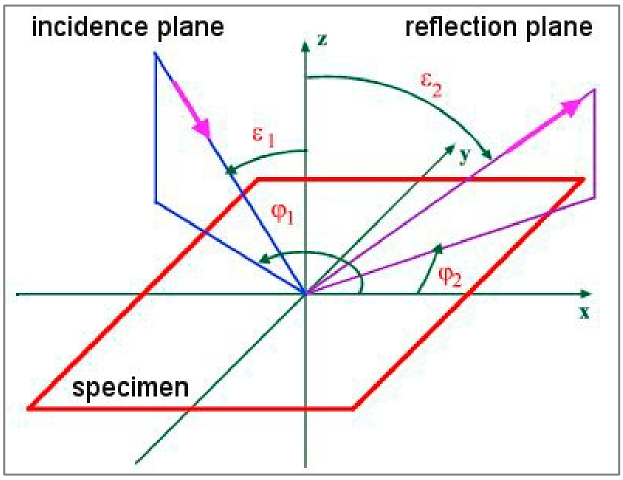

FIGURE 63 - POLAR COORDINATE SYSTEM FOR THE SPECTROMETRIC MEASUREMENTS

The measurement geometries are distinct in relation to the applications. Those most widely used for reflectance measurements are established by the “Commission Internationale de l’Eclairage” (CIE) in order to obtain comparable results. In Table 19 (Oleari C., 1998), "d" indicates the angle of the diffused light. In the case of directional illumination and observation, the respective solid angles correspond approximately to 0. In the real situation, the illumination and observation beams show a solid angle of 5-8°.

Geometry	**Irradiation**		**Observation**		**Specular reflection**	**CIE quantity**	**Quantity symbol**
	ε_1	**σ_1**	**ε_2**	**σ_2**			
0/d SCI	± 10°	± 5°	diffuse	diffuse	included	diffuse reflectance	$\rho_{0/d}$
0/d SCE	± 10°	± 5°	diffuse	diffuse	excluded	diffuse reflectance	$\rho_{0/d}$
d/0 SCI	diffuse	diffuse	± 10°	± 5°	included	reflectance factor, d/0	$R_{d/0}$
d/0 SCE	diffuse	diffuse	± 10°	± 5°	excluded	reflectance factor, d/0	$R_{d}/0$
d/d	diffuse		diffuse		included	reflectance for diffuse irradiance	$\rho_{d/d}$
0/0	± 10°	± 8°	± 10°	± 8°	included	specular reflectance	$\rho_{0/0}$
45/0	45° ± 2°	± 8°	± 10°	± 8°	excluded	reflectance factor, 45/0	$R_{45/0}$
0/45	± 10°	± 8°	45° ± 2°	± 8°	excluded	reflectance factor, 0/45	$R_{0/45}$

TABLE 19 - CIE GEOMETRY OF IRRADIATION AND OBSERVATION FOR REFLECTION MEASUREMENTS AND RELATIVE QUANTITIES

Image spectroscopy collects backscattered light in a narrow solid angle. It foresees to illuminate the area of interest with lamps (300 W halogen lamps, in our tests), positioned symmetrically at about 45° of incidence in order to get a reasonably uniform brightness, and observe it perpendicularly. Therefore, the measured quantity is the reflectance factor $R_{2x45/0}$ (Figure 64).

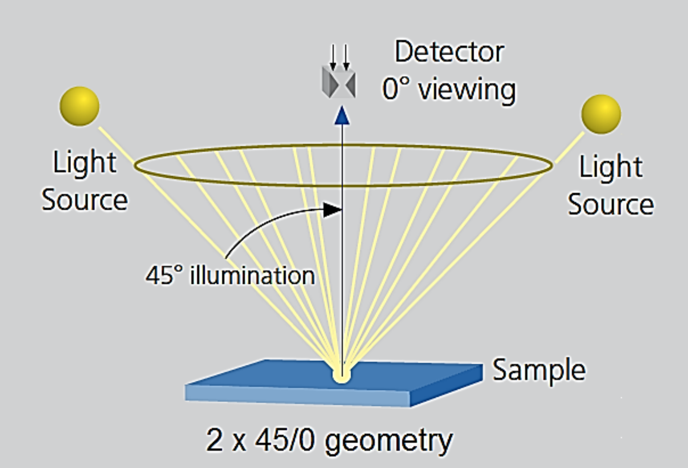

FIGURE 64 – REPRESENTATION OF 45/0 GEOMETRICAL CONFIGURATION FOR REFLECTION MEASUREMENTS

The technique is based on multi-wavelength imaging where a sequence of images of the samples is acquired and digitised in narrow spectral bands, from the visible to the near IR. The reflectance spectrum, which is a physical property of the object, is derived from the image sequence by a calibration procedure and suitable software. The result of IS measurements represents a relative quantity, called spectral reflectance factor R_λ, which is expressed by the ratio between the detected radiation diffused from the sample I_{RD} and the intensity of the radiation reflected by reflectance standard I_{ref} (Daffara C., 2010):

$$R_\lambda = \rho_{ref} \frac{I_{RD}}{I_{ref}}$$

where

ρ_{ref} is the certified value for the reflectance standard.

This equation, generally valid for the visible range, can be extended up to near infrared range, since until 2.5 μm the thermal emission of both standard and sample is negligible.

IS performs measurements on a large region of the sample and requires no contact with the sample. Therefore, the region of interest can be chosen after the image acquisition. Concerning quantitative comparisons, they may be effective, if the same geometry is preserved.

4.3 SET UP AND TESTS IN LABORATORY

4.3.1 OBJECTIVE

The main goal of this task was to understand if image spectroscopy could be a reliable technique to analyse edible oils, being able to distinguish among different varieties of extra virgin oils or even to identify any adulteration with refined oils. The final aim would be to build a portable and low cost device for a beginning individuation of possibly counterfeited samples to be labelled for further and deeper analyses with more specific techniques.

The technique is usually carried out in archaeometric studies to detect at different times the alterations of the pictorial layer not yet perceptible to the human eye. Therefore, the experimental work of this thesis was focused to understand the possible extension and applicability of image spectroscopy to the field of food research. The challenge was to achieve results similar to the reflectance spectra obtained with the spectrophotometer, in particular the identification of the absorption peak at 670 nm, which is the most distinctive feature allowing to recognize extra virgin oils towards refined ones.

4.3.2 EXPERIMENTAL APPARATUS

4.3.2.1 SPECTROPHOTOMETER

The University of Molise carried out the measurements with the spectrophotometer. The device used was LAMBDA 25 UV/VIS Perkin Elmer and the cuvettes were HELLMA quartz with optical path of 10 mm. The measurements were performed in double-beam mode using air as reference. Each sample was analysed in the range between 300 and 1050 nm, with bandwidth of 1 nm.

At the Institute of Applied Physics of the Italian National Research Council (IFAC-CNR), other two Perkin Elmer double-beam double-monochromator spectrophotometers were used, namely LAMBDA 19 and LAMBDA 1050. The samples were analysed in transmittance mode with both devices. In addition, in the spectrophotometer LAMBDA 1050, also a 60 mm integrating sphere was mounted, which allowed to detect the overall transmission, i.e. direct transmission plus diffuse transmission, including beam deviation. Two different references were used: an empty cuvette with LAMBDA 19 and a cuvette filled with pure alcohol 95° with LAMBDA 1050. The same cuvettes used for image spectroscopy were analysed, i.e. standard cuvettes of light polystyrene with optical path of 10 mm filled with 3 ml of oil. Each sample was examined in the range between 350 and 1100 nm, with bandwidth of 1 nm.

4.3.2.2 IMAGE SPECTROSCOPY

The acquisition of the images at different wavelength values is achieved using a monochrome digital camera (Pulnix TM-1325 CL©). It is equipped with a revolving wheel placed between the objective and the silicon CCD (1288 x 1026 pixel), containing 16 interferential optical filters (1'' in diameter) with a narrow bandwidth of 10 nm, covering the sensitivity range of the detector from 450 to 970 nm (Table 20).

This device was designed and built by the collaboration between INFN Section of Ferrara and the Department of Physics of Ferrara University[2] (Figure 65) (Albertin F., 2012) (Pellicori V., 2013).

---

[2] S. Chiozzi, F. Evangelisti, S. Squerzanti, of INFN – Section of Ferrara, and L. Landi of Ferrara University

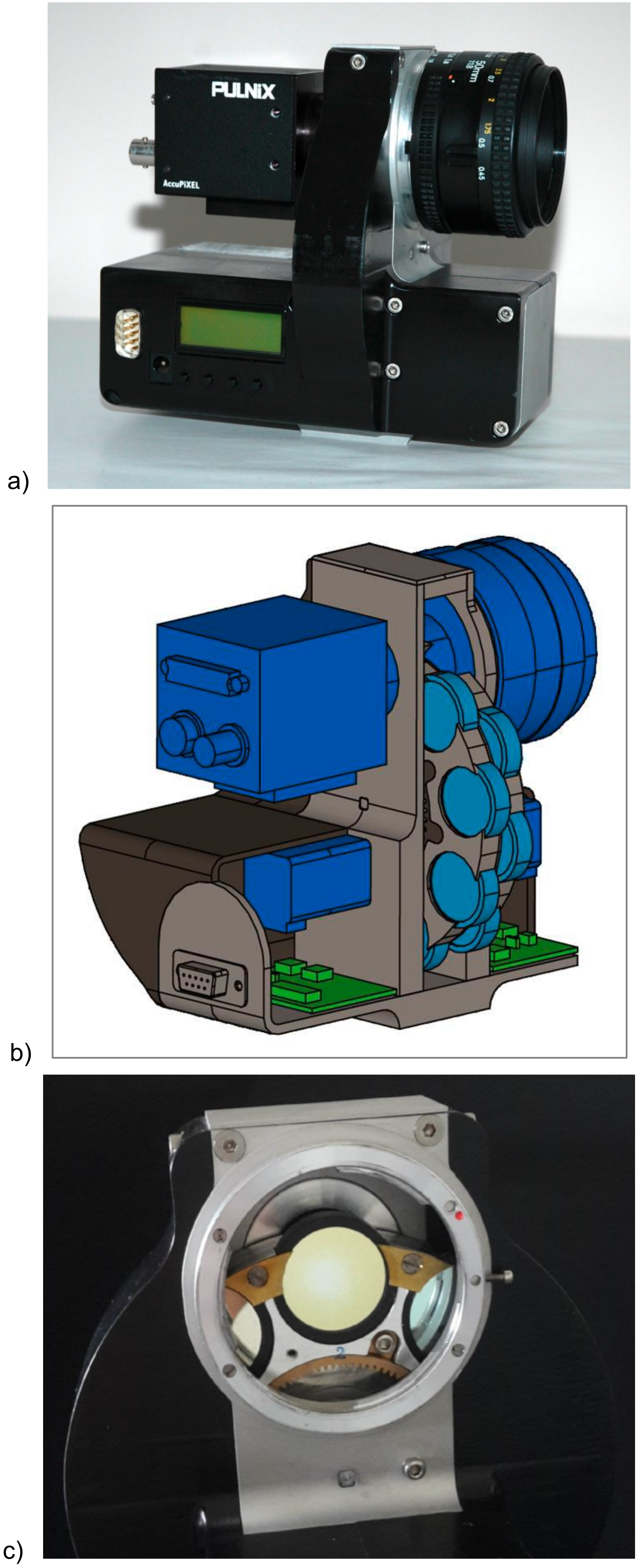

Figure 65 - Image spectroscopy device, equipped with Pulnix TM-1325 CL camera (a) and its internal structure (b-c)

Filter	λ (nm)	Filter	λ (nm)	Filter	λ (nm)	Filter	λ (nm)
1	**450**	5	**612**	9	**680**	13	**790**
2	**490**	6	**649**	10	**690**	14	**850**
3	**514**	7	**660**	11	**710**	15	**910**
4	**570**	8	**670**	12	**730**	16	**970**

TABLE 20 – PEAK TRANSMISSION WAVELENGTH (NM) OF THE INTERFERENCE FILTERS EMPLOYED IN THE MULTISPECTRAL IMAGING

The filters are changed manually, while a PC is used for the image acquisition. The PC is interfaced with the camera via a 8-bit video digital acquisition card (PCI-1428) provided by National Instrument. The acquisition is controlled through two interface programs: 'IMAQ Measurement and Automation' of National Instrument and Mean3.vi[3], developed in the LabView© platform. The first software operates in video mode, allowing to control the acquisition field and to adjust the diaphragm and focus of the camera. The second software operates in snapshot mode and is responsible of the final acquisition. It is possible to set the number of multiple image per single acquisition, choose the output format file and the folder to store it in the PC. In our tests, the images are obtained from the average of 10 acquisitions and are stored as 8-bit TIFF files.

4.3.3 CALCULATION OF REFLECTANCE SPECTRA WITH IMAGE SPECTROSCOPY

Each image, acquired with image spectroscopy, carries the information related to the reflectance diffused by the sample in the spectral band transmitted by the interferential filter. The whole set of images using the 16 filters can be acquired and saved sequentially, allowing focussing and diaphragm settings at each wavelength value.

The elaboration and the calculation of the reflectance for the whole multispectral sequence are carried out through a software specially developed in the Windows environment, called Tele32[4].

Before calculating the reflectance value of the selected zones, the image must be corrected by some "defects" due to the acquisition, mainly the statistical noise and the unevenness of the field.

Statistical noise is due to signal fluctuations and is reduced averaging multiple images.

The unevenness of the field depends both on causes external to the apparatus, such as the lack of homogeneity of lighting of the sample, and other related to the apparatus itself, such as loss of brightness at the edges of the lens, the presence of dust on the lens or on the CCD.

---

[3] Developed by S. Chiozzi at the Electronic Service of INFN in Ferrara

[4] Developed by I. Bortolotti at Ferrara University

Field unevenness can be corrected by software:

- the image of a grey surface with uniform reflectance is acquired, called "topographic white", with the same acquisition conditions of the IS sequence, like distance from sample, illumination, lens aperture and focus;
- each sample acquisition image is associated with that of the topographic white at the same wavelength;
- the correction takes place through an algorithm, usually multiplicative, that divide the grey level value of each pixel of the image by the grey level value of the corresponding pixel of the relative white topographic. The formula is the following:

$$I_\lambda(x;y) = i_\lambda(x;y)\frac{< \overline{b_\lambda(x;y)} >}{b_\lambda(x;y)}$$

Where

$I_\lambda(x;y)$ = pixel value of the image corrected with white topography

$i_\lambda(x;y)$ = pixel value of the image to correct

$b_\lambda(x;y)$ = pixel value of the white topographic image

$< \overline{b_\lambda(x;y)} >$ = mean value of white image grey levels

On all the acquired images at the various wavelengths, "regions of interest" (ROI) are plotted, on which to perform the reflectance measurements.

ROIs can be:

- reference, if drawn on the reflectance standards Figure 66 (A);
- generic, if drawn on certain areas of the sample, as uniform as possible Figure 66 (B).

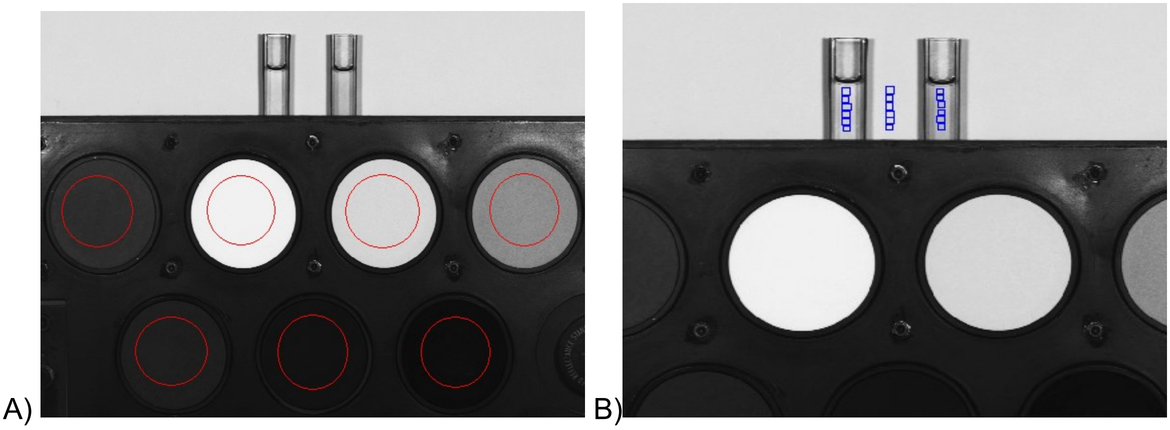

Figure 66 – Plot of “regions of interest" (ROI) on: A) reflectance standards (ROI of reference); B) areas of the sample (generic ROI)

Absolute reflectance measurements taken as an average in the region of interest of an acquired image are then performed by interpolation between the levels of grey of the surrounding standards (Figure 67):

1) the average grey level is calculated on each reference standards, whose diffuse reflectance value is well known. Diffuse reflectance standards with average values of reflectance ranging from 2% to 99% are produced (Labsphere Inc., USA – distributed in Italy by LOT-ORIEL, Milan), with reasonably constant values over a wide range of wavelengths;
2) a calibration curve is constructed, based on which the reflectance values of the measuring zones are calculated;
3) Interpolation of the grey level scale is performed by using a polynomial curve, usually third-degree.

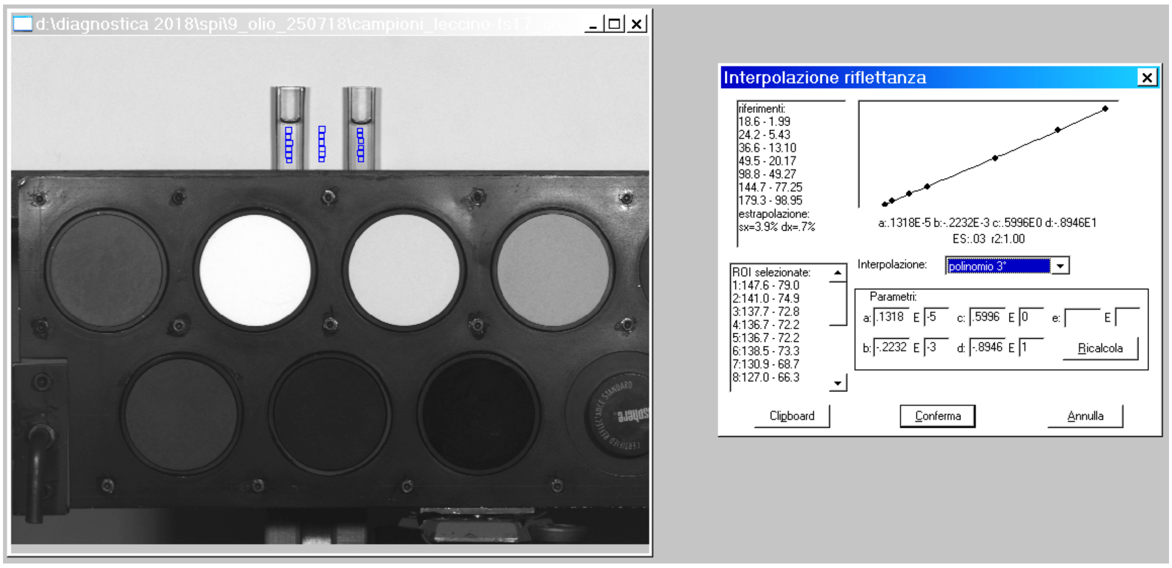
d:\diagnostica 2018\spi\9_olio_250718\campioni_leccino-fs17_co

Interpolazione riflettanza

riferimenti:
18.6 - 1.99
24.2 - 5.43
36.6 - 13.10
49.5 - 20.17
98.8 - 49.27
144.7 - 77.25
179.3 - 98.95
estrapolazione:
sx=3.9% dx=.7%

a:.1318E-5 b:-.2232E-3 c:.5996E0 d:-.8946E1
ES:.03 r2:1.00

ROI selezionate:
1:147.6 - 79.0
2:141.0 - 74.9
3:137.7 - 72.8
4:136.7 - 72.2
5:136.7 - 72.2
6:138.5 - 73.3
7:130.9 - 68.7
8:127.0 - 66.3

Interpolazione: polinomio 3°

Parametri:
a: .1318 E -5
c: .5996 E 0
e: E
b: -.2232 E -3
d: -.8946 E 1

FIGURE 67 – CONSTRUCTION OF THE CALIBRATION CURVE TO CALCULATE THE REFLECTANCE OF THE SAMPLE BY INTERPOLATION OF THE GREY LEVELS OF GENERIC ROI WITH THE ONES OF REFERENCE ROI

This operation is repeated on the whole sequence of acquisition in order to create the reflectance spectrum on the entire spectral range (Figure 68).

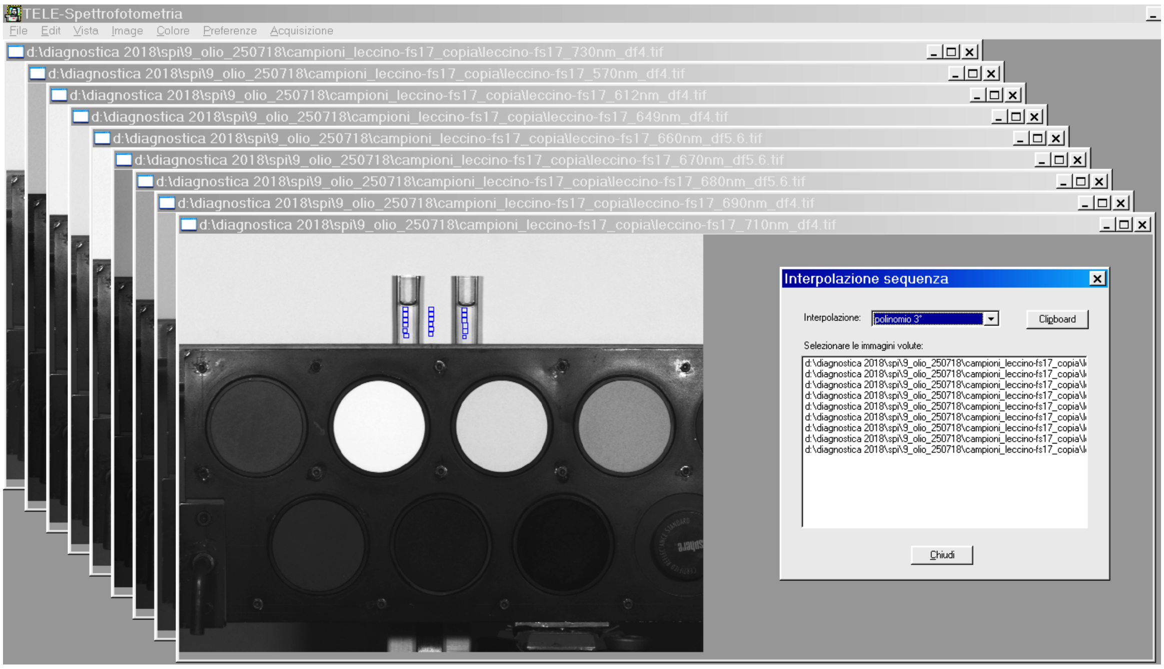

```
d:\diagnostica 2018\spi\9_olio_250718\campioni_leccino-fs17_copia\leccino-fs17_730nm_df4.tif
d:\diagnostica 2018\spi\9_olio_250718\campioni_leccino-fs17_copia\leccino-fs17_570nm_df4.tif
d:\diagnostica 2018\spi\9_olio_250718\campioni_leccino-fs17_copia\leccino-fs17_612nm_df4.tif
d:\diagnostica 2018\spi\9_olio_250718\campioni_leccino-fs17_copia\leccino-fs17_649nm_df4.tif
d:\diagnostica 2018\spi\9_olio_250718\campioni_leccino-fs17_copia\leccino-fs17_660nm_df5.6.tif
d:\diagnostica 2018\spi\9_olio_250718\campioni_leccino-fs17_copia\leccino-fs17_670nm_df5.6.tif
d:\diagnostica 2018\spi\9_olio_250718\campioni_leccino-fs17_copia\leccino-fs17_680nm_df5.6.tif
d:\diagnostica 2018\spi\9_olio_250718\campioni_leccino-fs17_copia\leccino-fs17_690nm_df4.tif
d:\diagnostica 2018\spi\9_olio_250718\campioni_leccino-fs17_copia\leccino-fs17_710nm_df4.tif
```

Interpolazione: polinomio 3°

Selezionare le immagini volute:

```
d:\diagnostica 2018\spi\9_olio_250718\campioni_leccino-fs17_copia\
d:\diagnostica 2018\spi\9_olio_250718\campioni_leccino-fs17_copia\
d:\diagnostica 2018\spi\9_olio_250718\campioni_leccino-fs17_copia\
d:\diagnostica 2018\spi\9_olio_250718\campioni_leccino-fs17_copia\
d:\diagnostica 2018\spi\9_olio_250718\campioni_leccino-fs17_copia\
d:\diagnostica 2018\spi\9_olio_250718\campioni_leccino-fs17_copia\
d:\diagnostica 2018\spi\9_olio_250718\campioni_leccino-fs17_copia\
d:\diagnostica 2018\spi\9_olio_250718\campioni_leccino-fs17_copia\
d:\diagnostica 2018\spi\9_olio_250718\campioni_leccino-fs17_copia\
```

FIGURE 68 – INTERPOLATION ON THE WHOLE SEQUENCE OF ACQUISITION

The reflectance standards are 2-inch diameter discs (Figure 69) and are made with a mixture of Spectralon®, high reflectance synthetic resin, and carbon powder. This material diffuses in an isotropic way all the light it receives; it is stable over time and strongly resistant. The standards used are 7 with reflectance of 2%, 5%, 10%, 20%, 50%, 75%, 99%.

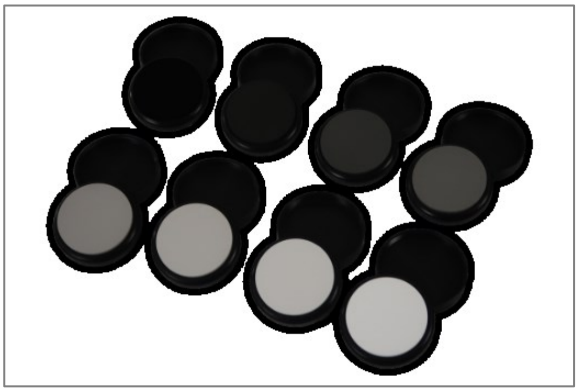

FIGURE 69 - 2-INCH DIAMETER SPECTRALON®DISCS USED AS REFLECTANCE STANDARDS IN IMAGE SPECTROSCOPY

Accuracy in the determination of the absolute reflectance is as good as 2% in the most sensitive region of CCD, between 520 nm and 860 nm, reducing to 5% in the blue (450-480 nm) and NIR (900-1050 nm) regions (Petrucci F., 2004).

The detection of spectra according to multispectral images sequence is performed with the help of a dedicated software and takes place in two phases:

- identification of the reference regions on the reflectance standards;
- identification of the measurement regions on the acquired images.

The program is responsible to:

- copy the selected regions in an image to all the other counterparts corresponding to the other wavelengths in the sequence;
- perform interpolations at each wavelength between the pre-set reference regions, based on the reflectance values of the samples;
- return the results in an ASCII text file, for further processing with other software.

4.3.4 FIRST TRIALS

The first tests were performed in order to verify the possible drift of reflectance of the reference standards from the values of the last calibration, carried out by the manufacturer Labshpere in 2013.

The same ROIs on the 7 grey standards were used both as generic and reference. The comparison of the reflectance values is shown in Figure 70, which demonstrates that the curves between the Labsphere calibration and the acquisition do not differ, except at 1050 nm.

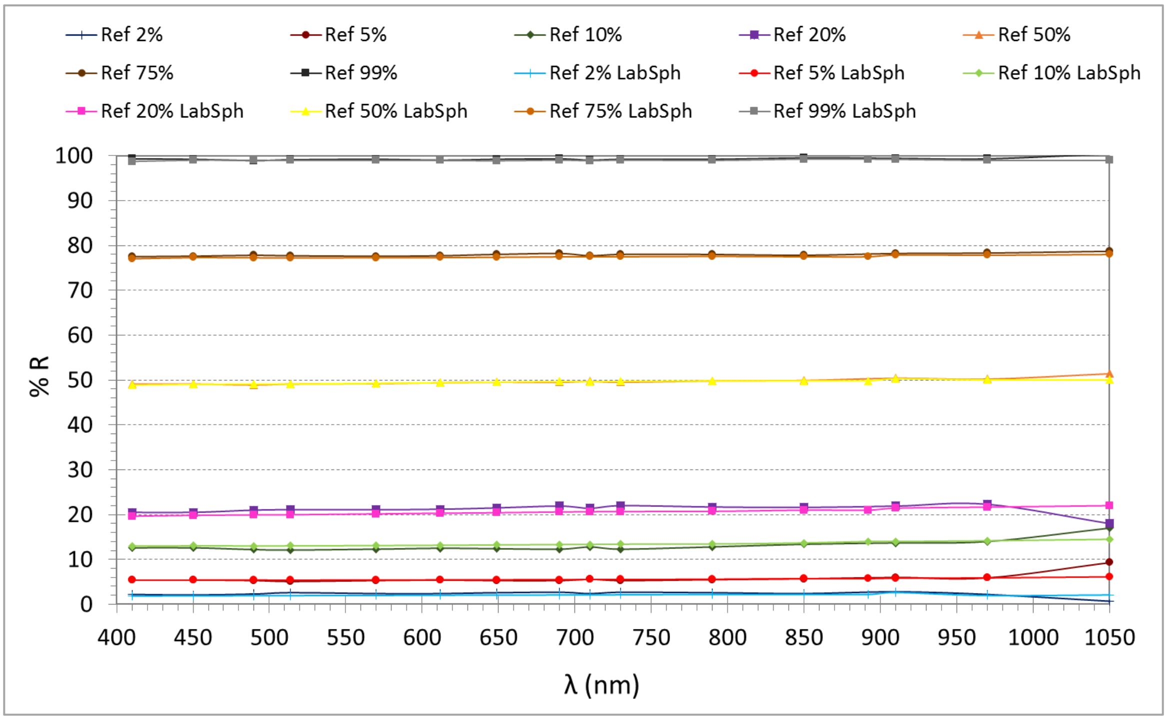

FIGURE 70 – COMPARISON OF REFLECTANCE VALUES OF THE STANDARDS BETWEEN LABSPHERE CALIBRATION AND ACQUISITION

The next step was to check the unevenness of the filters at each wavelength. A rectangular plot (1250 x 100 pixels) was drawn on the white sheet used as background. The relative graph displays the intensities of pixels along this rectangular selection: in particular, the X-axis represents the horizontal distance through the selection and the Y-axis the vertically averaged pixel intensity, expressed as grey level. As shown in Figure 71, there is a decrease of grey levels at the edges of the image, due both to the camera lens and the filters, which transmit less light at the edges.

This information is worthwhile for the set up: taking advantage of the smallness of the samples (cuvettes of oils), it can be exploited the centre of the area to be acquired to obtain the maximum of illumination and homogeneity in the reflectance response.

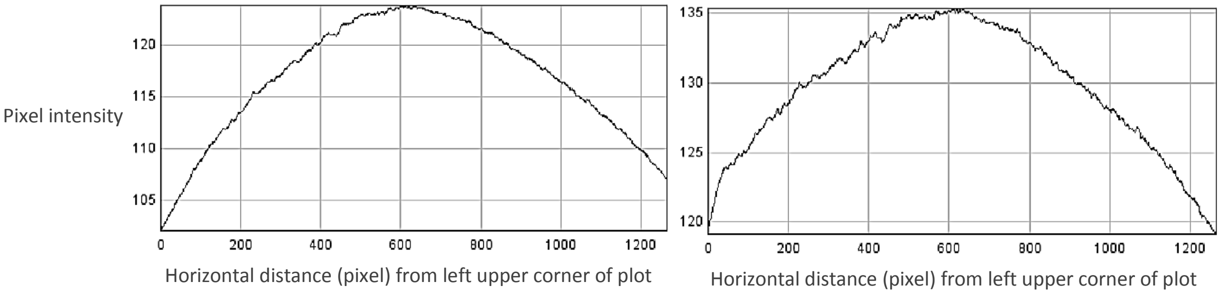

FIGURE 71 – GREY VALUES OF THE PLOTTED AREA ON A WHITE SURFACE AT 450 (LEFT) AND 970 NM (RIGHT) AS EXAMPLE

4.3.5 RESULTS OF MEASUREMENTS ON OILS

The samples were prepared by transferring 3 ml of oil in standard cuvettes made of light polystyrene (PS), with an optimal transparency in the spectral range 340-900nm and an optical path of 10 mm. Three varieties of extra virgin oils were examined, namely *Coratina* (cultivar mainly diffused in Puglia) – *Leccino* (widespread at national level, probably of Tuscan origins) – *FS17* (*Favolosa*, widespread at national level). Next to these, other three kind of oils were analysed, i.e. *Lampante*, refined and *Olive* oil.

A brief note is needed to explain the qualitative characteristics of the oil. After pressing, the oil is divided into three product categories based on its quality characteristics. If it has no defects and acidity of less than 0.8%, it is classified as “extra virgin” olive oil. If it presents a minimum quantity of defect but the acidity is less than 2%, one has “virgin” olive oil. If the quality defects are marked and the acidity exceeds 2%, the oil is declassified as "lampante" and re-worked until refined oil is obtained. With the addition of a small percentage of extra virgin olive oil, it becomes olive oil. In our case, the *Olive* oil was composed by 85% of refined oil and 15% of extra virgin olive oil.

Since the measurements with the spectrophotometer are related to the transmittance of the samples, it was first necessary to understand how to transform the reflectance measurements obtained with the image spectroscopy into transmittance values, in order to be able to compare the results of the two techniques. In addition, we had to correct the reflectance measurements by taking into account the contribution both of the background and the cuvette, in order to separate the only reflection of the oil.

Considering the path of the light, as outlined in Figure 72, we have incident rays (I_0) which pass through the cuvette, the oil, and then they are reflected by the background; finally, they retrace the same path in the opposite direction.

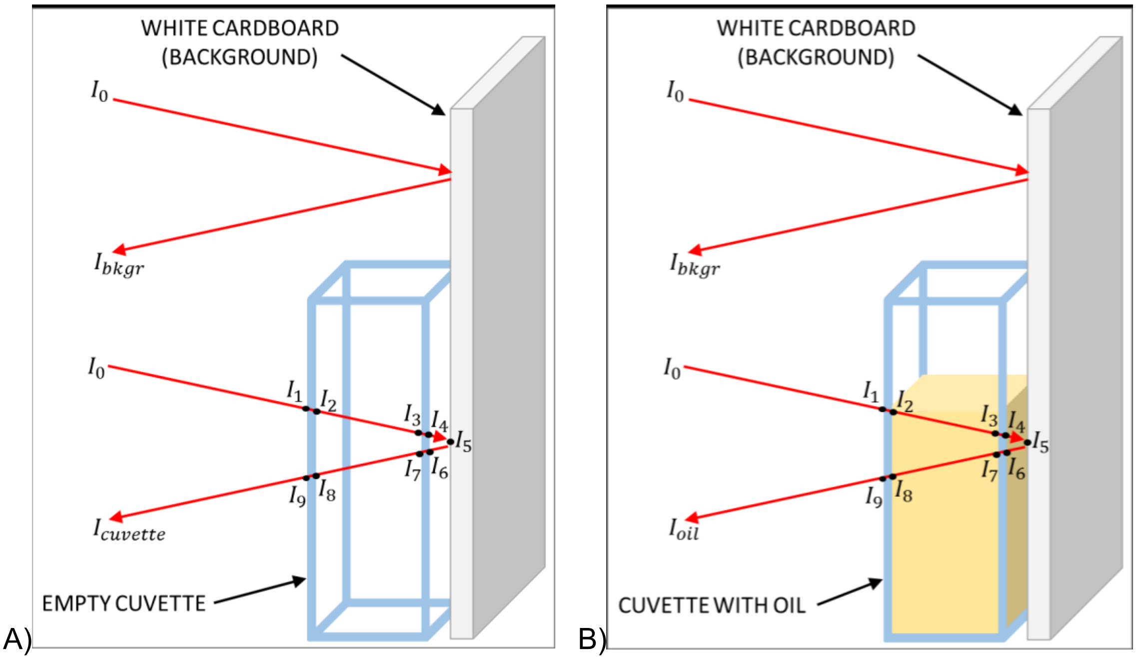

FIGURE 72 – OUTLINE OF THE REFLECTED AND TRANSMITTED COMPONENT OF THE INCIDENT LIGHT MEASURED WITH IMAGE SPECTROSCOPY, IN CASE OF AN EMPTY CUVETTE (A) AND A CUVETTE FILLED WITH OIL (B)

In the hypothesis that there is no scattering, the light is partially reflected and partially transmitted at each interface.

The normal component of reflection (R) is reduced at each median crossing as follows:

$$R = \left(\frac{n_1 - n_2}{n_1 + n_2}\right)^2$$

In the case of the empty cuvette, the refraction index are $n_1 = 1.6$ (PS) and $n_2 = 1$ (air). Thus, applying the equation above, the reflection is reduced by 5% of the light power at each interface air/polystyrene ($\boldsymbol{R_{air/ps}}$):

$$\boldsymbol{R_{air/ps}} = \left(\frac{n_1 - n_2}{n_1 + n_2}\right)^2 = \left(\frac{1.6 - 1}{1.6 + 1}\right)^2 = \mathbf{0.053}$$

In the case of the cuvette filled with oil, the refraction index are $n_1 = 1.6$ (PS) and $n_2 = 1.3$ (oil). In this case, the reflection is reduced by 1% of the light power at each interface oil/ polystyrene ($\boldsymbol{R_{oil/ps}}$):

$$\boldsymbol{R_{oil/ps}} = \left(\frac{n_1 - n_2}{n_1 + n_2}\right)^2 = \left(\frac{1.3 - 1.6}{1.3 + 1.6}\right)^2 = \mathbf{0.011}$$

Considering the path of the incident light in the empty cuvette, we have 4 interfaces air/polystyrene (I_1, I_2, I_3, I_4 in Figure 72-A), so we can calculate the transmitted light after each interface as follows:

$$I_1 = I_0\,(1 - R_1)$$

$$I_2 = I_1\,(1 - R_2)$$

$$I_3 = I_2\,(1 - R_3)$$

$$I_4 = I_3\,(1 - R_4)$$

where $R_1 \cong R_2 \cong R_3 \cong R_4$, which correspond to $R_{air/ps}$.

When the light encounters the background, we suppose that it is completely reflected (R_5). Therefore, considering the reflectance of the background (I_{bkgr}) as:

$$\boldsymbol{I_{bkgr} = I_0\,R_5}$$

at point I_5, we obtain the following equation:

$$I_5 = I_4 R_5 \rightarrow I_5 = I_0\,(1 - R_1)(1 - R_2)(1 - R_3)(1 - R_4)R_5 \rightarrow I_5 = I_0\,\left(1 - R_{air/ps}\right)^4 R_5$$

The light retrace then the same path (by crossing points I_6, I_7, I_8, I_9 in Figure 72-A), where $R_6 \cong R_7 \cong R_8 \cong R_9$ correspond again to $R_{air/ps}$.

At the end, the reflectance of the empty cuvette ($\boldsymbol{I_{cuvette}}$) is calculated as the sum of the background reflection and the transmitted light after 8 air/polystyrene crossings (Figure 72-A):

$$I_{cuvette} = I_5\left(1 - R_{air/ps}\right)^4 \rightarrow \boldsymbol{I_{cuvette} = I_0\left(1 - R_{air/ps}\right)^8 R_5}$$

By substituting the term $I_0\,R_5$ with the equivalent term I_{bkgr}, we obtain the following equation:

$$\frac{I_{cuvette}}{I_{bkgr}} = \left(1 - R_{air/ps}\right)^8 \rightarrow \left(1 - R_{air/ps}\right) = \sqrt[8]{\frac{I_{cuvette}}{I_{bkgr}}}$$

Considering the cuvette filled with oil, the light crosses 4 times the interface air/polystyrene (at points I_1, I_4, I_6, I_9) and 4 times the interface oil/polystyrene (at points I_2, I_3, I_7, I_8) (Figure 72-B). Therefore, in this case the reflectance $\boldsymbol{I_{oil}}$ is calculated as the sum of the background reflection, the transmitted light after 4 air/polystyrene crossings and 4 oil/polystyrene crossings, and the double transmission through the oil (T^2):

$$\boldsymbol{I_{oil} = I_0\, R_5 \left(1 - R_{air/ps}\right)^4 (1 - R_{oil/ps})^4\, T^2}$$

Considering $\left(1 - R_{oil/ps}\right) \approx 1$, we can neglect this term and, by substituting the term $I_0\, R_5$ with the equivalent term I_{bkgr}, we obtain the following equation:

$$\frac{I_{oil}}{I_{bkgr}} = \left(1 - R_{air/ps}\right)^4\ T^2$$

Considering $\left(1 - R_{air/ps}\right) = \sqrt[8]{\frac{I_{cuvette}}{I_{bkgr}}}$, as by previous equation, we can substitute the term $\left(1 - R_{air/ps}\right)^4$ as follows:

$$\left(1 - R_{air/ps}\right)^4 = \left[\left(\frac{I_{cuvette}}{I_{bkgr}}\right)^{1/8}\right]^4 = \left(\frac{I_{cuvette}}{I_{bkgr}}\right)^{4/8} = \left(\frac{I_{cuvette}}{I_{bkgr}}\right)^{1/2}$$

Thus, at the end it results the following equation:

$$T^2 = \frac{I_{oil}}{I_{bkgr}}\left(\frac{I_{bkgr}}{I_{cuvette}}\right)^{1/2} \rightarrow T^2 = \frac{I_{oil}}{\left(I_{bkgr}\, I_{cuvette}\right)^{1/2}} \rightarrow \boxed{\boldsymbol{T = \frac{\sqrt{I_{oil}}}{\left(I_{bkgr}\, I_{cuvette}\right)^{1/4}}}}$$

This last equation was used to calculate the transmittance spectra of the oil from the reflectance values recorded with image spectroscopy, in order to have a direct comparison with the transmittance values obtained with the spectrophotometry. Notwithstanding, some approximations, in applying the ideal conditions leading to the formulation of these equations, could be the reason why the two techniques differ in the resulting absolute values. For instance, we neglected the small scattering induced by oil and the finite solid angle of acceptance of the detector.

Even the use of an empty cuvette as a reference can be another cause of error. Normally, in fact, spectroscopic measurements on liquids are carried out on a solution, and only the solvent is used as a reference, after separation from the solute. This gives the certainty of measuring the only contribution of the component under investigation. In the case of pure liquids, such as oil, the analysis is carried out by comparing the sample under test with a known sample as reference, or the relative measurements between one sample and another.

After this premise, we started to perform several tests to find the best position both of the lamps and of the cuvettes filled with oil, placed on an easel used as support. A couple of cuvettes were analysed at a time, spaced between them, with a white no-fluorescent cardboard behind them as background. Two lamps of 300 W, positioned almost frontally to the samples, illuminated them the most uniformly as possible, avoiding shadows and reflections. Pieces of a thin black cardboard were used to cover two opposite sidewalls of the cuvettes (leaving free the front and rear ones to receive and reflect the light back), and also on the supporting shelf of the easel, again to avoid reflections. This configuration is shown in Figure 73.

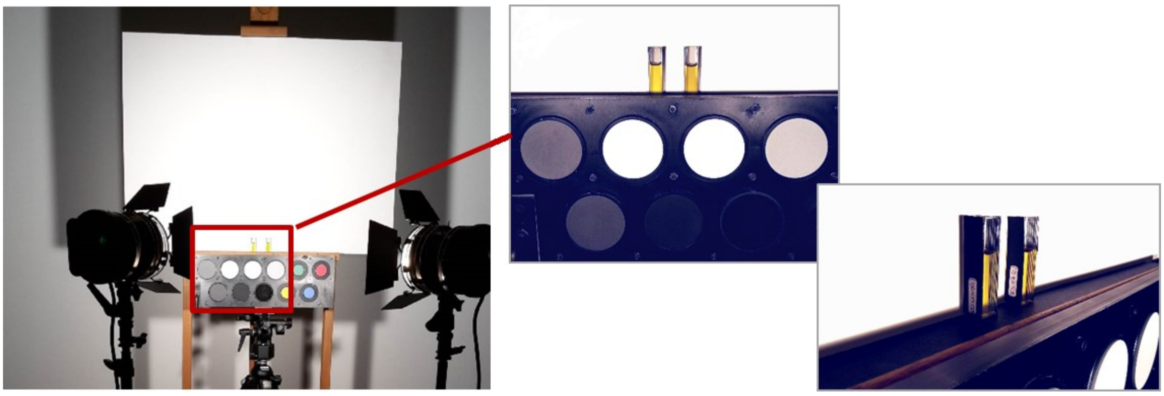

FIGURE 73 – CONFIGURATION OF LAMPS, CUVETTES AND REFLECTANCE STANDARDS FOR IMAGE SPECTROSCOPY ANALYSIS

The next step was to verify the correct selection of the filters mounted on the camera. Three new filters were mounted, with narrow bandwidth centred at 660 – 670 – 680 nm (Table 20). Indeed, next to verify the general trend of the spectra, we were interested in finding the absorption peak observed with spectrophotometry at 670 nm in particular, rather than to detect the absolute values of transmittance. In fact, having spectra obtained with a spectrophotometer, it is useful to determine a priori the bands of interest with very fine spectra (bandwith of 1 nm).

The absorption peak centred at 670 nm was clearly detected in all three reflectance spectra of the analysed extra virgin oils (Figure 74). In addition, by comparing the reflectance spectra obtained with image spectroscopy with the ones obtained with the spectrophotometer (Figure 75), it is worthwhile to notice that they are very similar and also the slight differences between the three varieties of oils were measured as well, i.e. a greater absorption of *Coratina* and *FS17* with respect to *Leccino* cultivar.

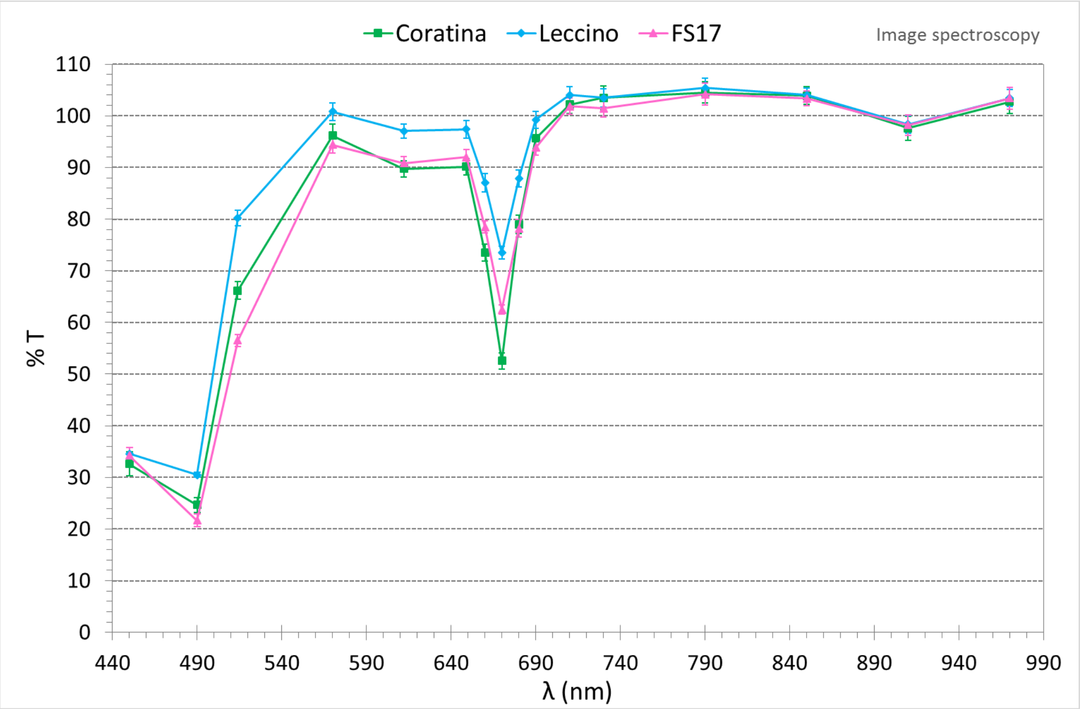

FIGURE 74 – CALCULATED TRANSMITTANCE SPECTRA OF THREE ANALYSED EXTRA VIRGIN OILS OBTAINED WITH IMAGE SPECTROSCOPY

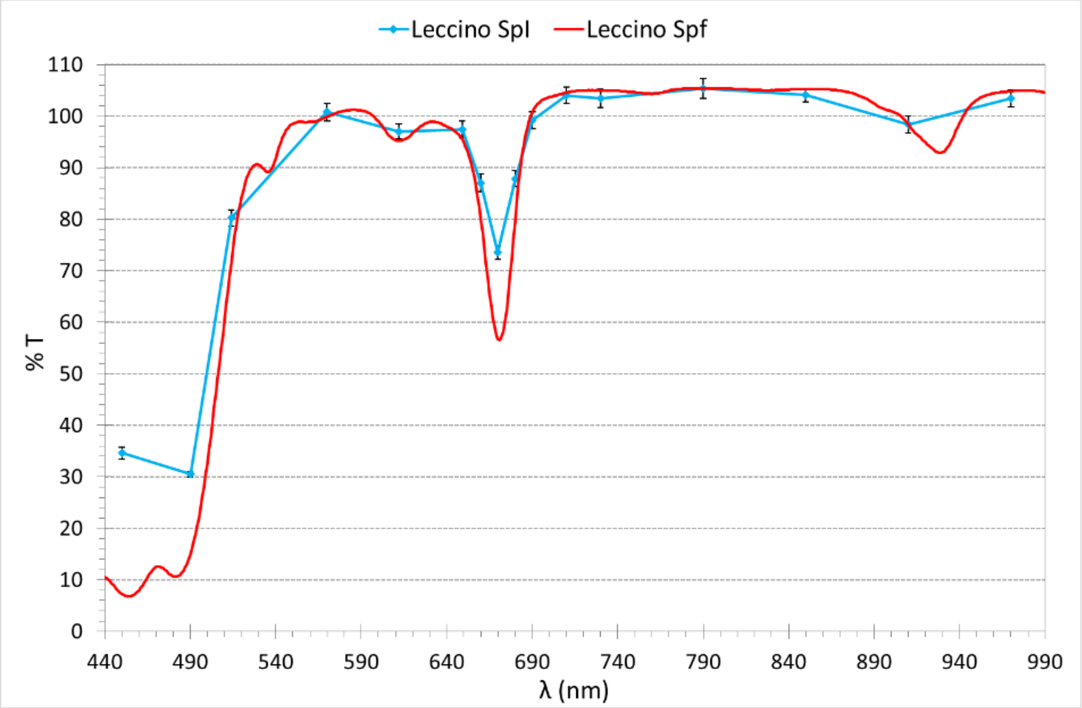

A)

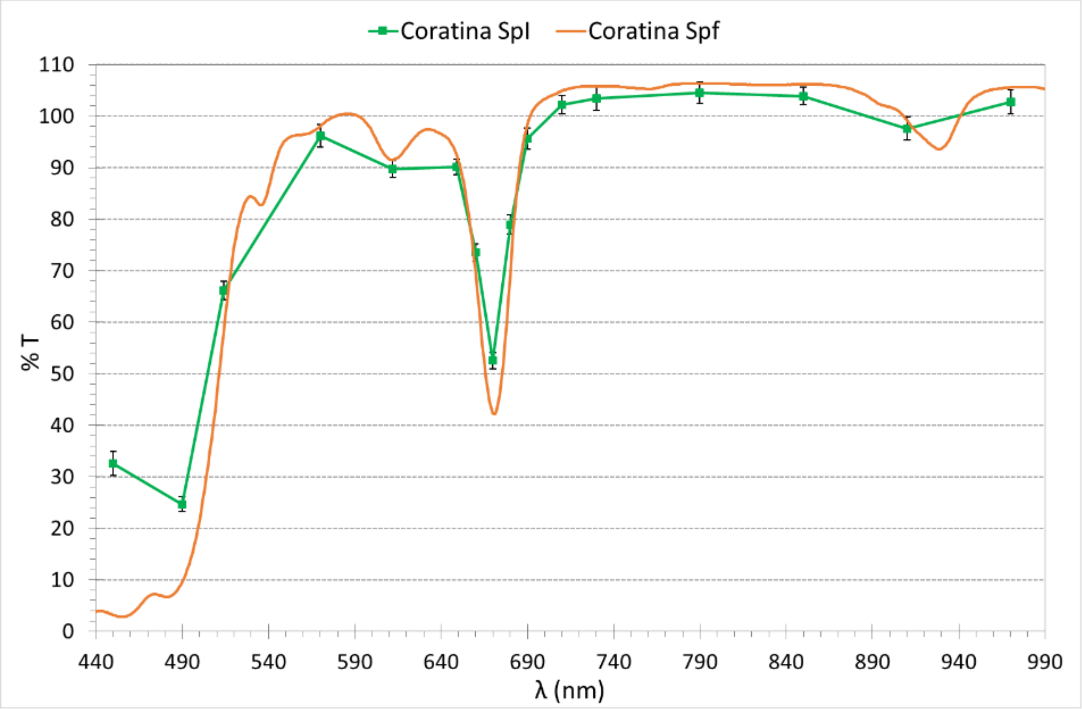

B)

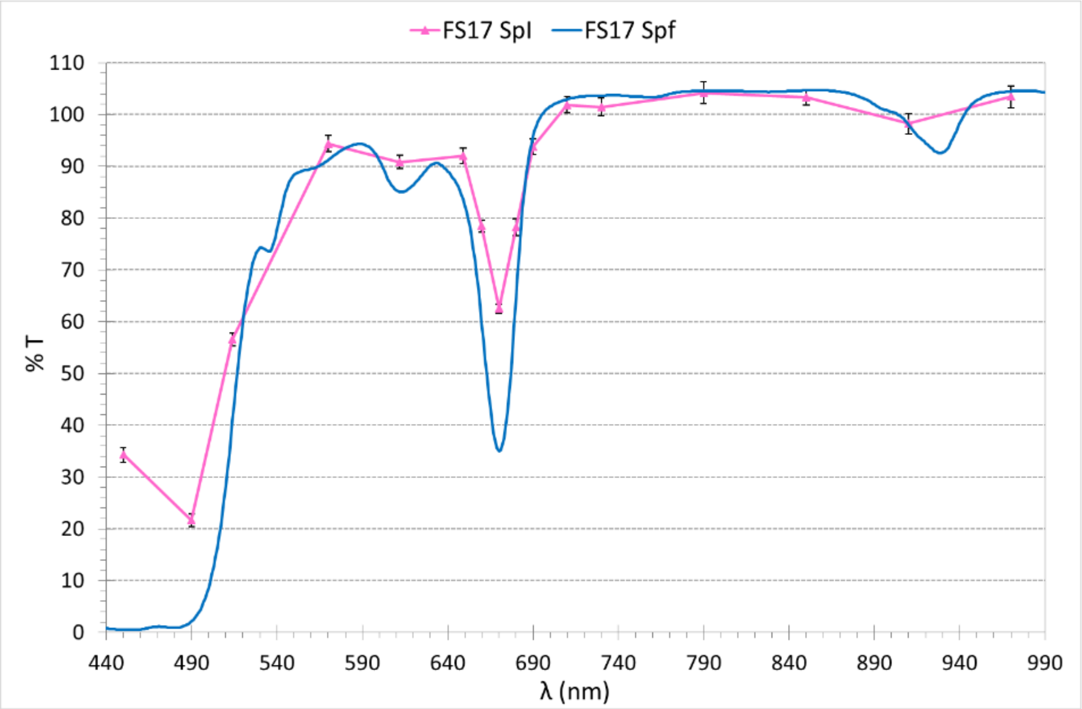

C)

FIGURE 75 – COMPARISON OF TRANSMITTANCE SPECTRA OBTAINED WITH IMAGE SPECTROSCOPY (SPI) AND SPECTROPHOTOMETER (SPF) FOR THREE VARIETIES OF EXTRA VIRGIN OILS:
A) *LECCINO*, B) *CORATINA*, C) *FS17*

As shown in Figure 75, the transmittance values obtained at 450 nm were very different from the spectrophotometer measurement and not in line with the rest of the spectrum trend. The cause is attributable to the poor sensitivity of the technique at that wavelength. Henceforth, the corresponding acquisition will not be taken into consideration.

Another remark should be notice concerning the maximum values significantly exceeding 100%, both with the image spectroscopy and the spectrophotometer. The reason relies in a misinterpretation of the reference. Indeed, usually when analysing liquid with spectrophotometry, the sample consists of solvent added with the solute, while the reference in the solvent alone. In the case of oil, where this methodology could not be applied, the spectra of the samples were modulated on references that were completely different from the oil, i.e. air (empty cuvette), alcohol and water, as shown hereafter.

The analysis of the three other kind of oils gave again results well comparable between image spectroscopy and spectrophotometer. In particular, the absorption peak at 670 nm was clearly detected in the *Lampante* and *Olive* samples (Figure 76-A and C). In addition, the different entity of absorption, much greater in the *Lampante* oil, was evidently reflected even in image spectroscopy. In the same way, it is remarkable the absence of this absorption peak in the spectra of the refined sample with both techniques (Figure 76-B).

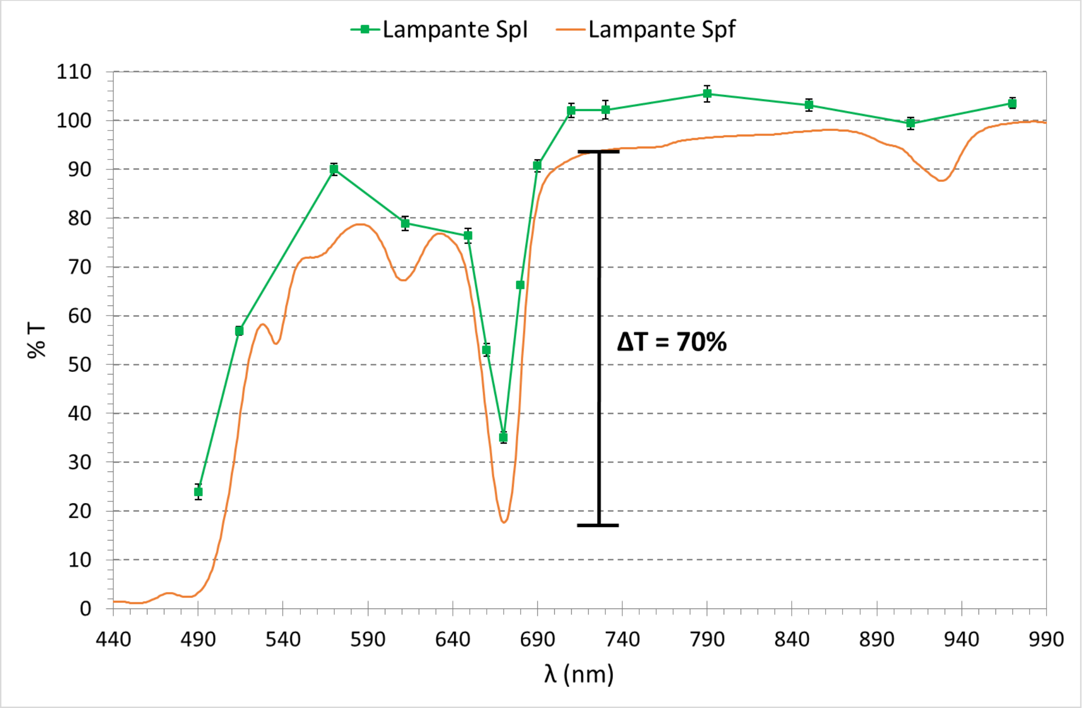

A)

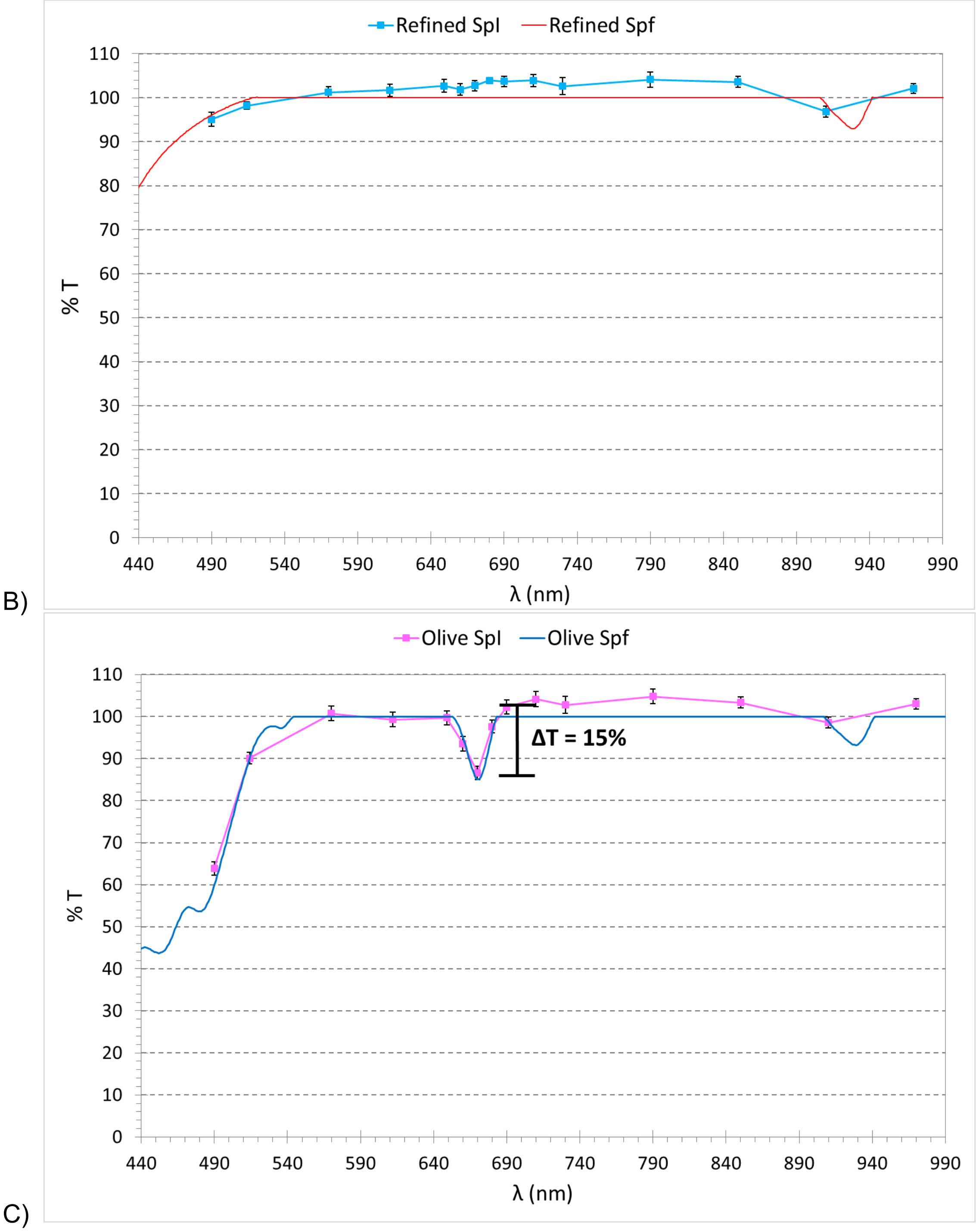

FIGURE 76 - COMPARISON OF TRANSMITTANCE SPECTRA OBTAINED WITH IMAGE SPECTROSCOPY (SPI) AND SPECTROPHOTOMETER (SPF) FOR *LAMPANTE* (A), REFINED (B) AND *OLIVE* OIL (C)

4.3.6 COMPARISON WITH OTHER SPECTROPHOTOMETER MEASUREMENTS

We turned to "Nello Carrara" Institute of Applied Physics of the Italian National Research Council (IFAC-CNR), where, thanks to Dr. Marcello Picollo, we obtained other spectroscopic references by using two Perkin Elmer double-beam double-monochromator spectrophotometers, namely LAMBDA 19 and LAMBDA 1050.

The analyses were performed in transmittance mode on the whole set of oil samples, by using an empty cuvette and a cuvette filled with pure alcohol 95°, as reference. At the end, these spectra were compared with the ones obtained with both image spectroscopy and the spectrophotometer used by the University of Molise.
The results are reported in the graphs included in Figure 78, which show the spectra obtained with image spectroscopy (SpI), the spectrophotometer LAMBDA 25 of the University of Molise (Spf) and the spectrophotometer LAMBDA 19 (Spf IFAC), all using an empty cuvette as reference. The spectra obtained with LAMBDA 19 were quite noisy in the region of NIR because of the detector; moreover, the automatic change of the sensor inside the device at 860 nm appeared as marked step.

For each variety of oil, all the spectra obtained with the two different techniques and the different spectrophotometer devices, showed a similar trend. Some differences were observed only in the absolute values of transmittance. The only exception was a slight positive peak around 900 nm, in case the alcohol was used as reference (Figure 77); this is due to the transmittance spectra of the alcohol itself. For this reason and for ease of reading, since the rest of the trend is anyway similar to the others spectra, this spectrum has not been included in the graphs of Figure 78.

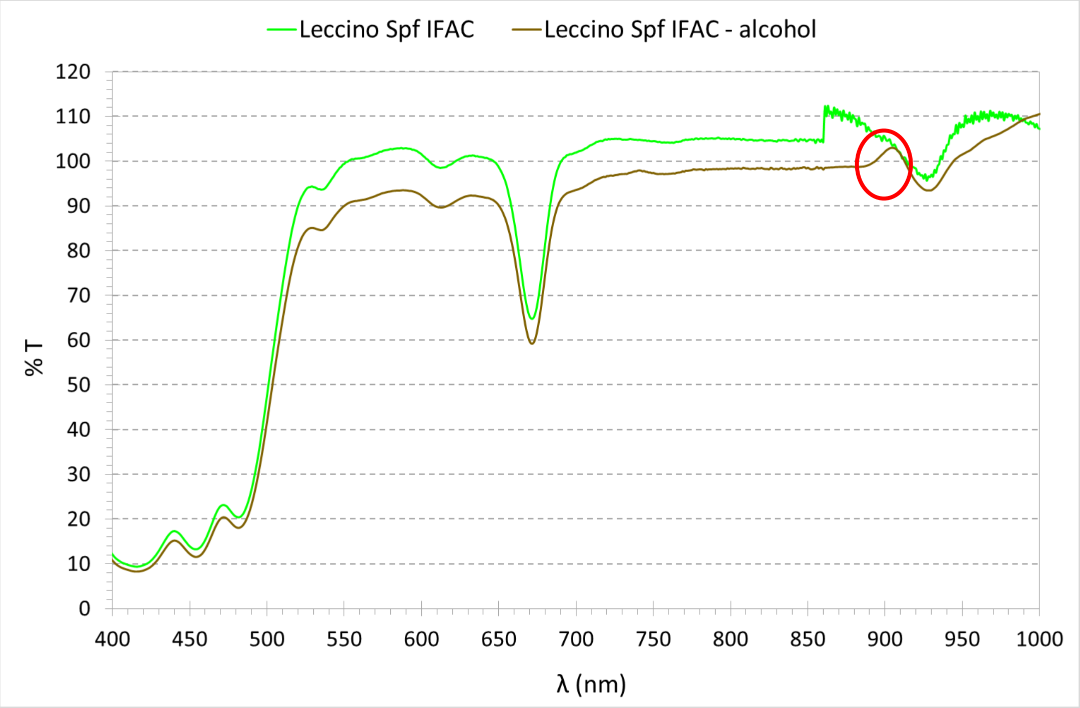

FIGURE 77 – TRANSMITTANCE SPECTRA OF *LECCINO* OIL OBTAINED WITH AN EMPTY CUVETTE (SPF IFAC) AND A CUVETTE FILLED WITH PURE ALCOHOL (SPF IFAC – ALCOHOL), AS REFERENCE

A)

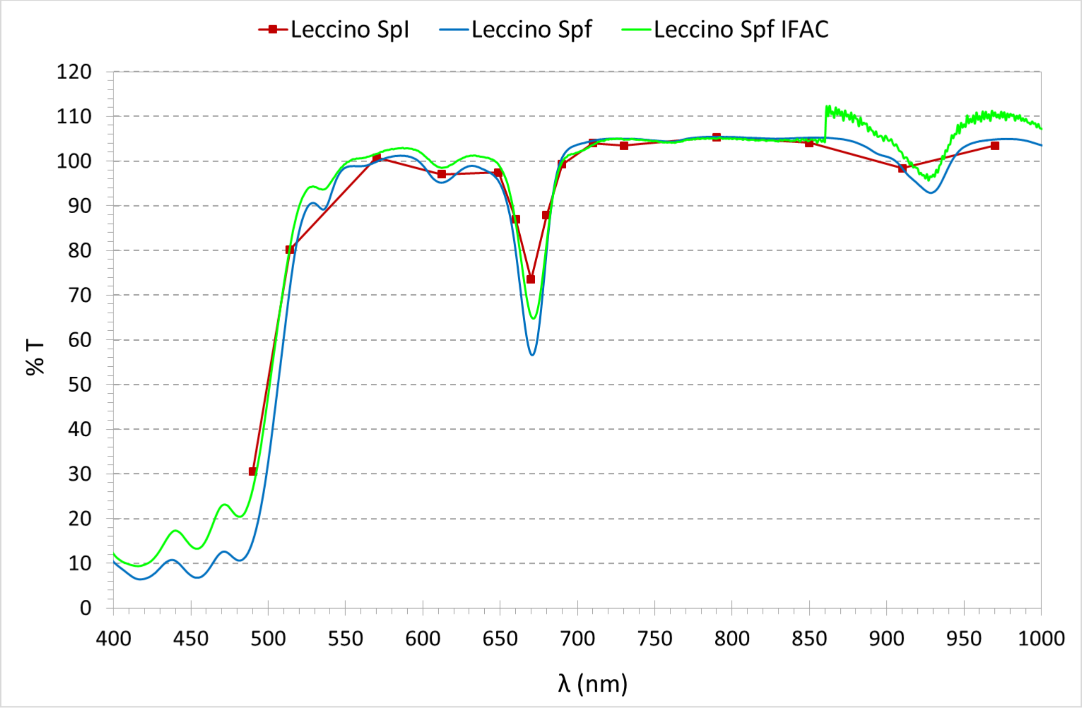

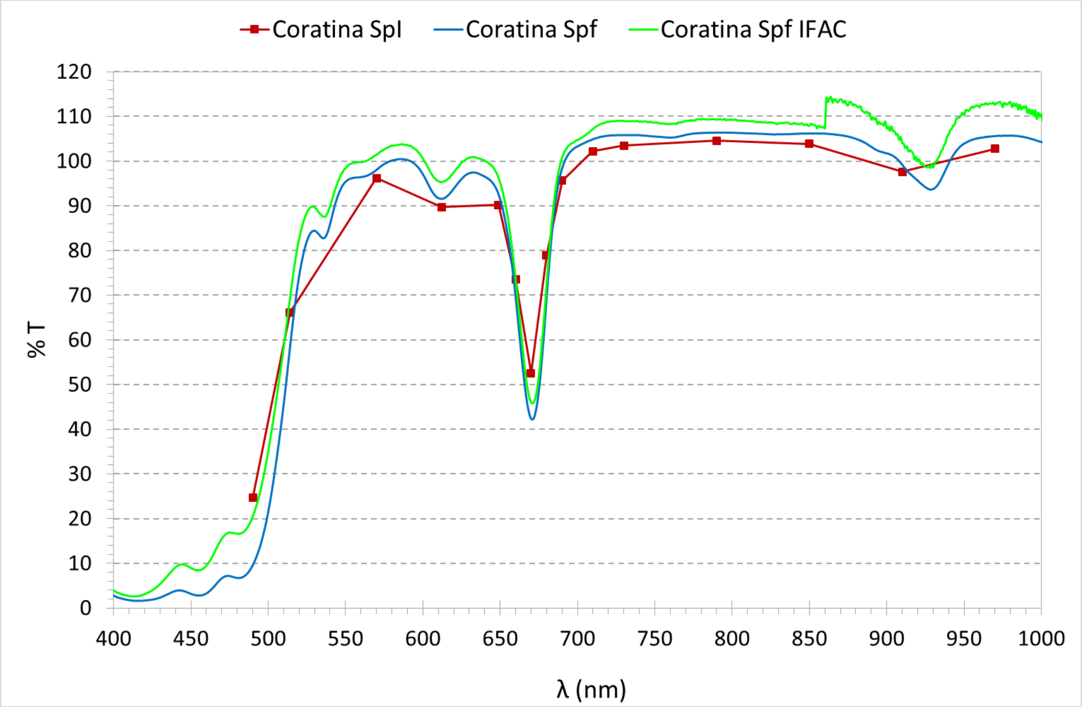
Coratina Spl
Coratina Spf
Coratina Spf IFAC
% T
λ (nm)
0
10
20
30
40
50
60
70
80
90
100
110
120
400
450
500
550
600
650
700
750
800
850
900
950
1000

B)

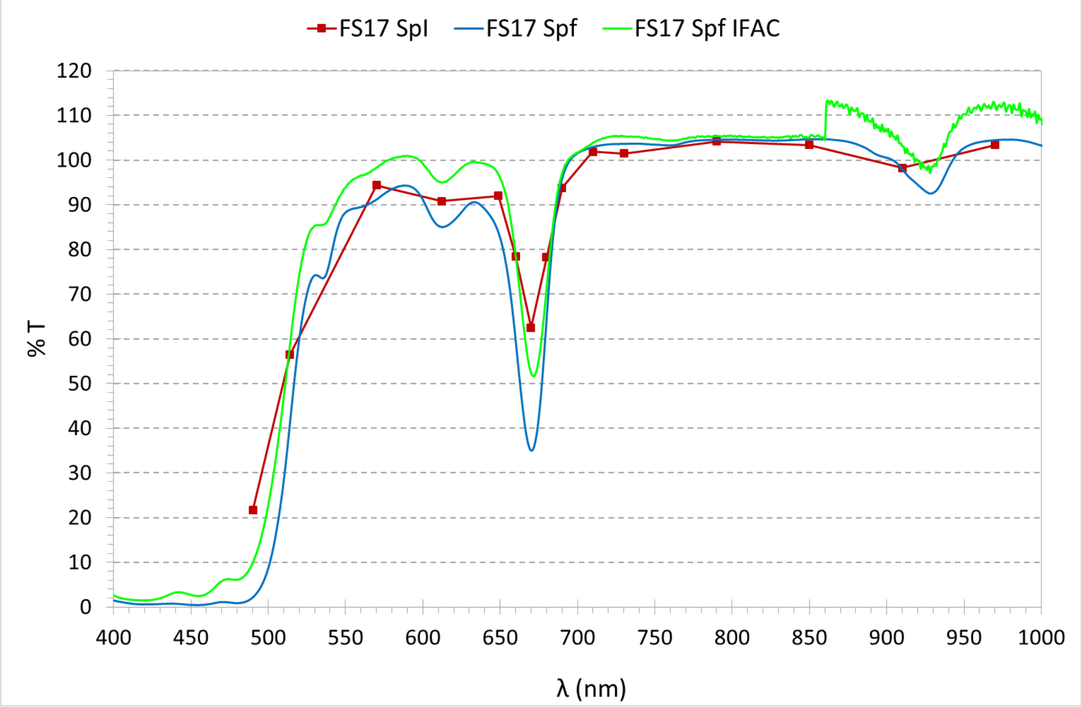
FS17 Spl
FS17 Spf
FS17 Spf IFAC
% T
λ (nm)
0
10
20
30
40
50
60
70
80
90
100
110
120
400
450
500
550
600
650
700
750
800
850
900
950
1000

C)

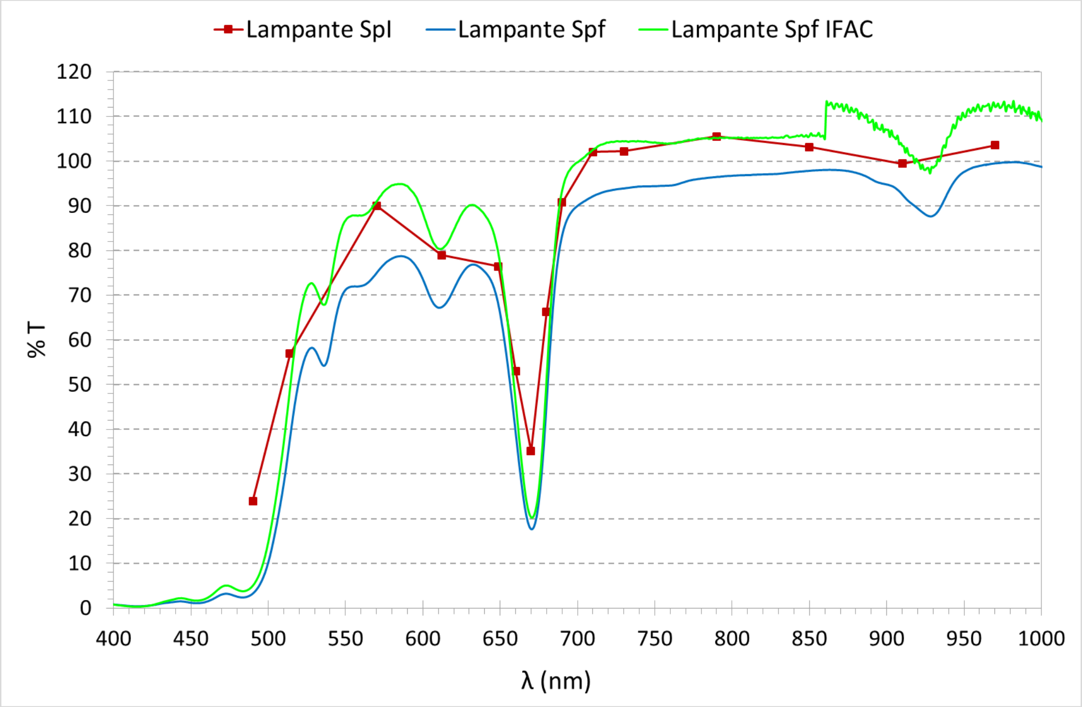
Lampante SpI
Lampante Spf
Lampante Spf IFAC
% T
λ (nm)
0
10
20
30
40
50
60
70
80
90
100
110
120
400
450
500
550
600
650
700
750
800
850
900
950
1000

D)

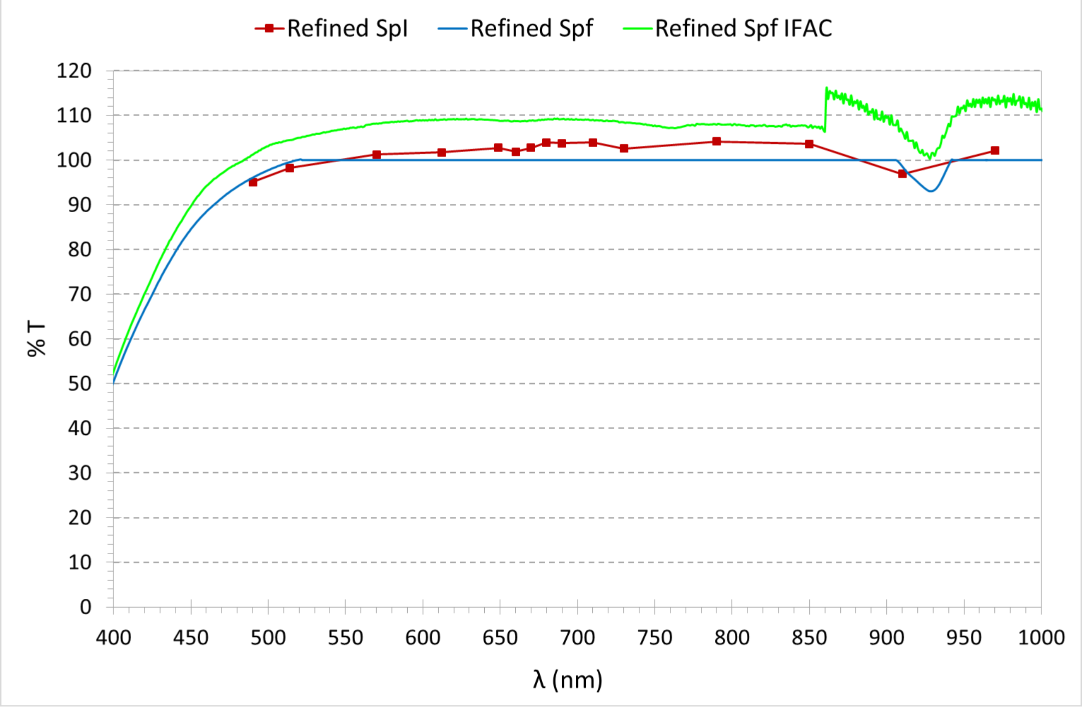
Refined SpI
Refined Spf
Refined Spf IFAC
% T
λ (nm)
0
10
20
30
40
50
60
70
80
90
100
110
120
400
450
500
550
600
650
700
750
800
850
900
950
1000

E)

F)

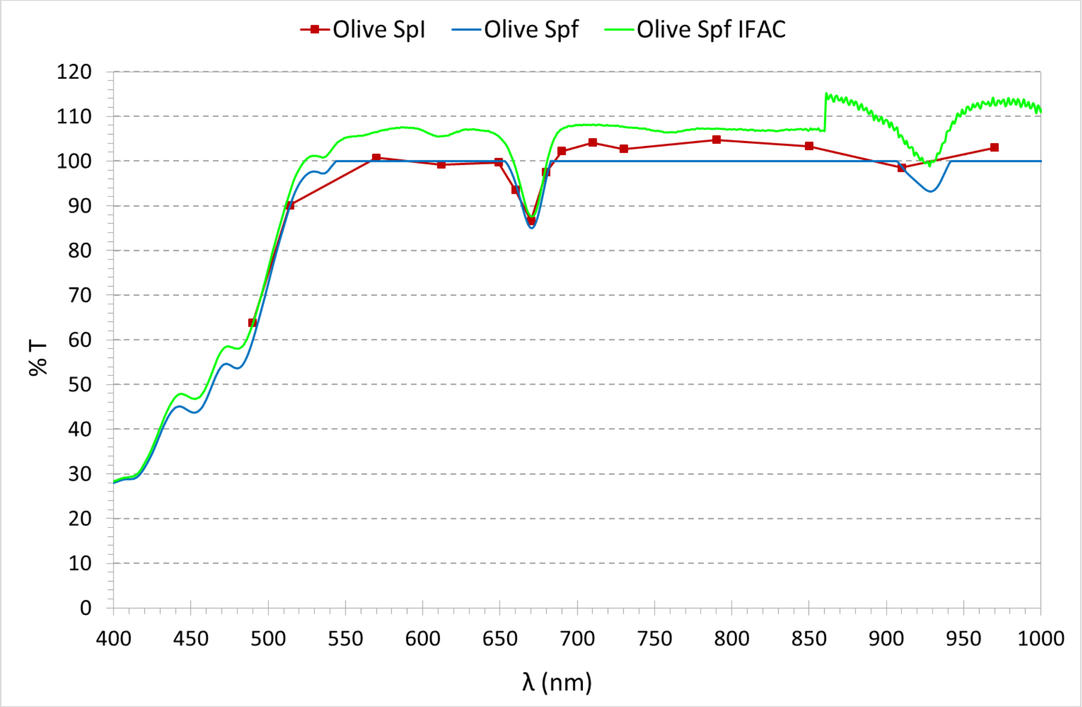

FIGURE 78 – COMPARISON OF TRANSMITTANCE SPECTRA OBTAINED WITH IMAGE SPECTROSCOPY (SPI), SPECTROPHOTOMETERS LAMBDA 25 (SPF) AND LAMBDA 19 (SPF IFAC) FOR THE SAMPLES A) *LECCINO*, B) *CORATINA*, C) *FS17*, D) *LAMPANTE*, E) *REFINED* OIL, F) *OLIVE* OIL

In spite of the difference in the transmittance measured between image spectroscopy and spectrophotometry, up to 10 percentage points, the spectral position of the absorption peaks is detected with adequate precision by the various systems involved.

Another trial was performed by using a cuvette filled with distilled water as reference. Nevertheless, this methodology was discarded because of the trend beyond 920 nm, which reached values around 160 % in the spectra of oils, as a result of the absorption peak of the water (Figure 79).

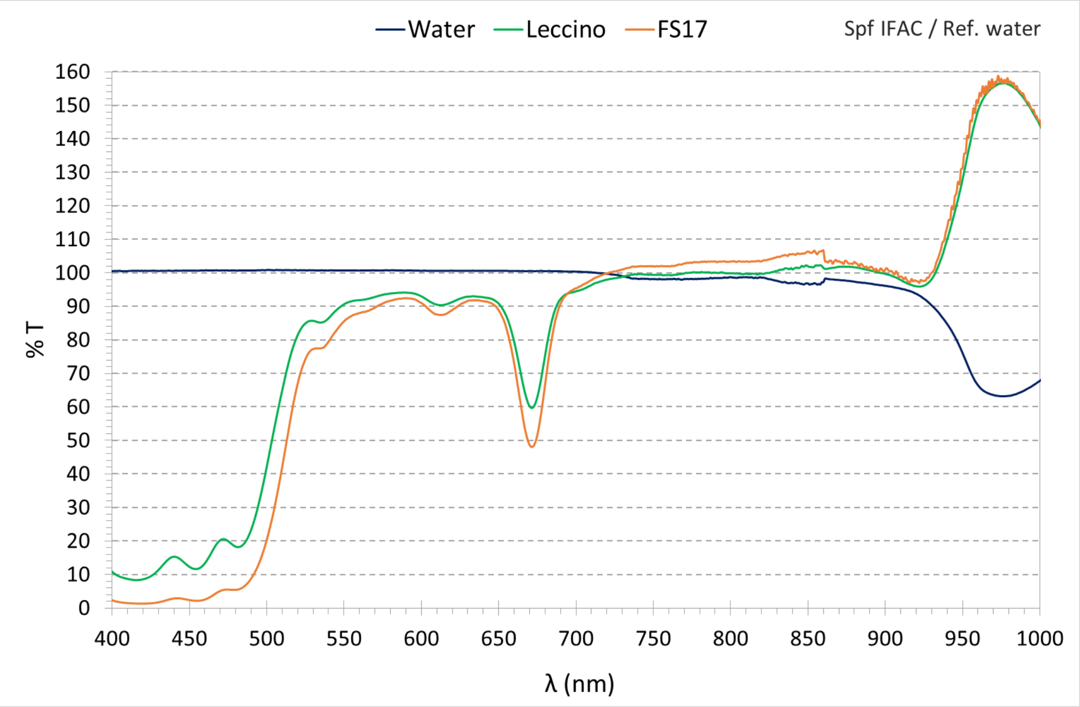

FIGURE 79 –TRANSMITTANCE SPECTRA OF *LECCINO* AND *FS17* WITH CUVETTE FILLED WITH DISTILLED WATER AS REFERENCE OBTAINED WITH LAMBDA 1050

4.3.7 REPEATABILITY OF THE MEASURES

The acquisition of the topographic whites at two different times, after dismounting / mounting the whole set up, were divided for each other, then the minimum, maximum and average values of the grey levels were calculated on the resulting image. This operation was repeated at the different wavelengths next to the interesting peak at 670 nm, i.e. in the range 612-710 nm. The results are reported in Table 21, both for the whole image and for a selection on the most uniform central area after processing with maximum contrast (Figure 80, Figure 81).

λ (nm)	**A) Image**			**B) Selection**		
	min	**max**	**avg**	**min**	**max**	**avg**
612	0.824	1.123	**0.958**	0.904	1.123	**0.961**
649	0.876	1.135	**0.982**	0.933	1.135	**0.991**
660	0.83	1.145	**0.951**	0.897	1.145	**0.959**
670	0.781	1.066	**0.915**	0.861	1.061	**0.921**
680	0.812	1.092	**0.93**	0.882	1.084	**0.939**
690	0.971	1.189	**1.065**	1.027	1.152	**1.076**
710	0.832	1.126	**0.945**	0.892	1.126	**0.948**

TABLE 21 - MINIMUM, MAXIMUM AND AVERAGE VALUES OF THE GREY LEVELS OF THE IMAGE RESULTING FROM THE DIVISION BETWEEN THE TOPOGRAPHIC WHITES ACQUIRED ON TWO DIFFERENT DATES: A) ENTIRE IMAGE; B) SELECTION ON THE MOST UNIFORM CENTRAL AREA AFTER PROCESSING THE WHOLE IMAGE WITH MAXIMUM CONTRAST

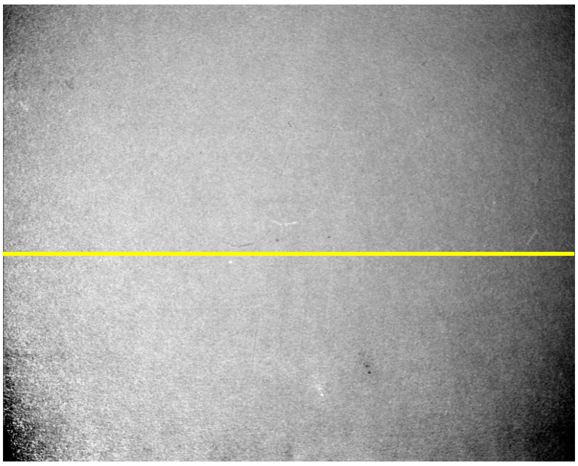

FIGURE 80 – IMAGE RESULTING FROM THE DIVISION OF TWO TOPOGRAPHIC WHITES ACQUIRED AT 612 NM AFTER ELABORATION OF MAXIMUM CONTRAST

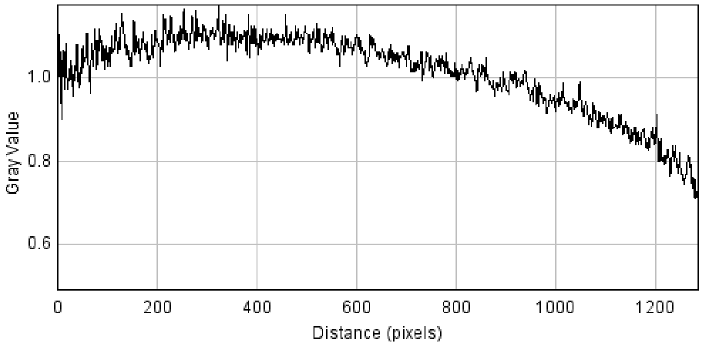

FIGURE 81 – GREY VALUES IN CORRESPONDENCE OF THE PLOTTED YELLOW LINE OF FIGURE 80, FROM THE LEFT TO THE RIGHT

The average values fluctuate around 1, demonstrating the goodness of the topographic white as a tool to correct the acquired images of the samples, as well as the good repeatability of the technique.

Another exercise was carried out by comparing the acquisition at two different times on *Leccino* and *FS17* oil samples in the range 570-730 nm. In this case, the “pure” reflectance values were considered, avoiding the calculation to get the transmittance values. As shown in Figure 82, the spectra of the two oils acquired at time 1 and 2 overlap quite completely, with very small differences of 3.5% at maximum.

Thus, even if by dismounting and mounting the whole set up we are not sure to restore the exact geometrical configuration as in a compact device, we obtained a very good repeatability of the measures.

For comparison, we made the same graph (Figure 83) including the spectra obtained with two different analysis with the spectrophotometer LAMBDA 25. In this case, the spectra of *Leccino* and *FS17* oils differ of maximum 9% and 14% respectively.

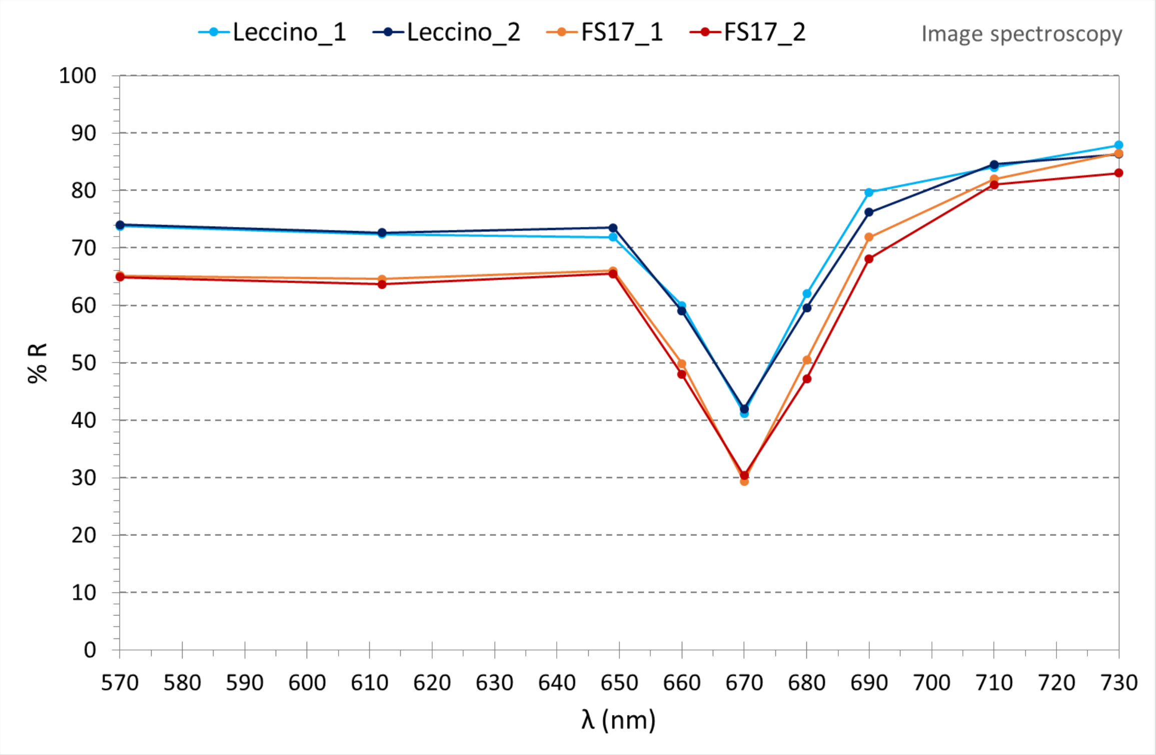

FIGURE 82 – REFLECTANCE SPECTRA OF *LECCINO* AND *FS17* OILS OBTAINED WITH IMAGE SPECTROSCOPY AT TWO DIFFERENT TIME OF ACQUISITION (1 AND 2)

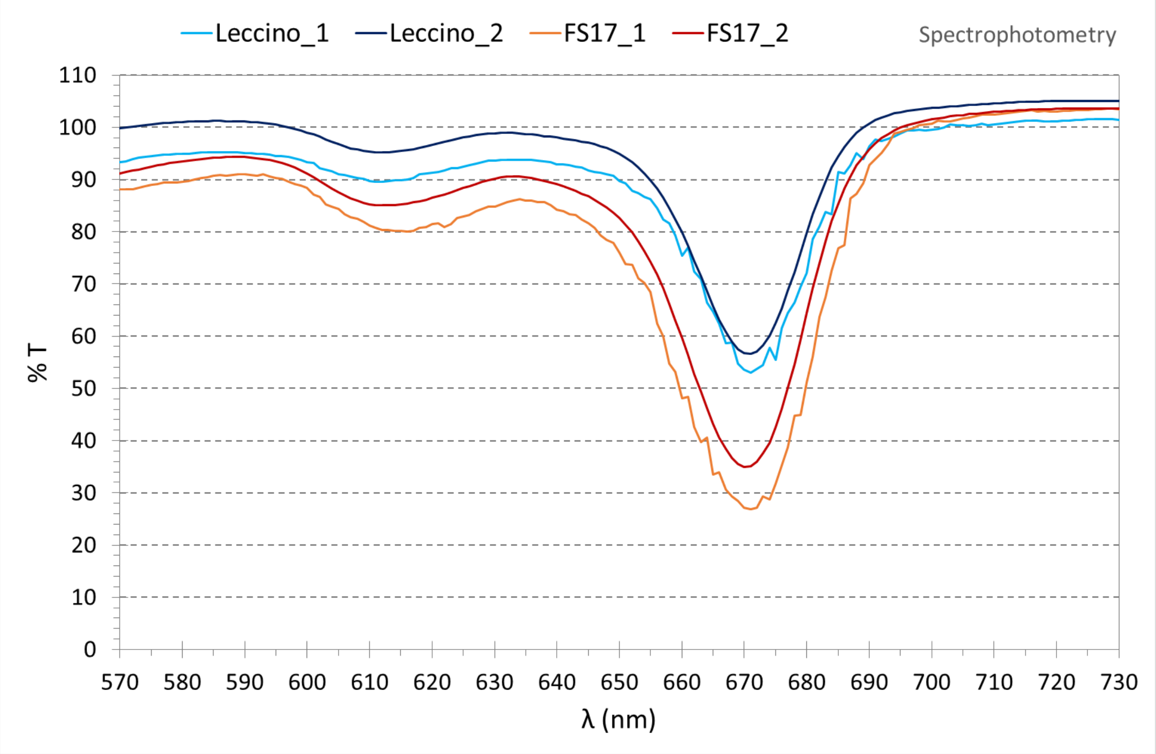

FIGURE 83 - TRANSMITTANCE SPECTRA OF *LECCINO* AND *FS17* OILS OBTAINED WITH SPECTROPHOTOMETRY AT TWO DIFFERENT TIME OF ACQUISITION (1 AND 2)

CONCLUSION OF SECTION B

Two experimental techniques were properly configured and adapted for specifically requested purposes and they were analysed in terms of performance and reliability. The imaging instruments based on Schlieren effect and reflectance spectroscopy respectively were implemented at the stage of 'proof of concept'. Anyway, the first interesting results demonstrated the possibility to study more in deeply their future developments.

The first objective was to build a Schlieren optical system able to visualize the airflows through small changes in the refractive index, due to variations in pressure/temperature. The idea to develop a portable instrument for the imaging of air movement, to be applied to the HVAC studies, is very promising thanks to its real-time imaging capability and no interference with the air flow. The system could be applied everywhere ventilation problems occurs, such as hospital environments, laboratory fume hoods, clean rooms, etc. Moreover, it could give a worthy contribution to indoor air quality studies or validate complex computational flow patterns, being a valid alternative to traditional systems using gas tracer or particle velocity. The experimental work focused on understanding the potentiality of the system built in the laboratory and the basic conditions to work in real environments.

A single-mirror Schlieren system was mounted on an optical bench, equipped with a concave parabolic mirror, a white LED light, a pinhole to create a point light source, a knife-edge to cut the maximum zero order of diffraction and, separately on a tripod, a digital camera (Thorlabs Inc., USA) for image acquisition.

The first tests were performed to display the heat "plume" from the tip of a welder and from the hand in order to estimate the sensitive volume of the working area along the optical bench. The volume of the working area was estimated as equal to the focal length of the mirror (86.4 cm). Indeed, the display of the Schlieren effect decreased considerably over 50-60 cm away from the mirror and then got lost when the focal length of 86 cm was exceeded. The maximum yield was very close to the mirror, especially when the temperature gradient with respect to air room temperature was low.

In order to quantify the sensitivity to variations of the refraction index (n), a helium gas flow was used. The gas flow, from turbulent to stable "plume", was clearly displayed, demonstrating that a change from 1.000293 (n of air) to 1.000036 (n of helium) is visible.

Further tests were carried out with compressed air, demonstrating the sensitivity of the system to pressure variations in both static and perturbed conditions. The results confirmed that the Schlieren effect was more evident with pressure over 2 bar and if the flow was subjected to movements.

The second objective was to configure properly the technique of image spectroscopy for the analysis of olive and refined oil samples and to test the reliability of the results in comparison with spectrophotometric analysis.

Thus, from one side, one has finely discretized spectra obtained with multispectral devices, useful for identifying the optimal bands in which to concentrate the spectroscopic filters of image spectroscopy and for validating the technique as equally effective. From the other side, the use of image spectroscopy instead of multispectral devices allows portability and affordability in terms of costs, even at the expense of spectral resolution. Hence, it would be feasible a first individuation of possibly counterfeit samples with image spectroscopy, to be labelled for further and deeper analyses with techniques that are more specific.

The technique of image spectroscopy consists of the acquisition of images at different wavelengths with a monochromatic digital camera equipped with a rotating wheel, containing 16 interferential optical filters, which cover the sensitivity range of the silicon semiconductor detector from 490 to 970 nm with a bandwidth of 10 nm. Each image carries the information related to the reflectance diffused by the sample in the spectral band transmitted by the interferential filter. The reflectance measurements of the sample are performed by interpolation with the reflectance values on reference standards.

After several preliminary tests for the identification of the appropriate configuration, six samples of oil were analysed. The reflectance values were then processed to obtain the corresponding transmittance values to be compared to those collected with the spectrophotometer.

The intent was to obtain reflectance / transmittance spectra similar to those obtained with the spectrophotometer, in particular to identify the absorption peak at 670 nm, which allows distinguishing extra virgin oils from refined ones.

The absorption peak centred at 670 nm was clearly detected in all three reflectance spectra of the analysed extra virgin oils. The slight differences between the three varieties of extra virgin oils were measured as well, i.e. a greater absorption of *Coratina* and *FS17* with respect to *Leccino* cultivar.

Concerning the analysis of the three other oil (not extra virgin), the absorption peak at 670 nm was noticed in both the *Lampante* and *Olive* samples, reflecting also the different entity of absorption, much greater in the first one.

In general, all the transmittance curves obtained by image spectroscopy overlapped with good approximation the ones obtained with all the spectrophotometer devices used (LAMBDA 19 -25- 1050). Some differences were observed only in the absolute values of transmittance, partially due to the uncertainty of the measures of both of techniques, and to the calculations necessary to pass from reflectance to transmittance values.

In conclusion, image spectroscopy has proven to be a valid technique being very precise in giving the correct spectral position of the absorption peaks of the examined oil samples.

APPENDIX 1

List and description of parameters (THORLABS, 2016) set in the ThorCam software to enhance the quality of Schlieren images.

- CAMERA
    - PIXEL CLOCK: it determines the speed at which the sensor cells can be read out.
    - FRAME RATE: the possible range of settings depends on the selected pixel clock. You can select a lower frame rate without changing the pixel clock, whilst you need to increase the pixel clock to set a higher frame rate.
    - EXPOSURE TIME: it depends on the selected frame rate and is pre-set to its reciprocal value, i.e. a lower frame rate allows for longer exposure times. You can select a shorter exposure time without changing the frame rate, whilst you need to reduce the frame rate to set a longer exposure time.
- IMAGE
    - MASTER GAIN: a voltage proportional to the amount of incident light is output by the sensor. To increase image brightness and contrast, this signal can be amplified by an analogical gain and offset before the digitizing process. The results of analogical signal processing are usually better than the results of digital post-processing. Depending on the sensor type, a global gain value for all pixels (master gain) or a separate gain value for each colour (RGB gain) can be set: in our case, the auto gain feature is used.
    - BLACK LEVEL (OFFSET): every digital image sensor has light-insensitive cells next to the active image area. These dark pixels are used to measure a reference voltage (black level) which is subtracted from the image signal. This compensates thermally generated voltages on the sensor, which would otherwise falsify the signals. Normally, the sensor adjusts the black level automatically. If the environment is very bright or if exposure times are very long, it may be necessary to adjust the black level manually.
    - SOFTWARE GAMMA: when imaging a scene, the shape of the grey level characteristic is crucial for displaying differences in brightness. With image processing, linear characteristics are generally required. The human eye, on the other hand, perceives differences in brightness based on a logarithmic characteristic, which often approximates a gamma characteristic in practice. <u>Linear characteristic</u>: if a system yields double the output value for double the brightness, the system features a linear characteristic (Figure 84).

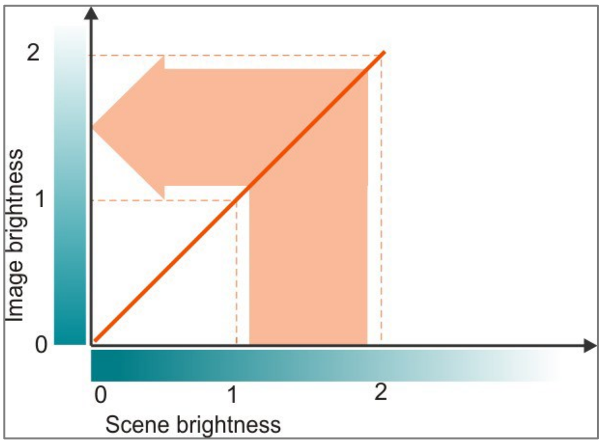

FIGURE 84 – IMAGING WITH LINEAR CHARACTERISTIC

Gamma characteristics: gamma curves are power functions of the form $y = x^{1/\gamma}$, with γ values included in the range 1-2.2 (i.e. $1/\gamma < 1$), as limited in the software. Gamma characteristic brightens dark areas of an image, which corresponds more to the perception of the human eye; whilst in light areas of an image, the differences in brightness are condensed (Figure 85). A gamma value of 1 generates a linear characteristic again.

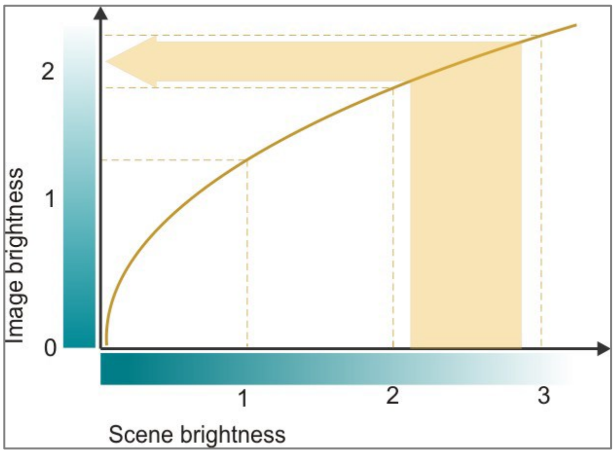

FIGURE 85 – IMAGING WITH GAMMA CHARACTERISTIC

Logarithmic characteristic: the logarithmic characteristic follows the function $y = \log(x)$. Very large jumps in brightness in light areas of a scene only cause small changes in image brightness (Figure 86). This explains why image sensors with a logarithmic characteristic, in particular, are ideal for imaging scenes with very wide dynamic range.

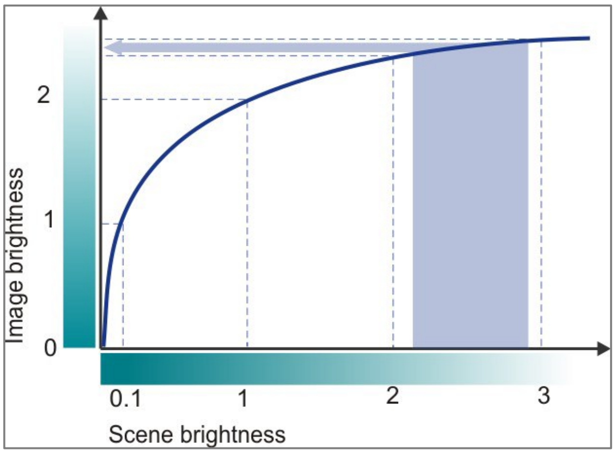

FIGURE 86 - IMAGING WITH LOGARITHMIC CHARACTERISTIC

- SHUTTER:

  The image is recorded in the sensor in four phases:

  a. Reset pixels of the rows to be exposed
  b. Exposure of pixel rows
  c. Charge transfer to sensor
  d. Data readout

  The sensors of the camera have no mechanical shutters, but work with electronic shutter methods instead. The control of the average brightness is preferably achieved by adjusting the exposure, i.e. you set the highest possible exposure time before gain is controlled.

  - GLOBAL AREA: with a global shutter sensor, all pixel rows are reset and then exposed simultaneously. At the end of the exposure, all rows are simultaneously moved to a darkened area of the sensor. The pixels are then read out row-by-row (Figure 87). Exposing all pixels simultaneously has the advantage that fast-moving objects can be captured without geometric distortions.

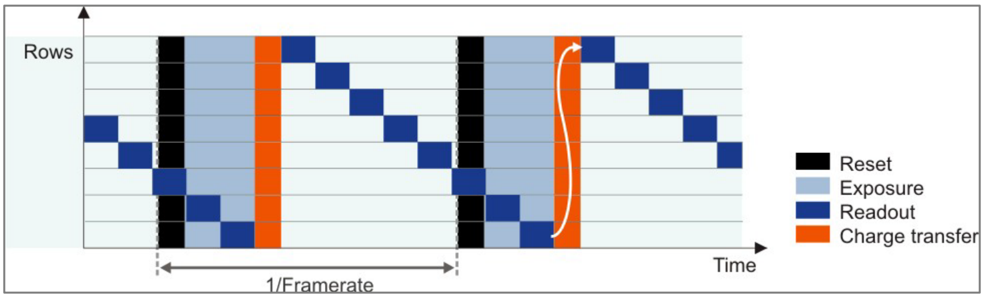

FIGURE 87 - TIMING OF GLOBAL SHUTTER SENSOR IN LIVE MODE

  - MANUAL LOG MODE: in the manual Log mode, it is possible to display the information in the overexposed image areas. This mode is effective for very short exposure times, when there may occur the so-called crosstalk effects in the global shutter mode, which have the effect that the image content appears brighter in vertical line, from top to bottom. When using the manual Log mode no master gain is possible.
  - LOG MODE GAIN: the Log Manual Gain class provides methods for setting the gain, which can be adjusted in 5 levels. The level "3" corresponds to a gain factor of 1 for monochrome or colour sensors. A low level results in a low gain and may display more details in the overexposed image areas; on the contrary, a higher level gives a higher gain, thereby a darker image can be brightened.
  - LOG MODE VALUE: the Log Manual Value class provides methods for setting the threshold at which the linear sensitivity pass over into a logarithmic characteristic. It can be adjusted in 13 levels: the value "0" represents the lowest active level and "12" corresponds to the highest level.

REFERENCES

Albertin F., Boselli L., Peccenini E., Pellicori V., Petrucci F., Tisato F. 2012. Image spectroscopy for conservation and diagnostics of contemporary painting materials. *Proceedings of the Meeting Science for Contemporary Art.* 2012, p. 93-102.

ASHRAE. 2004. ASHRAE 55-2004R. *Thermal Environmental Conditions for Human Occupancy.* Atlanta, GA : American Society of Heating, Refrigerating and Air-Conditioning Engineers, 2004.

Atcheson B., Heidrich W., Ihrke I. 2009. An evaluation of optical flow algorithms for background oriented schlieren imaging. *Experiments in Fluids.* 2009, Vol. 46, 3, p. 467–476.

Auliciems, A. 1981. Towards a psychophysiological model of thermal perception. *International Journal of Biometeorology.* 1981, Vol. 25, p. 109–122.

Baglivo L., Lucchi E., Roberti F., Frick J., Reichert M., Schönberger E., Grün G., Garmendia Arrieta L., Casado A.M., Verhey B., Brocken H., Menmuir S., Fairnington I., Gouas V., Hermann C., Ochoa M. 2015. *D4.4 Results of laboratory and outdoor tests for the validation of new materials.* s.l. : Deliverable of FP7 project EFFESUS (Grant no. 314678, FP7-2012-NMP-ENV-ENERGY-ICT-EeB), 2015.

Becherini F., Lucchi E., Gandini A., Barrasa M.C., Troi A., Roberti F., Sachini M., Di Tuccio M.C., Arrieta L.G., Pockelé L., Bernardi A,. 2018. Characterization and thermal performance evaluation of infrared reflective coatings compatible with historic buildings. *Building and Environment.* 2018, Vol. 134, p. 35-46.

Bernardi A., Becherini F., Romero-Sanchez M.D. , Lopez-Buendia A., Vivarelli A., Pockelé L., De Grandi S. 2014. Evaluation of the effect of Phase Change Materials technology on the thermal stability of Cultural Heritage objects. *Journal of Cultural Heritage.* 2014, Vol. 15, 5, p. 470-478.

Bernardi A., Becherini F., Vivarelli A., De Grandi S., Pockelé L. 2010. *Monitoraggio microclimatico presso il Museo dell'Opera di Santa Croce a Firenze – Anno 2010.* 2010. Technical report to the Opera of Santa Croce di Firenze, Italy.

—. 2011. *Museo dell'Opera di Santa Croce - Campagne di misura manuali.* 2011. Technical report to the Opera of Santa Croce di Firenze, Italy.

Bernardi A., Vivarelli A., Becherini F., Broström T., Hermann C., Hrabovszky-Horváth S., Rodwell D., Stuart J., Troi A. 2013. *D1.2 Establishment of Impact indicators.* s.l. : Deliverable of FP7 project EFFESUS (Grant no. 314678, FP7-2012-NMP-ENV-ENERGY-ICT-EeB), 2013.

Brager G.S., de Dear R.J. 1998. Thermal adaptation in the built environment: a literature review. *Energy and Buildings.* 1998, Vol. 27, p. 83-86.

Brocken H. 2014. *D4.3 New lime based mortar.* s.l. : Deliverable of FP7 project EFFESUS (Grant no. 314678, FP7-2012-NMP-ENV-ENERGY-ICT-EeB), 2014.

Burton, R.A. 1949. A Modified Schlieren Apparatus for Large Areas of Field. *Journal of the Optical Society of America.* 1949, Vol. 39, 11, p. 907-908.

Cabeza L. F., Castell A., Barreneche C., De Gracia A., Fernandez A.I. 2011. Materials used as PCM in thermal energy storage in buildings: A review. *Renawable and Sustainable Energy Reviews.* 2011, Vol. 15, p. 1675-1695.

Casado M., Tsoutis C., Garmendia L., Gouas V., Gouas F., Özgür K. 2014. *D4.1 New radiation cost-effective selective coating.* s.l. : Deliverable of FP7 project EFFESUS (Grant no. 314678, FP7-2012-NMP-ENV-ENERGY-ICT-EeB), 2014.

Casado M., Vivarelli A., Becherini F., Di Tuccio M., Bernardi A., Mezzasalma G., Menmuir S.,, Schumacher P. 2016. *D7.3 Assessment of the performance and validation of the systems after renovation.* s.l. : Deliverable of FP7 project EFFESUS (Grant no. 314678, FP7-2012-NMP-ENV-ENERGY-ICT-EeB), 2016.

CEN, European Committee for Standardization. 1995. *Moderate thermal environments. Determination of the PMV and PPD indices and specification of their conditions for thermal comfort.* Brussels, Belgium : s.n., 1995.

Chen C., Guo H., Liu Y., Yue H., Wang C. 2008. A new kind of Phase Change Material (PCM) for energy storing wallboard. *Energy and Buildings.* 2008, Vol. 40, p. 882-890.

Daffara C., Pampaloni E., Pezzati L., Barucci M., Fontana R. 2010. Scanning Multispectral IR Reflectography SMIRR: An advanced tool for art diagnostics. *Accounts of Chemical Research.* 2010, Vol. 6, 43, p. 847-856.

de Dear R.J. 1998. A global database of thermal comfort field experiments. *ASHRAE Transactions.* 1998, Vol. 104, 1b, p. 1141–1152.

de Dear R.J., Brager G.S. 1998. Developing an adaptive model of thermal comfort and preference. *ASHRAE Transactions.* 1998, Vol. 104, p. 145–167.

—. 2002. Thermal comfort in naturally ventilated buildings: revisions to ASHRAE standard 55. *Energy and Buildings.* 2002, Vol. 34, 6, p. 549–561.

Edmund Optics Ltd. https://www.edmundoptics.eu/optics/optical-mirrors/focusing-concave-mirrors/4.25-diameter-x-34-fl-protected-aluminum-parabolic-mirror/#resources. [Online]

Epstein Y., Moran D.S. 2006. Thermal Comfort and the Heat Stress Indices. *Industrial Health.* 2006, Vol. 44, p. 388-398.

Fanger P.O. 1982. *Thermal comfort.* Florida : Kreiger, 1982.

Farid M.M., Khudhair A.M., Razack S. A. K., Al-Hallaj S. 2004. A review on phase change energy storage: materials and applications. *Energy Conversion and Management.* 2004, Vol. 45, p. 1597-1615.

Felix Regin A., Solanski S.C., Saini J.S. 2008. Heat transfer characteristics of thermal energy storage system using PCM capsules: A review. *Renewable and Sustainable Energy Reviews.* 2008, Vol. 12, p. 2438-2458.

Gouas, DWE, Rodwell, HOR-BER, Fraunhofer, NTNU e Acciona, RED, Historic Scotland. 2015. *D7.2 Developed systems installed, commissioned and started-up.* s.l. : Deliverable of FP7 project EFFESUS (Grant no. 314678, FP7-2012-NMP-ENV-ENERGY-ICT-EeB), 2015.

Hargather M. and Settles G.S. 2010. Natural-background-oriented schlieren imaging. *Experiments in Fluids.* 2010, Vol. 48, 1, p. 59–68.

Hecht E. and Zajac A. 1979. *Optics.* s.l. : Addison-Wesley Publishing Company, 1979.

ISO. 2005. 7730-2005. *Ergonomics of the thermal environment - Analytical determination and interpretation of comfort using calculation of the PMV and PPD indices and local thermal comfort criteria.* Geneva : International Standards Organization, 2005.

—. 2004. 8996-2004. *Ergonomics of the thermal environment. Determination of metabolic rate.* Geneva : International Standards Organization, 2004.

—. 2007. 9920-2007. *Ergonomics of the thermal environment - Estimation of thermal insulation and water vapour resistance of a clothing ensemble.* Geneva : International Standards Organization, 2007.

—. 2014. BS EN ISO 9869-1. *Thermal insulation. Building elements. In-situ measurement of thermal resistance and thermal transmittance. Part 1: Heat flow meter method.* 2014.

Khudhair A.M., Farid M.M. 2004. A review on energy conservation in buildings applications with thermal energy storage latent heat using phase change materials. *Energy Conversion and Management.* 2004, Vol. 45, p. 263-275.

Kuznik F., Virgone J., Johannes K. 2011. In situ study of thermal comfort enhancement in a renovated building equipped with Phase Change Material wallboard. *Renawable Energy.* 2011, Vol. 39, p. 1458-1462.

Lucchi E., Becherini F., Di Tuccio M.C., Troi A., Frick J., Roberti F., Hermann C., Fairnington I., Mezzasalma G., Pockelé L., Bernardi A. 2017. Thermal performance evaluation and comfort assessment of advanced aerogel as blown-in insulation for historic buildings. *Building and Environment.* 2017, Vol. 122, p. 258-268.

Mazumdar, A. 2013. *Principles and techniques of Schlieren imaging systems.* Columbia University. New York : s.n., 2013.

Meier G.E.A. 2002. Computerized background-oriented schlieren. *Experiments in Fluids.* 2002, Vol. 33, 1, p. 181-187.

Nicol J.F., Humphreys M.A. 2002. Adaptive thermal comfort and sustainable thermal standards for buildings. *Energy and Buildings.* 2002, Vol. 34, p. 563–572.

Oleari C. 1998. *Misurare il colore. - Spettrofotometria, fotometria e colorimetria. Fisiologia e percezione.* Milano : Hoepli Ed., 1998.

Pellicori V. 2013. *Image spectroscopy for diagnostic and conservation of contemporary art materials.* 2013. Tesi di Dottorato in fisica, A.A. 2010-2012.

Petrucci F. 2004. Image spectroscopy for diagnostics and conservation of contemporary art. [aut. libro] Società Italiana di Fisica. [a cura di] M. Milazzo, M. Piacentini M. Martini. *Physics methods in Archaeometry - Proceedings of the Internation schoold of Physics "Enrico Fermi" (Course CLIV).* 2004, p. 331-345.

Romero M.D., Lopez A.M., Becherini F., Bernardi A. 2012. *D8.1 PCM storage barriers and possible solutions to CH buildings.* s.l. : Deliverable of FP7 project MESSIB (Grant no. 211624, NMP-2007-4.0-5), 2012.

Romero-Sanchez M. D., Guillem-Lopez C., Lopez-Buendia A. M., Stamatiadou M., Mandilaras I., Katsourinis D., Founti M. 2012. Treatment of natural stones with Phase Change Materials: Experiments and computational approaches. *Applied Thermal Engineering.* 2012, Vol. 48.

Rossi G., Iacomussi P., Sarotto M., Soardo P. 1998. Misurazioni gonioriflettometriche per la colorimetria. *Proceedings of colorimetry 1998, SIOF.* 1998, p. 71-86.

Runming Y., Baizhan L., Jing L. 2009. A theoretical adaptive model of thermal comfort – Adaptive Predicted Mean Vote (aPMV). *Building and Environment.* 2009, Vol. 44, p. 2089–2096.

Schardin H. 1942. Schlieren methods and their applications. *Ergebnisse der exakten Naturwissenschaften.* 1942, Vol. 20, 303.

Settles G.S. and Via G. 1986. A Portable Schlieren Optical System for Clean Room Applications. *The Journal of Environmental Sciences.* 1986, Vol. 30, 5, p. 17-21.

Settles G.S. and Via G.G. 1989. Measurement and Control of Particle-Bearing Air Currents in a Vertical Laminar Flow Clean Room. [a cura di] K.L. Mittal. *Particles in Gases and Liquids.* Boston : Springer, 1989, Vol. 1.

Settles G.S. 2004. Important developments in schlieren and shadowgraph visualization during the last decade. *International Symposium on Flow Visualization.* 2004.

—. 2006. *Schlieren and Shadowgraph Techniques: Visualizing Phenomena in Transparent Media.* s.l. : Springer, 2006. 2 edition.

—. 1997. Visualizing Full-Scale Ventilatin Airflows. *ASHRAE Journal.* July 1997, p. 19-26.

Spectabit Optics LLC. https://www.spectabit.com/index.php/analog-schlierenscope. [Online]

Spectabit Optics LLC. https://www.spectabit.com/index.php/digital-focusing-schlieren. [Online]

—. https://www.spectabit.com/index.php/focusing-schlieren. [Online]

Steskens P., Loomans M. 2010. *T1.3 Performance Indicators for Health and Comfort.* s.l. : Deliverable of FP7 project PERFECTION (Grant no. 212998, FP7-ENV 2007-1), 2010.

Strikolith B.V. http://www.strikolith.com/product/generate_information/?id=1495. [Online]

Tang J.W., Liebner T.J., Craven B.A., Settles G.S. 2009. A schlieren optical study of the human cough with and without wearing masks for aerosol infection control. *Journal of the Royal Society Interface.* 2009, Vol. 6, Suppl. 6, p. S727–736.

Tang J.W., Nicolle A.D.G., Pantelic J., Jiang M., Sekhr C., Cheong D.K.W., Wai Tham K. 2011. Qualitative Real-Time Schlieren and Shadowgraph Imaging of Human Exhaled Airflows: An Aid to Aerosol Infection Control. [a cura di] J.C. Benjamin. *PLOS One.* 2011, Vol. 6, 6.

Tang J.W., Settles G.S. 2009. Images in clinical medicine. Coughing and masks. *The New England Journal of Medicine.* 2009, Vol. 361, 26.

THORLABS. 2016. *DCx Camera Functional Description and SDK Manual - v. 4.80.* 8 11 2016.

Tyagi V.V., Buddhi D. 2007. PCM thermal storage in buildings: A state of art. *Renewable and Sustainable Energy Reviews.* 2007, Vol. 11, p. 1146-1166.

Tyagi V.V., Kaushik S.C., Tyagi S.K., Akiyama T. 2011. Development of phase change material based microencapsulated technology for buildings: A review. *Renawable and Sustainable Energy Reviews.* 2011, Vol. 15, p. 1373-1391.

UNI. 2003. 11097:2003. *Gestione per la qualità - Indicatori e quadri di gestione della qualità - Linee guida generali.* 2003.

Verma, Prashant, Varun, Singal. 2008. Review of mathematical modeling on latent heat thermal energy storage systems using phase-change material. *Renewable and Sustainable Energy Reviews.* 2008, Vol. 12.

Vivarelli A., Bernardi A., Pockelé L., Becherini F., Mezzasalma G., Schumacher P., Schoenberger E. 2015. *D7.1 Assessment of the performance of the districts before renovation.* s.l. : Deliverable of FP7 project EFFESUS (Grant no. 314678, FP7-2012-NMP-ENV-ENERGY-ICT-EeB), 2015.

Vogel A., Apitz I., Freidank S., Dijkink R. 2006. Sensitive high-resolution white-light schlieren technique with a large dynamic range for the investigation of ablation dynamics. *Optics Letters.* 2006, Vol. 31, 12, p. 1812-1814.

Weinstein L.M. 2010. Review and update of lens and grid schlieren and motion camera schlieren. *European Physical Journal Special Topics.* 2010, Vol. 182, p. 65-95.

Wetzstein G., Raskar R., Heidrich W. 2011. Hand-held schlieren photography with light field probes. *IEEE International Conference on Computational Photography ICCP.* 2011.

Wohlwill J.F. 1975. Behavioral response and adaptation to environmental stimulation. [a cura di] Damon A. *Physiological anthropology.* Cambridge, MA : Harvard University Press, 1975, p. 295–334.

Wolkoff P., Kjaergaard S.K. 2007. The dichotomy of relative humidity on indoor air quality. *Environment International.* 2007, Vol. 33, 6.

Zalba B., Marin J. M., Cabeza L. F., Mehling H. 2003. Review on thermal energy storage with phase change: materials, heat transfer analysis and applications. *Applied Thermal Engineering.* 2003, Vol. 23, p. 251-283.

LIST OF FIGURES

LIST OF TABLES

LIST OF ACRONYMS

AKNOWLEDGEMENTS

The first people I would thank are my supervisors, Prof. Ferruccio Petrucci and Dr. Adriana Bernardi, who allowed me to realize this doctorate and conclude this thesis, guiding me in every phase and spending long time to discuss methodology and results.

I thank all the people involved in the various research topics addressed in this thesis, from the staff of RED srl, with whom we collaborated closely for the experiments within the European MESSIB and EFFESUS projects, to the numerous partners of the two respective projects.

Another special thanks to Prof. Sante Mazzacane and Prof. Pasquale Catalano, from which came the ideas related to the Schlieren system and image spectroscopy, respectively. For the latter, I would like to mention also Prof. Paolo Russo, the first intermediary between us and the University of Molise; Prof. Maria Cristina Messia, for conducting the spectrophotometric analyses on oil samples, and Dr. Marcello Picollo for granting me his time and the use of his laboratory for further spectrophotometric analysis.

Thank Prof. Giuseppe Schirripa and Dr. Paolo Bison, the referees, for their effort, comments and guidance in the final phase of this thesis.

Then I thank a lot my former colleagues of the CNR of Padua, Dr. Maria Concetta Di Tuccio in particular and Dr. Francesca Becherini, for the many years spent together and for their support at work and not only. Thank also to Dr. Anna Impallaria for her help at the laboratory of archaeometry.

Finally, I am very grateful to all my family, to my parents and to Andrea in particular, who accompany me every day and always support my choices. To Irene, because her advent has brought a new life.